Universidad de Oviedo

ESCUELA POLITÉCNICA DE INGENIERÍA DE GIJON

MÁSTER EN INGENIERÍA DE TELECOMUNICACION

ÁREA DE TEORIA DE LA SEÑAL Y COMUNICACIONES

TESIS DE MÁSTER N.º 201903

DISEÑO DE REFLECTARRAYS PARA MEDIDAS EN APLICACIONES 5G – RESUMEN DE CONTENIDOS.

IMAZ LUEJE, Borja
TUTOR: D. Marcos Rodríguez Pino

FECHA: Julio 2019

Agradecimientos.

Tras finalizar esta etapa de mi vida quiero aprovechar para mencionar aquellas principales personas que han sido participes y catalizadores de haber superado todos los retos a lo largo de estos dos años.

Para empezar, quiero agradecer a las personas mas cercanas y pilares fundamentales de mi vida: mis padres Jesús y Amelia, mis hermanas Cristina e Irene o mi querido abuelo Serapio. Todos siempre han estado ahí estos años de Máster apoyándome en lo personal y siempre impulsándome a conseguir superar todas las dificultades que me he encontrado.

En este sentido también quiero agradecer a otra persona muy importante, como es Sara. Gracias por estar siempre a mi lado en las buenas y en las malas, animándome en todas las decisiones y oportunidades que se me han presentado.

Quiero dar las gracias también a todos mis compañeros de Máster, aquellos con los que ya había compartido experiencias en el grado. Vuestra experiencia y trabajo en equipo han sido determinantes para poder superar todas las adversidades que se nos han presentado.

Centrándose en este trabajo, quiero agradecer a mis compañeros de departamento en la empresa, como Constantine o Mehmed, los cuales siempre han estado ahí para ayudarme en el ámbito interno de la empresa. También por supuesto dar las gracias a mi supervisor Corbett, el cual ha sido de gran ayuda durante el desarrollo de todo el proyecto. Como profesor en la Universidad, hay que destacar a Marcos, quien ha sido el principal punto de referencia ante las distintas dificultades que han aparecido a lo largo del proyecto.

¡Muchas gracias a todos!

Dedicado a mis padres Jesus y Amelia,

a mis hermanas Cristina e Irene y

a mi abuelo Serapio,

por siempre estar a mi lado

0.- RESUMEN DE CONTENIDOS.

0.1.- Introducción.

La nueva generación de móviles 5G tiene por objetivo el incremento de las prestaciones en comparación con sus predecesoras, así como dar cabida a la integración de un amplio abanico de servicios. Los nuevos requisitos marcados en esta tecnología suponen también importantes desafíos en la instrumentación electrónica encargada de evaluar que los dispositivos electrónicos 5G cumplan con los requisitos marcados.

Dentro del campo de medida del comportamiento electromagnético generado por un dispositivo, los nuevos retos hacen que sea necesario la irrupción de nuevos sistemas y estructuras de medida, como son los denominados sistemas de rango compacto (CATR). Estos sistemas se basan en el uso de reflectores parabólicos, antenas con un coste de fabricación a priori elevado debido a la complejidad de realizar superficies curvas.

Por su parte, las antenas reflectarray son elementos radiantes basados en reflectores planos de una o varias capas de sustrato que permiten colimar el campo eléctrico en una determinada zona del espacio, de la misma forma que lo realiza un reflector parabólico, pero con una mayor facilidad de integración, complejidad y por ende menor coste en fabricación.

La memoria que a continuación se expone, intenta plasmar el proyecto de investigación que lleva su nombre, y ha tenido por objetivo el diseño de antenas reflectarray para su uso en sistemas CATR, en concreto aquellos utilizados como sistemas de medida de dispositivos pertenecientes a la futura tecnología 5G. Dicho proyecto de investigación se ha realizado dentro de la empresa Rhode & Schwarz en su sede central, sita en Múnich, Alemania.

De este objetivo general, es posible discernir distintos subobjetivos. Así pues, el primer de ellos será realizar una evaluación del contexto en el que se enmarcan los diseños, desde los conceptos más generales de la tecnología 5G, así como, la definición y descripción de los sistemas CATR y las antenas reflectarray. Consecuentemente con este contexto, se describirán los requisitos que deben satisfacer los diseños, a partir de los cuales hará falta construir una metodología a seguir basada en algunos de los conceptos básicos de este tipo de antenas.

Con esta metodología será posible entonces crear distintos diseños prototipo de antena ajustados a los requisitos marcados. Como parte final del proyecto, se realizará un estudio a cerca del coste económico que supone el proyecto en su conjunto, teniendo en cuenta el desarrollo de la metodología, el diseño y la fabricación de los distintos prototipos.

El documento resumen que a continuación se muestra, se organiza en 8 puntos siguiendo la línea de estos objetivos marcados, donde se añade un último capítulo donde se resumen las conclusiones a las que se ha llegado tras la realización del proyecto.

0.2.- Tecnologías 5G.

Una de las tecnologías actualmente en boga dentro de las telecomunicaciones es la nueva generación de comunicaciones celulares 5G. A parte de buscar la mejora en las principales prestaciones móviles como la velocidad de transmisión, latencia… etc., esta quinta generación busca abarcar y dar soporte a multitud de servicios variopintos. Se pretende entonces englobar en una misma infraestructura tecnologías que requieran amplias zonas de cobertura con anchos de banda poco exigentes (como los servicios IoT) así como tecnologías que requieran altas capacidades de transmisión sobre zonas más pequeñas.

Para hacer frente a tales retos, han surgido numerosas investigaciones cuya finalidad es mejorar distintas partes de la infraestructura. Dicho esto, aparecen nuevas formas de onda, métodos mejorados de dúplex, el denominado *Massive* MIMO o el estudio acerca del uso de frecuencias milimétricas.

Para dar cabida a esta conglomeración de servicios, en 5G se pretende abarcar un amplio rango de frecuencias. Desde este punto de vista, se podrán destacar dos franjas en el espectro radioeléctrico.

- **FR1(0.45-6.00 GHz).** Banda actualmente utilizada por las comunicaciones celulares predecesoras (3G y 4G) u otras tecnologías microondas con anchos de banda reducidos pero capaces de cubrir áreas extensas sin necesidad de grandes cantidades de energía.
- **FR2(24.25 – 52.60 GHz).** Nuevo rango de frecuencias que se pretende utilizar al ofrecer grandes anchos de banda. Al trabajar en alta frecuencia, las perdidas serán altas y por tanto las zonas a cubrir serán reducidas. La planificación de sub-bandas dentro de FR2 se ajustarán debido a diversos factores, como por ejemplo en función de las perdidas por absorción atmosférica.

Los requisitos comentados que implica 5G repercuten significativamente sobre la instrumentación electrónica dedicada a esta tecnología celular. Los futuros dispositivos 5G dispondrán de una alta integración, especialmente a frecuencias milimétricas. Es por ello que, dentro de la medida de antenas y radiación generada por un dispositivo, se propone el uso de los sistemas OTA (*Over-The-Air*). Sistemas que permiten la medida de los distintos patrones de radiación que ofrece un dispositivo sin conexiones con el dispositivo bajo estudio (DUT).

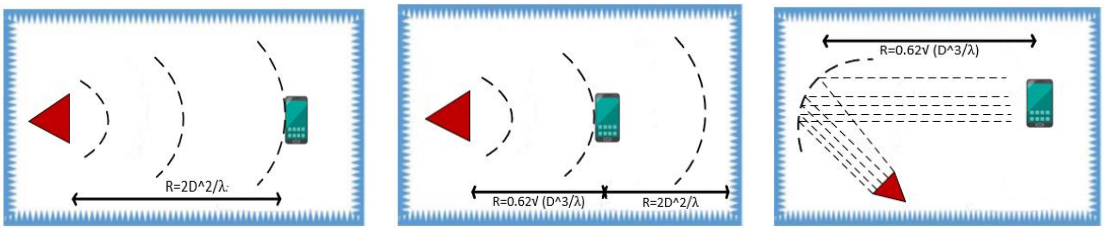

(a) (b) (c)

Fig. R1 – Grupos de métodos de medida de antenas en los sistemas OTA: (a) Método campo lejano;(b) Método campo cercano; (c) Métodos campo lejano indirecto.

Los sistemas OTA pueden realizar la medida utilizando distintas configuraciones entre antena y DUT. De acuerdo con el estándar 3GPP es posible distinguirlos en 3 grupos: los métodos campo lejano directo, métodos de campo cercano y métodos campo lejano indirecto (Fig. R1). La principal desventaja de los primeros será la distancia entre antenas, cuando se trabaje a altas frecuencias o con antenas de grandes dimensiones. El método campo cercano, permitirá realizar medidas a distancias de separación más bajas, con el inconveniente de necesitar un mayor coste de computación en el procesado de las medidas. Por último, los métodos de campo lejano indirecto permiten resolver los inconvenientes vistos en los dos anteriores, ya que su objetivo es crear un área, en la zona cercana de la antena, donde el campo eléctrico se comporta como si se trabajase en campo lejano. De los distintos métodos con los que se puede crear esta zona del espacio, destacan los sistemas en los que se basa este proyecto, también llamados sistemas CATR.

0.3.- Sistemas CATR.

Se denominan sistemas de rango compacto o CATR, a aquellos sistemas que, mediante el uso de uno o varios reflectores, permiten colimar el campo eléctrico proveniente de un alimentador sobre una zona determinada del espacio, donde el campo se propagara como una onda plana. Por regla general, este reflector mencionado suele ser una superficie parabólica ya que, gracias a sus propiedades geométricas, transforma las ondas esféricas del alimentador en ondas planas, lo que permite que el campo eléctrico se comporte de forma similar en campo cercano, como así lo haría en campo lejano. A la zona del espacio cercana al reflector que cumple tales características también se denomina zona tranquila (*quiet zone*).

Aunque teóricamente, el uso de reflectores parabólicos sobre sistemas CATR ofrecen estas prestaciones, en la práctica aparecerán algunos efectos que pueden limitar el tamaño de esta zona tranquila, algunos de ellos se muestran en la Fig. R2**.**

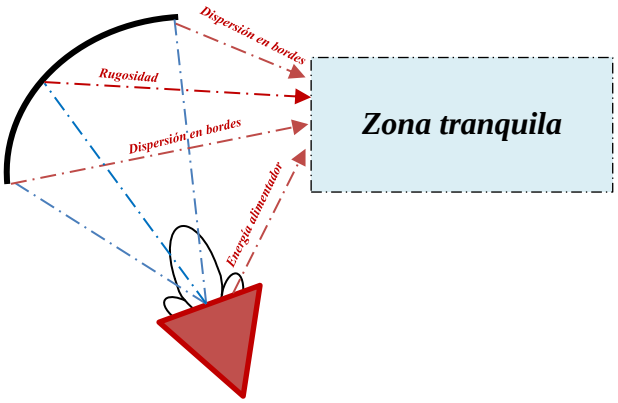

Fig. R2 – Contribuciones que distorsionan la zona tranquila.

0.4.- Antenas Reflectarray.

Las antenas reflectarray consisten en estructuras offset conformadas por un reflector y un alimentador en un formato idéntico a los sistemas CATR. Sin embargo, el reflector será una superficie plana conformada por un conjunto de elementos radiantes, agrupados siguiendo una distribución array.

Al igual que en los reflectores parabólicos, los reflectarrays buscan conformar un determinado campo eléctrico reflejado a partir del campo que incide sobre su superficie. Sin embargo, mientras que el reflector parabólico también utiliza su geometría para colimar el campo, el reflectarray utilizara la distribución y forma de los elementos radiantes. Esto le dotará de una mayor libertad para conformar distintos patrones de radiación.

Los reflectarrays también se constituyen como antenas directivas, lo que implica que concentraran el campo en un determinado haz. En función de este haz, es posible distinguir 2 tipos de antenas reflectarray: reflectarrays de haz fijo y variable.

Los primeros, fijan el haz en una dirección determinada del espacio no modificable tras la fabricación. Este tipo es el mas desarrollado e investigado al ser más sencillo de implementar.

Por su parte, los reflectarrays de haz reconfigurable, permiten modificar el haz después de la fabricación, mediante el uso de dispositivos activos (diodos PIN, MEMS) en los elementos radiantes. Este subgrupo de antenas tendrá mayor versatilidad que los anteriores, si bien su implementación y diseño requerirán un mayor esfuerzo.

Las antenas reflectarray por definición, disponen de una naturaleza intermedia entre las antenas array y los reflectores parabólicos, de los que toman sus principales ventajas. Los reflectarrays convencionales (haz fijo), se constituyen enteramente de elementos pasivos, lo que reduce las perdidas con respecto al uso de arrays convencionales. Frente a los reflectores parabólicos, a parte de la versatilidad mencionada anteriormente, las antenas reflectarray tienen mayor capacidad de integración, facilidad de implementación y escalabilidad. Estas características son las que hacen a estas antenas muy interesantes como sustitutivo de los reflectores parabólicos en los sistemas CATR.

Como contrapartida, la principal desventaja de los reflectarrays es, al igual que los arrays, su reducido ancho de banda. Esta limitación viene derivada especialmente por el ancho de banda de los elementos radiantes y los desfases debidos a los distintos caminos espaciales.

0.5.- Requisitos de la antena.

Una vez descrito el contexto en el que se enmarca el proyecto, se dispone a definir los requisitos electromagnéticos que debe satisfacer el campo eléctrico.

Se realizan diseños de antenas reflectarray para frecuencias en los dos rangos frecuenciales en los que se posicionará 5G, en concreto las frecuencias a 1.7 y 28 GHz. Las antenas a 1.7 GHz deben generar una zona tranquila de dimensiones 500 x500 x 500 mm^3 a una distancia del reflector no superior a 3 metros. Por su parte los diseños a 28 GHz deberán crear zonas quietas de 10x10x10 cm^2 a una distancia máxima de 50 cm del reflector.

Para la fabricación del reflector es posible utilizar el sustrato Taconic-TSM DS3b y excepcionalmente, para la banda de 1.7GHz, es posible utilizar también FR4. Ambos sustratos son muy utilizados dentro de la empresa para la fabricación de placas de circuito impreso (PCB). Para diseños de más de una capa, es posible también el uso de pegamentos compatibles con estos sustratos si se desea la implementación de reflectores de varias capas.

En cuanto a los valores cuantitativos que definen la zona tranquila objetivo, se considera que el campo eléctrico en dicha zona no debe tener un rizado mayor de 1.5 dB en amplitud y 22º en fase.

Como último requisito impuesto, para el diseño de las antenas, Rhode ofrece la posibilidad de utilizar dos plataformas software comerciales como son Matlab ® y CST Studio Microware ®.

0.6.- Metodología.

Previo al diseño de los reflectarrays, será necesario definir una metodología o conjunto de pasos a seguir para llegar a un punto o configuración que tenga un comportamiento electromagnético ajustado al os requisitos. Por ello, en este proyecto se describe una metodología conformada por los bloques que se detallan en la Fig. R3.

Estos bloques además pueden agruparse en tres subprocesos ordenados según su ejecución: diseño individual, diseño global y evaluación.

En el primero de ellos, se evalúan de manera independiente dos componentes principales que conforman la antena: el alimentador y los parches dispuestos sobre el reflector. Del primer bloque se extrae información a cercad e la relación entre las características físicas de la celda y el campo reflejado que esta genera. En este caso, la onda reflejada en cada celda será igual a la onda incidente en la misma, sobre la que se aplica un determinado desfase, dependiente del tamaño de la celda. En el estudio del alimentador se evalúa las características y se extraen modelos equivalentes para su uso en los modelos de la metodología.

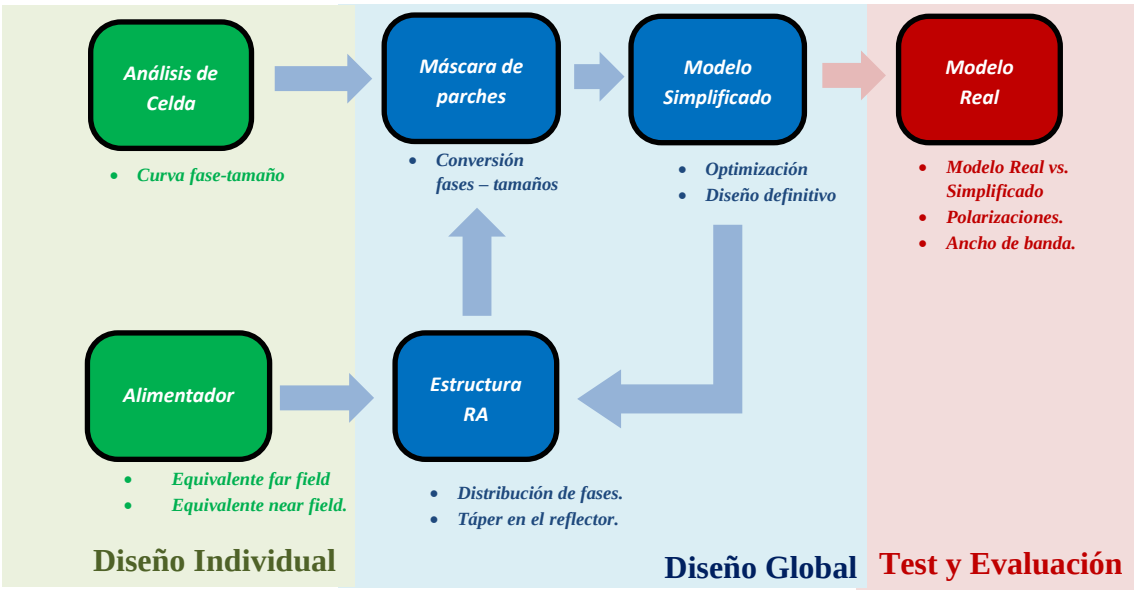

Fig. R3 – Esquema flujograma de la metodología para el diseño de antenas reflectarray.

Con dicha información se pasará al diseño de la estructura en su conjunto. Este subproceso consistirá en la iteración de tres bloques donde en primer lugar se dimensionará el reflector y que fases debe ofrecer este para que el campo reflejado global del reflector se ajuste al campo eléctrico que se busca. La configuración de antena resultante sirve como punto inicial en el proceso de optimización.

Con la información de celda, estas fases se traducen en tamaños de parche (máscara de parches) con la que, junto a la información recabada de la estructura, es posible realizar un modelo en CST del diseño (modelo simplificado) y evaluar su comportamiento. El proceso de optimización se ejecutará en este bloque.

Si tras la optimización, el resultado de la antena difiere en exceso de los requisitos marcados, se probará con una nueva configuración de reflectarray. Si, por el contrario, se consigue una configuración adecuada, se realizará un modelo detallado de la antena (diseño definitivo).

Por último, en el proceso de evaluación, se crea un modelo CST del diseño optimizado más ajustado a la realidad, con el que se calculará el ancho de banda de la antena y su comportamiento en la otra polarización (téngase en cuenta que esta antena ofrece polarización lineal y el proceso de optimización se basará sobre una de ellas, en concreto la polarización Y).

A continuación, se exponen algunos aspectos concretos de cada uno de los bloques que conforman la metodología:

0.6.1.- Análisis de Celda.

Los elementos radiantes que se han escogido para esta metodología son los parches pasivos cuyos parámetros se muestran en la Fig. R4**.** Para simplificar el elemento, se considerarán parches cuadrados ($a = b, a_1 = b_1$, $a_2 = b_2$,…,$a_n = b_n$,….).

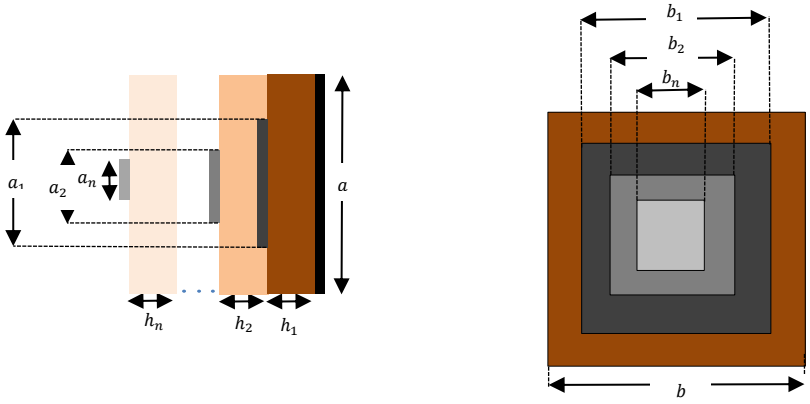

Fig. R4 – Estructura genérica de la celda. Vista frontal y de perfil. En escala de grises los parches, a color los substratos.

El principal objetivo de este bloque será conseguir una relación lineal entre el tamaño de los parches y el desfase que introducen. Una zona lineal que aporte un rango de desfases alto con una pendiente no demasiado pronunciada. Estos dos aspectos de la curva tienen una relación inversa (cuando aumenta uno, se reduce el otro) lo que supondrá

tener que lidiar con una relación de compromiso entre ambos. La curva fase-tamaño se ajustará mediante la configuración de parámetros del parche como su periodicidad, frecuencia de diseño, altura de sustrato….

El ángulo con el que incide la onda sobre el parche también será un factor que deberá tenerse en cuenta, dado que se pretende crear estructuras reflectarray en offset. Dicho esto, se evaluará el comportamiento de la celda en diferentes ángulos de incidencia, almacenando la información en una matriz tridimensional denominada matriz de diseño, la cual será muy útil los posteriores pasos de la metodología.

0.6.2.- Alimentador.

En la mayoría de las antenas que siguen una estructura en offset, el alimentador será por regla general una antena tipo bocina, ya que esta permite generar diagramas de radiación pincel directivos, que enfoquen la mayoría de la energía sobre el reflector. En este sentido se creará un modelo CST de la bocina escogida y se extraerán distintos modelos equivalentes de la misma para los modelos CST de la estructura en conjunto.

0.6.3.- Estructura RA.

Como primer bloque dentro del diseño general, se dispone a dimensionar las características del reflector y marcar una configuración inicial de la antena con la información ya recabada del alimentador y las celdas.

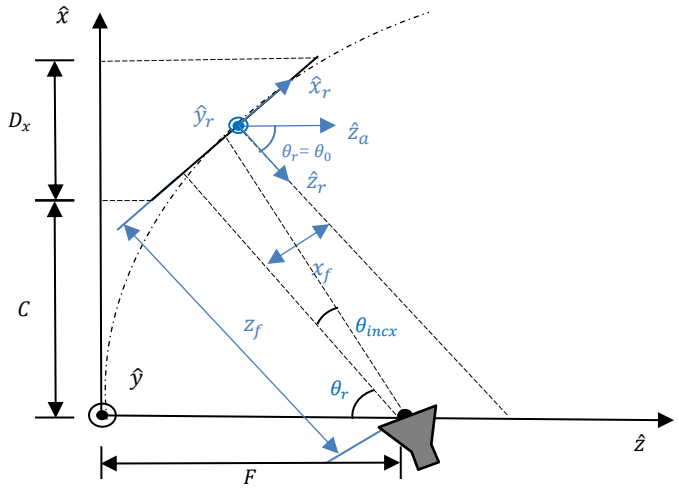

Fig. R5 – Estructura geométrica de una antena reflectarray. Modelo equivalente parabólico.

Una antena reflectarray puede definirse geométricamente utilizando un modelo equivalente parabólico tal y como se muestra en la Fig. R5**.** También resultará interesante, a la hora de modelar dicha antena en CST, utilizar el sistema de referencia propio del

reflector, el cual considere como punto de referencia, el centro del reflectarray. Será preciso entonces calcular las relaciones entre los parámetros de ambos sistemas de referencia.

Para dimensionar de manera correcta todos estos parámetros, en este punto se realizarán dos estudios importantes:

- **Distribución de fases.** Apoyándose en la teoría de arrays, es posible calcular la distribución de fases que debe haber en el reflector para que este genere un frente de ondas con fase constante, condición teórica que tienen los reflectores parabólicos. Se espera que, si se consigue recrear el campo lejano de un reflector parabólico, la antena reflectarray se comporte en campo cercano de manera similar a lo que haría el reflector parabólico.
- **Campo sobre el reflector.** Juntamente con el anterior punto, se deberá evaluar la diferencia de campo eléctrico a lo largo de la superficie reflectora. Basándose en previos estudios de reflectarrays, este efecto deberá ser tenido en cuenta para encontrar un punto inicial adecuado.

0.6.4.- Máscara de parches.

Este bloque actuará como bloque intermediario entre la estructura RA y la creación del modelo CST. Con la distribución de fases calculada y la matriz de diseño, es posible obtener el tamaño que debe tener cada parche que conforme el reflector. Estos tamaños permanecerán invariantes durante todo el proceso de optimización.

0.6.5.- Modelo Simplificado.

Con todas las características conocidas de la configuración inicial, se dibujará un modelo de la antena en CST bajo ciertas premisas que simplificarán el modelo, reduciendo así su coste computacional.

En primer lugar, se realizará una simulación con la configuración inicial obtenida. Seguidamente, se analizará el efecto de algunos parámetros geométricos, en aras de mejorar el comportamiento del campo eléctrico y por ende la zona tranquila generada. En este punto se modificarán parámetros como la distancia entre alimentador y reflector, o el ángulo de apuntamiento de la bocina sobre este. También se valorará la introducción de elementos radiantes que actúen como bloqueante de cierto campo eléctrico residual.

En los distintos estudios realizados en este bloque, se evaluará el campo eléctrico en cortes transversales al reflectarray y en distintos planos sobre el eje Z. Tomando como referencia los requisitos de campo dentro de la zona tranquila, es posible obtener los tamaños de zona tranquila en distintos puntos del eje Z, con los que se calculará a que distancia del reflector se consigue que la zona tranquila alcance las dimensiones

impuestas. La principal figura de mérito durante el proceso de optimización el tamaño mínimo de zona tranquila que se consigue para cada configuración bajo análisis.

La configuración reflectarray más idónea se estudiará con mayor detalle, con el fin de poder ser comparada en el siguiente bloque.

0.6.6.- Modelo Real.

Como último bloque de la metodología, se creará en CST un modelo más realista de la estructura reflectarray, donde se consideran las propiedades más realistas de la antena. Este modelo tiene por objetivo su uso en los siguientes estudios.

- **Comparativa con el diseño simplificado.**
- **Comparativa entre polarizaciones.**
- **Estudio en banda.**

Con este bloque, finaliza el proceso de diseño y se está en disposición de extraer aquellos datos necesarios para la fabricación del prototipo.

0.7.- Diseños Reflectarray.

Como principal punto del trabajo, se realizan tres diseños de antenas reflectarrays ejemplo apoyándose en la metodología creada. Dos diseños se enfocarán en la banda de 28 GHz y otro en la de 1.7 GHz.

0.7.1.- Diseño 28 GHz Monocapa.

Como primer diseño a realizar, se comienza considerando un reflectarray conformado por una capa de sustrato y una capa de parches. De acuerdo con el análisis de celda, se consigue una relación lineal de fases y tamaños de parches adecuada cuando se utiliza una periodicidad de $\frac{3\lambda_0}{8}$ (4.018 mm) junto con una altura de sustrato de 0.76 mm. Esta relación es robusta frente a distintos ángulos en incidencia oblicua, así como en banda, donde el principal efecto es una variación de la pendiente en dicha curva. Como contrapartida, y al tratarse de un diseño monocapa, no se conseguirá un rango de fases de 360º.

Como alimentador se escogerá el tipo de antena *Axial Chokes Conical Horn*. Una bocina cónica con polarización lineal con interesantes propiedades electromagnéticas para su uso en los sistemas CATR. El diseño de esta bocina a 28 GHz proporcionará un diagrama de radiación quasi-simetrico en ambos cortes con una ganancia de 20 dBi. No obstante, dada la relación entre propiedades eléctricas y físicas, será un diseño de bocina con una considerable complejidad para su fabricación.

Con respecto a la estructura global de la antena, se dimensionará un reflector de 96x82 elementos. Con la posición inicial del alimentador, se calculan los ángulos con los que incide la onda proveniente del alimentador. En vista del comportamiento de la celda frente a las combinaciones de ángulos que se obtienen, la incidencia oblicua no causará efectos significativamente nocivos al campo eléctrico.

En la simulación bajo el modelo simplificado de esta configuración se observa una zona tranquila de tamaño reducido, derivada principalmente por la dispersión en los bordes del reflector. En vista de esto, se optimizará la posición del alimentador y el ángulo de apuntamiento de este.

Tras estos estudios, se consiguen tamaños de zona tranquila que se acercan al límite de 10 cm marcado, aunque no se alcanza este límite a distancias del reflector menores de 50 cm. En vista de esto, se prueba a introducir algunos elementos a la estructura como son un plano PEC sobre la bocina con el fin de reducir los efectos que provoca el campo generado por la bocina en direcciones distintas a la de apuntamiento. También se probará, junto con este nuevo elemento, a colocar la bocina en posiciones por debajo del reflector, que no generen bloqueo sobre el campo reflejado. Sin embargo, no se consigue mejorar de manera significativa la zona tranquila y por tanto el modelo optimizado en ángulo y posición será el escogido como configuración definitiva.

En el análisis del modelo definitivo, se observa que la zona tranquila aumenta de tamaño a medida que el campo se aleja del reflector. Se consigue alcanzar una zona tranquila ajustada en requisitos, aunque a una distancia del reflector por encima de la máxima marcada. En estas simulaciones se aprecia una desviación del haz principal en el campo reflejado. Una desviación tanto en su ángulo de apuntamiento como en el punto del reflector donde se genera. Así pues, en el diseño definitivo se calcula el ángulo de deriva y offset sobre el eje Z de este haz principal, corrigiendo la estructura en su defecto.

Con respecto al modelo real, se comprueba su similitud con el modelo hasta ahora utilizado. Se corrobora también las reducidas diferencias en la zona tranquila para ambas polarizaciones, gracias a la simetría de radiación en el alimentador. Por último, en banda la antena tendrá un ancho de banda de 2 GHz tanto en amplitud como en fase, con un rango de frecuencias entre 26 y 28 GHz.

0.7.2.- Diseño 28 GHz Multicapa.

Con la introducción de una nueva capa de sustrato, se introduce al análisis de celda dos nuevas variables a configurar como son la altura de la segunda capa y la relación de parches entre ambas capas. No obstante, con este diseño se consigue eliminar la restricción de fases que se tenía en el diseño monocapa. Se consigue una zona lineal

adecuada en la curva fase-tamaño con una periodicidad de $\frac{\lambda_0}{2}$ (5.40 mm), unas alturas de sustrato $(h_1, h_2) = (0.72,1.52)$ mm y una relación de parches $\alpha = 0.75$.

En frecuencia, esta curva tendrá un comportamiento idéntico que en caso anterior mientras que en incidencia oblicua aparecerá una mayor distorsión de la curva, lo que se traduce en mayor sensibilidad a altos ángulos de incidencia.

Utilizando el mismo diseño de alimentador y buscando unas dimensiones similares al reflector de una capa, la configuración reflectarray inicial será similar a la que se obtiene en monocapa. Las diferencias radicarán en un menor número de parches (al aumentar la periodicidad) y una distribución de fases que abarcan en valor un rango de 360º.

La simulación inicial presenta una forma y tamaño de zona tranquila peor que el caso anterior, si bien también es susceptible de ser mejorada optimizando el tamaño y el ángulo de apuntamiento. Al igual que ocurría en monocapa, tras la optimización de estos dos parámetros no se consigue alcanzar una zona tranquila a distancias menores de 50 cm, aunque si para distancias más alejadas. En este diseño también aparece una desviación del haz principal ligeramente más acusada que en el diseño monocapa, que se corregirá siguiendo el mismo proceso que en el anterior caso.

En su modelo real, el diseño multicapa presenta más diferencias entre modelos, ya que el diseño multicapa introduce más variables a introducir en este modelo, como por ejemplo el pegamento a utilizar entre capas. Por su parte, la zona tranquila será prácticamente idéntica en ambas polarizaciones. A pesar de su peor comportamiento a la frecuencia de diseño, esta antena en banda será más robusta, consiguiendo un ancho de banda de hasta 4 GHz en amplitud y manteniendo los 2 GHz en fase. Tanto en amplitud como en fase, la zona tranquila tendrá un mejor comportamiento a las frecuencias por encima de los 28 GHz.

0.7.3.- Diseño 1.7 GHz Monocapa.

El análisis de celda a 1.7 GHz valora la posibilidad de utilizar también el sustrato FR4, con lo que se añade una etapa adicional en este análisis. Se observa que las alturas disponibles para ambos tipos de sustrato aportan relaciones lineales con altas pendientes, algo no deseable para el diseño. Dicho esto, se propone el uso de varias capas de sustrato superpuestas, para conformar capas con una mayor altura de sustrato.

Dicho lo cual y en vista de los resultados, se utilizará también el sustrato Taconic TSM-DS3 con una periodicidad de $\frac{\lambda_0}{2}$ (88.235 mm) y una altura de sustrato de $h =$ 3.81 mm (combinación de dos capas de sustrato 1.52 + 2.29 mm). La configuración de

celda propuesta tiene un comportamiento idéntico en banda a los anteriores diseños y una robustez frente a la incidencia oblicua como ocurría en el diseño de 28 GHz una capa.

Utilizando el mismo tipo de antena, se realiza un diseño de bocina a 1.7 GHz con menores restricciones en ganancia (15 dBi), lo que permite reducir la complejidad de fabricación de esta antena y características eléctricas más permisivas.

La estructura inicial del reflectarray a 1.7 GHz se asemeja a una versión escalada de los diseños a 28 GHz, estimada en base a los requisitos de zona tranquila que se han impuesto en esta banda. El reflector a utilizar tendrá unas dimensiones de 185.29 x 176.47 cm. Debido a esto los ángulos de incidencia serán similares a los anteriores diseños, aunque el táper sobre el reflector será ligeramente menor, dada la menor directividad de la antena.

A diferencia de los anteriores diseños, la simulación de la estructura inicial presenta buenas prestaciones de zona tranquila, consiguiendo cumplir los objetivos. En aras de buscar un diseño optimo, se seguirá un proceso de optimización similar a los anteriores casos, consiguiendo un modelo definitivo de reflector con aun mejores prestaciones. Gracias a esto, se consigue duplicar el tamaño de zona requisito en amplitud, consiguiendo superficies por encima del metro cuadrado en esta componente.

Sin embargo, en las distintas configuraciones evaluadas de este diseño se identifican áreas con alto rizado dentro de la zona tranquila. Esta sensibilidad al rizado provoca mayores discrepancias entre modelos real y simplificado, así como en el estudio en varias polarizaciones.

Con respecto al estudio frecuencial, se consigue un ancho de banda de 200 MHz ajustado, en términos relativos, a los anchos de banda que se consiguen con este tipo de antenas. Se tiene un rango de operación entre 1.7 y 1.9 GHz, siendo en estas frecuencias extremo donde la zona tranquila alcanza un mejor comportamiento.

0.8.- Proyecto y Presupuesto.

A cerca de la organización del trabajo que ha supuesto este proyecto, es posible dividirla en dos periodos temporales, acaecidos entre junio y septiembre de 2018 y entre Febrero y Julio del 2019 respectivamente.

En el primero de ellos, las tareas del proyecto se enfocaban en la búsqueda bibliográfica a cerca del contexto del trabajo y el tipo de antenas a utilizar, junto con la definición de los requisitos de la antena. Como segundo bloque en este periodo, se describió e implemento la metodología a utilizar, validándola por diseños preliminares de antena reflectarray.

El segundo período comenzó con la propuesta a cerca de ciertas mejoras a introducir en la metodología a la vez que se continuaba con la búsqueda bibliográfica. Gran parte de este periodo se ha centrado en el desarrollo de este documento y la realización de los diseños contenidos en el mismo.

Desde el punto de vista económico, este proyecto abarca dos fuentes de coste claramente diferenciables, como son los costes de diseño y los costes de fabricación. Especial atención tendrán estos últimos ya que se estima un coste mucho menor al coste que supondría la fabricación de un reflector parabólico para la misma aplicación.

0.9.- Conclusiones.

Basándose en los resultados que ha supuesto este proyecto, se concluye que las antenas reflectarray son un interesante candidato como sustituto de los reflectores parabólicos en los sistemas CATR, para su uso como dispositivos en 5G.

Al igual que estos, las antenas reflectarray, permiten concentrar el campo eléctrico sobre una determinada zona en campo cercano donde se consigue tener características eléctricas de campo lejano (zona tranquila). Además, lo consiguen con mayor facilidad de fabricación e integración con el resto del sistema, utilizando materiales estandarizados y ligeros.

Como contrapartida, se verifica que estas antenas disponen de un ancho de banda menor que los reflectores parabólicos, si bien ajustados a las bandas y sub-bandas que previsiblemente utilizara el futuro 5G.

Estas ventajas que presentan los reflectarrays se acentúan a frecuencias bajas del 5G, donde se buscan tamaños de zona tranquila amplios, que requieren de reflectores grandes. En este proyecto se verifica la escalabilidad de estas antenas, que permiten generar amplias zonas tranquila con reflectores de menor coste y mejor integrables que sus homólogos de reflector parabólico.

Respecto a la metodología empleada, se verifica su función para frecuencias bajas. Si bien para frecuencias milimétricas, los diseños basados en esta se acercan a los requisitos impuestos, pero no los consiguen cumplir.

En base a estas conclusiones, este proyecto abre la puerta algunas líneas de investigación, entre ellas se puede destacar la confección de un algoritmo que utilice como variables los parches en el proceso de optimización, o el diseño de nuevas estructuras reflectarray en otras bandas dentro de FR1.

Universidad de Oviedo

POLYTECHNIC SCHOOL OF ENGINEERING OF GIJÓN.

MASTER'S DEGREE IN TELECOMMUNICATIONS ENGINEERING

SIGNAL THEORY AND COMMUNICATIONS AREA

FINAL THESIS MASTER Nº 201903

REFLECTARRAY DESIGN FOR MEASUREMENTS IN 5G APPLICATIONS

IMAZ LUEJE, Borja
TUTOR: D. Marcos Rodríguez Pino

FECHA: July 2019

TABLE OF CONTENTS

LIST OF FIGURES

LIST OF TABLES

1.- INTRODUCTION

1.1.- Motivation.

One of the most important issues within telecommunications nowadays is the process of transformation towards the new generation of mobile communications, the 5th generation.

One of the main challenges that this technology must face is to have an important capacity of integration of services with very different features and requirements. For example, 5G technology is expected to allow speeds of tens of gigabytes for services in real time and in certain urban centers, but also to accommodate services that require broad coverage at low speeds.

The new requirements that mark the 5G technology also pose a challenge for the electronic instrumentation, responsible for verifying the devices that conform this future technology. In the case of the antenna instrumentation, the improvement of the technology and facing these new challenges is currently valued the use of measurements systems anciently restricted in a niche technology, such as compact range systems (CATR). These systems are based on the use of parabolic reflectors to generate areas with the desired electromagnetic conditions in a measurement process.

For its part, one of the antennas with greater evolution in recent years are reflectarray antennas (antennas that combine an array nature with the characteristics of reflectors). The main catalyst of its growth is the discovery and development of microstrip technology since the 1980s.

Due to their characteristics, reflectarray antennas can be compared with two types of traditional antennas such as arrays and parabolic reflectors. Compared to the first one, reflectarrays do not require distribution networks and therefore have much lower losses. Regarding parabolic reflectors, reflectarrays have a greater capacity to synthesize different radiation patterns, in addition to greater versatility, integration with other systems and less complexity in their manufacture.

Having said this, reflectarray antennas will then be a type of radiant elements that can be used for applications where parabolic reflectors are traditionally used, as CATR systems, where there are some studies such as [1]. This arouses interest in companies in the research sector, such as Rhode & Schwarz, where the project is being developed.

Based on all the aspects mentioned, the project described below aims to design reflectarray antennas prototype as a substitute for parabolic reflectors in CATR systems, for use within the 5G instrumentation.

1.2.- Objectives.

As it has been defined in the previous point, the fundamental axis of this project will be the design of different configurations of reflectarray that have an electromagnetic behavior similar to a parabolic reflector on a CATR system. To comply this goal, it will be essential to satisfy the following sub-goals.

First, it is necessary to describe in detail the problem and its technological context. A bibliographic search will then be carried out based on the three fundamental topics: 5G technology, CATR systems and reflectarray antennas. It will highlight the general lines and state of art of these 3 themes, as well as the relationship between them.

Focused on the problem to be faced in this project, the next step will be the definition of the requirements to be met by the antenna as well as the limitations in design and manufacture that exist. Adjusted to them, it is necessary to define and develop a methodology for the design of these antennas, based on their electromagnetic and geometric characteristics, the methodology will cover both the design and the subsequent study of aspects that remain outside this process as the study in band, its behavior in other polarizations and so on.

As a third step, a set of reflectarray designs will be made using the methodology described above. In this step it will also be necessary to clearly define the merit figures that allow to evaluate it the antenna fulfills or not the marked requirements.

Finally, the last goal is to carry out an economic evaluation of the entire process (both design and manufacture) that leads to the creation of a prototype reflectarray antenna. Apart from a technical comparison, this will allow a cost comparison between reflectarray and parabolic reflector antennas.

1.3.- Memory structure.

The following memory is composed by 7 chapters, within which a hierarchy of sections and sub-sections is defined. As mentioned before, chapter 1 details the motivation and the general goals of this project.

In the following two chapters, the context in which the project is placed will be described, from the most general aspect to the technological subgroup in which it is developed. Chapter 2 is based on the exposition of certain general lines about mobile communications and the future 5G. In a more specific way, chapter 3 defines the concept of CATR systems within the electronic instrumentation of devices and the type of the antenna that is proposed as a substitute element: reflectarray antenna.

Once the context is described, chapter 4 will define in detail the requirements to be met by the antenna. Besides this, the methodology of design of reflectarrays adjusted to these premises will be defined.

As the main block of this project, chapter 5 will detail the results obtained in each of the designs under study. For each of them and following the methodology described, the results will be shown in each of the stages, fully defining the performance of each antenna designed.

Chapter 6 will be based on describing two aspects at the project level: development and budget. Although this project covers the design, the cost of manufacturing these antennas will also be assessed since one of the project motivations is the economic improvement of this type of proposed antennas.

To summarize all the content, in chapter 7 the conclusions and main lines of work that the project opens will be mentioned.

2.- MOBILE COMUNNICATIONS

2.1.- Introduction.

Cellular technologies have advanced exponentially since their appearance in the 80's, always driven by the growing demands in terms of transmission and reception of information. Currently, the appearance of a new mobile generation, 5G which seeks to meet the countless requirements that are estimated in the future to be demanded by networks users. In addition, another of its goals is the integration of the mobile network with other technologies currently in vogue as the Internet of Things (IoT).

In the following chapter, the 5G mobile technology is briefly described, contextualizing it with its predecessor generations and defining the main challenges that this technology must face in order to implement it. The requirements to be met in the physical layer, in terms of waveforms, access technologies, … will be specially detailed. In this sense, the frequency spectrum occupied by 5G services will be an important factor to consider and therefore will be discussed in more detail.

Next, the repercussions of the 5G requirements on the instrumentation and measurement of the physical components that formed the system will be explained. For measurement of radiation patterns, where the use of OTA (Over-The-Air) test, common in other applications, is proposed for this purpose.

2.2.- Mobile generations. The future 5G

2.2.1.- Generations prior to 5G.

In the beginning of the mobile communications, 1st generation, dates from 1979, when several countries of the world, implement these cellular networks isolated from each other. These networks were based on circuit switching with speed between 1 and 2.4 kbps. They used frequency multiplexing (FDMA) using 832 duplex channels of 30 kHz each in the 800 – 900 MHz band. 1G had different standards such as the NMT (Nordic Mobile Telephone) used in northern European countries or the AMPS used in EEUU. The disadvantages of these original networks were their bad communications and poor call security.

The digitalization of mobile networks (1990) came from the hand of second generation (2G) networks, which worked in two frequency bands: the GSM band (850 – 1900 MHz) and CDMA (825 – 849 MHz) using bandwidths of 200 kHz and 1.23 MHz. Switching to Time Multiplexing (TDMA) and Code Multiplexing (CDMA) technologies

that increase the speed to a range between 14 and 64 kbps. The 1G standards were grouped into mobile standards conformed by a greater number of countries, such as GSM in Europe or CDMA in America or Asia. The better throughput and standardization of networks allowed the irruption of new services such as SMS, international roaming, calls on hold…

Faced with the need to provide higher speeds in communications, in 2000 emerged the third generation mobile (3G) hand in hand with the international group 3GPP that promulgated two international standards: UMTS and CDMA 2000 based on GSM and CDMA technologies. It goes to use a packet switching using different modes of multiplexing, offering speeds between 384 kbps and 2 Mbps. UMT and CDMA 2000 evolved over the years, achieving a substantial improvement in data speed and the appearance of the new services such as high-speed Internet access or videoconferencing.

As of 2010, the fourth generation (4G) appeared, which migrated cellular systems to IP technology. New multiplexing technologies appear (OFDM, MC-CDMA…) and a wider range of frequencies and bandwidths. The most important standards of this generation are the LTE (Long-Term Evolution) or the mobile WiMAX where speeds between 100 Mbps and 1Gbps are reached. In addition, there are high definition services (TV, VoIP, …) or access to dynamic information.

2.2.2.- The new mobile generation: 5G.

5G technology is defined as a set of researches and projects, within the field of cellular systems, which demonstrate the possibility of achieving a considerable increase in performance of 4G.

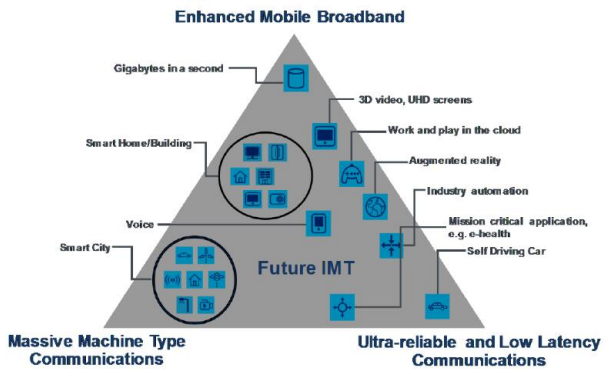

Fig. 2.1. - 5G usage scenarios [3].

The fifth generation aims to enable a communication system that can cope with the increase in connected devices, as well as open the door to the irruption of other technologies such as Internet of Things (IoT) and derivate thereof (*SmartCities*, Smart Homes, …).

Technically, the main challenges and requirements of the 5G generation are shown in the Fig. 2.2.

Fig. 2.2. - Challenge and Gaps of 5G. Comparison with 4G [3].

The new mobile generation does not yet have a global standardization, which is expected to be defined in 2020 (IMT-2020). Nevertheless, numerous investigations have been carried out to meet these imposed expectations. Some of them are:

- **Waveforms.** New wave formats are proposed to eliminate the limitations of OFDM modulations, such as GFDM (Generalized Frequency Division Multiplexing), FBMC (Filter Bank Multi-Carrier), …. It is foreseen that in 5G one or the other format will be used depending on the specific circumstances and requirements of the scenario, giving the technology greater flexibility.
- **Duplex methods.** It is valued the possibility of using the frequency division duplex (FDD) or time division duplex (TDD) methods adaptively depending on the load is evaluated.
- **Millimeter-wave technologies.** The use of frequencies located at the top of the radio spectrum allows the possibility of having a bandwidth greater than 4G. However, there are several regulatory difficulties for frequencies currently used by other applications and technological and technical difficulties for frequencies around tens of GHz. This point will be discussed in detail in the following section.
- **Massive MIMO.** By working with higher frequencies, it is possible to work with components of smaller physical dimensions. This has a great advantage in technologies such as MIMO, where it is possible to increase the number of antennas in each equipment improving the communication performance.

2.2.3.- 5G Spectrum.

The requirements and technologies that 5G intends to conglomerate are diverse, that is why, from the frequency point of view, it will be necessary to use frequencies in different points of the radio electric spectrum,

To meet capacity needs, it is necessary to have more bandwidth, which implies using frequencies in the high part of the spectrum. However, at these frequencies, the information will be more immune to the different distorting phenomena suffered by a wave in the air.

On the other hand, low frequencies allow a greater immunity to external factors, with a greater attenuation to the penetration in buildings but will have a reduced bandwidth, which translates into a lower transmission capacity.

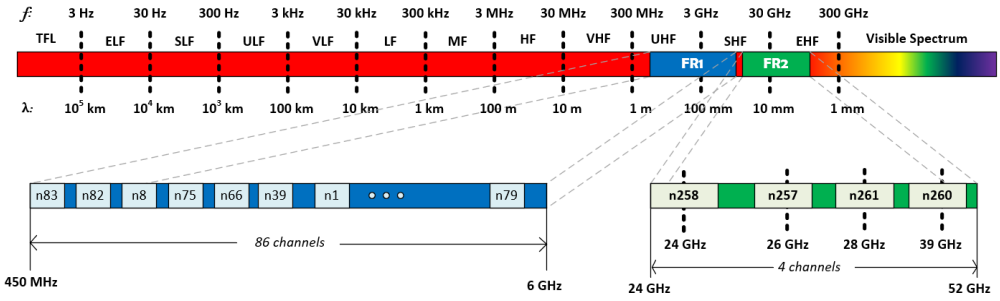

Fig. 2.3. - 5G New Radio: Frequency Allocation follow 3GPP Release 15.

Taking these factors into account, the 3GPP organization advocates for 5G a new wireless communications standard called 5G New Radio (NR) in which two wide frequency ranges are defined (Fig. 2.3):

- **FR1 (0.450 – 6.000 GHz).** This band is expected to allocate long distance mobile communications and technologies that do not require wide bandwidth, such as IoT services. Nowadays, this band is occupied mostly by previous mobile technologies (3G and 4G) along with television services. This frequency band will require cleaning band process for a coexistence between services without harmful interference.

- **FR2 (24.250 – 52.600 GHz).** In this range are grouped the so-called *milimiter waves* (mmWaves), by their size of wavelength. It is expected to host mobile communications in not very large areas with a dense mobile demand (e.g. cities). In this frequency range is more released although it is used by satellite applications which also forces the execution of sharing mechanisms or reorganization.

Apart from these two frequency ranges, other frequency bands have been proposed such as the 73 GHz [7].

The FR1 band consists of a wide range of sub-bands, it is estimated 86, with reduced bandwidths where it seeks to support a multitude of services. For example, the n66 band centered on 1.7 GHz is intended to accommodate cloud computing services over the bandwidth of 100 MHz.

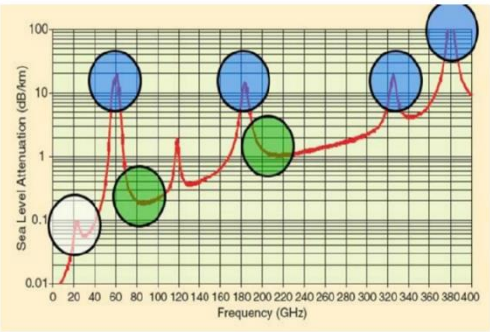

Fig. 2.4. - Atmospheric absorption across mmWave frequencies in dB/km [7].

Regarding FR2 band, a set of bands have been proposed for their availability and better performance with the communications channel. Fig. 2.4 shows how the band at 28 GHz are in a valley of the attenuation curve by atmospheric gases, what turns out to be very interesting for use as a 5G band.

The bandwidth around these frequencies varies from region to region. Each country proposes different frequency bands as shows in [8] [9], although the ITU and 3GPP organizations try to find a consensus between the different countries in order to standardize the technology globally.

2.3.- Instrumentation of components in 5G.

The new features of 5G present important challenges in the measurement and testing of RF components which will conform the entire mobile infrastructure. The challenges that arise in the measurement of the electromagnetic behavior of devices should be noted.

The massive MIMO technology requires adaptive antenna systems (AAS). Its main function will be conformed multiple radiation beams from the base station dedicated to each of the mobile devices. This achieves an efficient spectrum use and minimize the path loss.

The AAS is based on nxm phased array antennas which allow to generate different directive beams, controlled by their network feed. In previous mobile generation, the use

of frequencies below 6 GHz prevents arrays with many elements (in 4G 2x2 or 4x4 phase array antennas are used) given the physical limitations that exist in mobile devices. However, the irruption of millimeter frequencies, allows the use of arrays of tens or hundreds of elements in an array concentrated on very small surfaces, which significantly improves the performance of these adaptive systems.

Fig. 2.5. - Over-The-Air (OTA) drone measurement [10].

To verify the operation of these antennas, it is necessary to carry out measurements at a global level and once integrated with the whole system (mobile device), following a "black box" methodology [11]. Due to the high integration that exists in these devices, it makes it difficult or even impossible to measure these antennas using connectors.

In this context, the use of Over-The-Air (OTA) systems is proposed. It consists of configurations of measurements in which there are no power connectors available on the device under test (DUT) as it can see in Fig. 2.5. In them, it is the receiving antenna that is responsible for measuring the radiation pattern of the device in all directions. OTA methods also allow to measure the main tests in devices at *mmWaves*:

- **RF performance.** Minimum level of signal quality.
- **Demodulation/Data throughput performance.**
- **Radio Resource Management.** How the device access to the network, handover…
- **Signaling.** Upper layer signaling procedures.
- **Manufacturing test.** Calibration and validation of performance.

2.3.1.- Over-The-Air (OTA) Test Methods

The main target of an OTA test is the radiation pattern measurement of the DUT, at a sufficient distance to suppose the reception of a plane wave (*far field*). To achieve this there are several calculation methods that mark the physical implementation of these systems. According to [14], 3GPP defines the following methods of obtaining the *far field*:

2.3.1.1.- Direct Far Field Calculation.

The traditional method for calculating a radiation pattern is to distance the antennas, receiver and DUT, enough to assume that the incident waves in reception are considered plane waves.

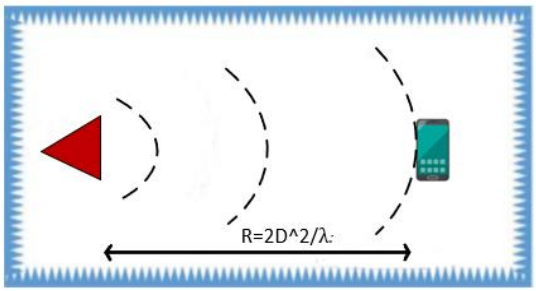

Fig. 2.6. - OTA test system using Direct Far Field Method.

The region of space where this is accomplished is called *Fraunhofer* zone. The distance from the antenna is calculated according to Fig. 2.6 where D is the maximum aperture of the antenna.

Considering the frequencies in FR2, the use of this method limits the maximum size of the antennas (according to 3GPP, less than 5 cm) so that this minimum distance is not triggered, difficult the measurement system.

2.3.1.2.- Near Field Method.

To avoid limitations on antenna size, there are methods of measuring in the near field. Within the near field, depending on the components that predominate over the field can be divided into near field reactive and radiated as shown in Fig. 2.7. Near Field methods work on the near field radiated in order not to modify the electromagnetic behavior of the antenna.

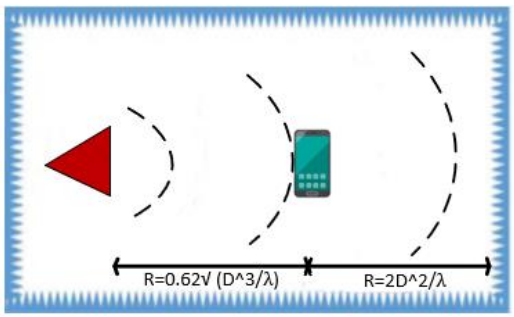

Fig. 2.7. - OTA test system using Near Field Method.

For obtaining the far field with these methods it is necessary to use transformations which require a higher computational cost. The measuring antennas used also have reduced bandwidths. According to [12], near field calculation, which are under development that do not require the use of transformations, are currently discussed as a viable option in RF tests according to the 3GPP standard.

2.3.1.3.- Indirect Far Field Calculation.

As a third group of methods, the indirect far field methods, which are an intermediate solution to the previous two. The objective of these methods is to generate a planar wave front on the near radiated field of an antenna. To do this, it is obtained an area of space near the antenna where the amplitude and phase of the waves is constant. With this, it is possible to measure antennas of greater aperture to an acceptable distance.

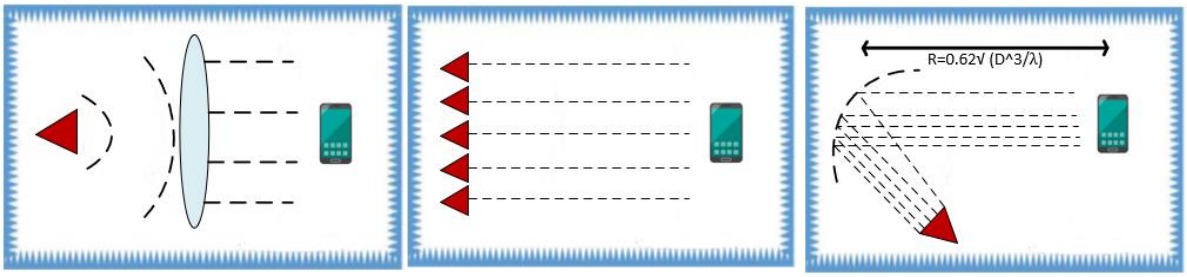

(a) (b) (c)

Fig. 2.8. - Different configurations using indirect Far Field Calculation: (a) Configuration with lens; (b) Configuration with array to plane wave synthesis; (c) CATR configuration.

To generate this type of waves, there are different configurations of antennas, such as the use of lens or synthesis of planar waves using antenna arrays. Each of them has their advantages and disadvantages. In addition to these two configurations, in this group are the compact test range systems (CATR) on which this project focuses and are detailed in the next chapter.

3.- CATR SYSTEMS AND REFLECTARRAYS.

3.1.- Introduction.

CATR systems are structures whose target is to generate a certain area of space close to the antenna, also called quiet zone, where it has a behavior like that existing in the far field. This behavior is interesting if it is desired to build HF measurement systems in compact spaces and therefore in the 5G measurements.

In the following chapter, we will define the concept of CATR systems, describing the main limitations of these systems. In addition to that explained in the previous chapter, the use of these systems for measurement of 5G devices is discussed, mentioning some examples of products currently on the market.

Once the concept of measurement systems has been explained, it will be described the type of antenna structure proposed in the project: reflectarray antennas. These consist of a flat reflector formed by a certain number of radiant elements on which a front of waves coming from an antenna that acts as a feeder falls. The joint action of these elements allows to conform different electromagnetic patterns on the broadside direction of the antenna.

The second part of this chapter describes the operation principle of these structures, their origin, state of art and their main advantages and disadvantages compared to antennas of similar behavior: array type antennas and parabolic reflectors. The comparison with the latter, the main structures used in CATR systems, justifies the interest in using reflectarray antennas in these measurement systems.

3.2.- CATR systems.

The compact antenna test range systems or CATR, are systems that make a certain region in space near the antenna in which the electromagnetic field propagates as a plane wave, thus simulate the antenna behavior in far field. This region is often called as a quiet zone.

The use of these systems was quiet reduced in its early years (the first CATR definition dates from 1969 by the hand of Johnson [15]) although with the accessibility to higher frequency bands, these systems were positioned as a candidate for radar applications, such as the measurement of RCS (Radar Cross Section) in anechoic chambers. The use of CATR systems expanded from the 80’s and, as mentioned above,

is currently proposed as measurement systems for frequencies in millimeter bands in the future 5G.

A traditional CATR system uses one or several parabolic reflectors taking advantage of the geometrical characteristics of these structures: they transform the spherical waves coming from a radiation source (feed) into waves whose electromagnetic fields are parallel to each other, thus generating a front of plane waves, as shown in the Fig. 2.8 (c). In order to reduce the blockage generated by the feed, CATR systems are always placed on offset structures. In Fig. 3.1, it shows some examples of these systems.

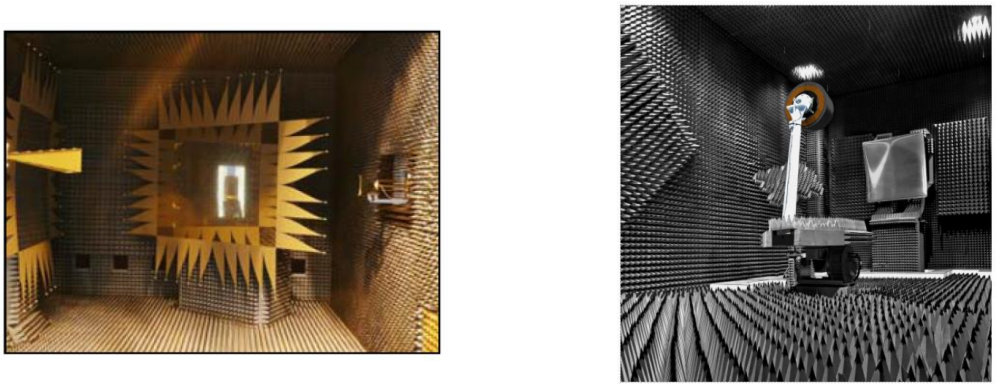

(a) (b)

Fig. 3.1. - CATR examples: (a) Dual reflector system, manufactured by March Microware Systems [16]; (b) CATR manufactured by MVG [17].

3.2.1.- Limitations of CATR systems.

Although from the theoretical point of view the CATR systems allow to generate a plane wave front, that is, a front with a constant phase and amplitude, this is not possible to obtain in practice due to several factors such as those shown below. In Fig. 3.2 the detailed effects are shown in a schematic way.

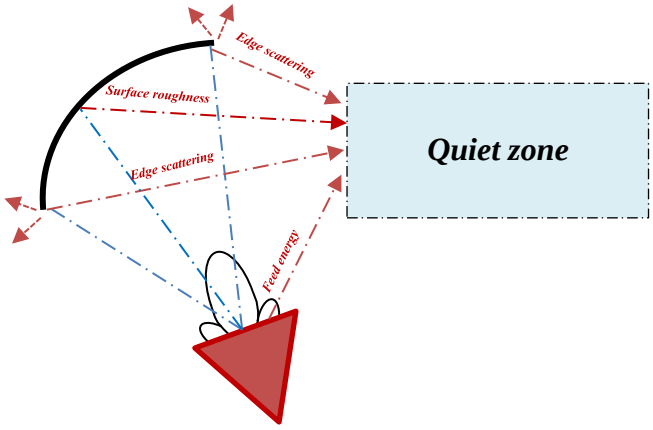

Fig. 3.2. - Contributions that distort the quiet zone.

- **Aperture size:** the finite size of the reflector delimits the maximum dimensions of the quiet zone and the proportion of its surface that generates the planar waves. The offset structure makes the equivalent aperture smaller than the size of the reflector, which makes the inclination angle of the reflector a critical factor. According to [1], it is typically estimated that a quiet zone diameter is less than 33% of the effective aperture.
- **Amplitude taper:** the difference in the amplitude of the field over the reflector or taper comes from two main causes: the difference in paths between the feed and the different points of the reflector; and the radiation pattern of the feed itself. It is important that this taper is as small as possible, in order to have a constant field on the surface. However, due to the beam pattern of the feeders, the distortion at the edges of the spillover increases. To compensate for these effects, it is usual to vary the pointing angle of the feeder slightly above the midpoint of the reflector, thus using the difference of paths to compensate for the incident field in the reflector. Another solution is the use of sub-reflectors that transform the field of the feeder in one with more uniform amplitude.
- **Edge Scattering:** another factor to consider is the effect of the edges of the reflector. Incident waves at the borders of the reflector diffract and can contaminate the quiet zone. This is an effect that limits the lower operating frequency. There are mainly two methods to minimize this phenomena: reduce the field at the edges, which is limited by the previous effect; and use surfaces at the borders that allow to minimize or cancel this dispersion, such as using curved or serrated edge [18].
- **Surface Roughness:** In practice, a parabolic reflector presents roughness on its surface due to the way to implement these structures (from tiny flat surfaces). These irregularities cause undesired reflections on the reflector, which can affect the quiet zone. This effect becomes important as the frequency increases. As an example, according to [18], the maximum roughness at 5G frequencies must be in the order of microns.
- **Unwanted feed energy:** the diagrams of the feeders in these systems are directive, although part of the radiated energy can be directed toward the quiet zone, being able to distort it. In order to solve it, it is interesting to obtain a good design structure, using blockers above the feeder which absorbs this spurious energy.
- **Far field of reflector:** the far field management behavior of the reflector causes the quiet zone to narrow as it moves away from the reflector.

Normally this problem does not affect CATR systems as the size of the reflectors used means that the far field is far from the area to be measured.

- **Antenna environment:** the possible reflections that exist in the environment can directly affect the behavior in the quiet zone. For this reason, these systems are normally found in environments surrounded by absorbent material as an anechoic chamber. It is especially critical the area immediately after the quiet zone.

3.2.2.- CATR systems and 5G measurement.

As a mentioned above, CATR systems are an attractive solution to the challenges of 5G measurements. Currently, several companies are under development of scale anechoic chambers incorporating these systems. Some examples of these products are shown below (Fig. 3.3):

- **MVG© Mini Compact Range.** Anechoic chamber capable of making measurements in the *mmWave* range (4 – 110 GHz) with quiet zone diameter of 50 cm. Its main applications are the aerospace industry, telecommunications and automotive.

- **R&S®ATS1000 Antenna Test System.** Anechoic chamber with a measuring ranges from 4 to 87 GHz that allows the measurement of the fundamental parameters of the antennas in the DUT (EIRP, TRP…). The CATR system generates quiet zones of 20 cm. From the use of a bubble on the device, it is possible to perform characterization in extreme temperature environments.

(a) (b)

Fig. 3.3. - 5G Measurements products with CATR systems: (a) MVG© Mini Compact Range [21]; (b) R&S®ATS1000 Antenna Test System [22].

3.3.- Reflectarray systems.

3.3.1.- Reflectarray definition.

A reflectarray antenna is a structure formed by a surface that combines the characteristics of a flat reflector with a radiating elements organized in an array distribution. This antenna has two main parts: a feed with a directive diagram pattern and a flat surface formed by a ground plane and one or several substrate layers.

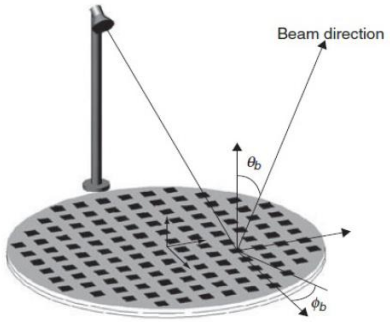

Fig. 3.4. - Generic structure of reflectarray [20].

The main target of these antennas is to modify the incident field on the reflector in order to achieve a certain reflected field. To control them, on the reflector, there is a mask of radiant elements whose size and shape directly affect the reflected electromagnetic wave.

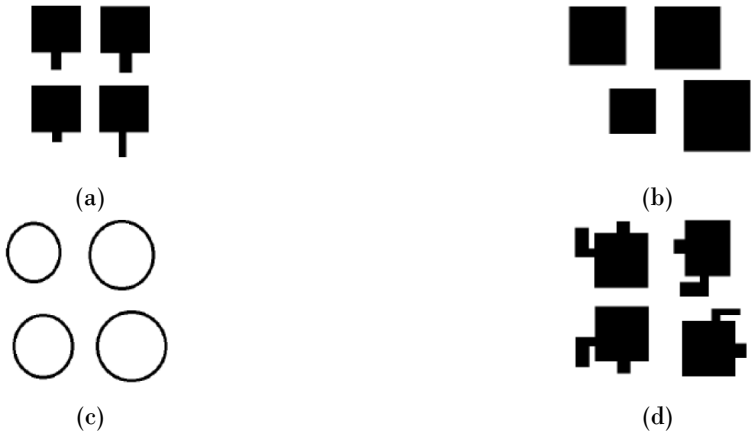

Fig. 3.5. - Different radiated elements in reflectarrays: (a) Patch with Transmission Lines; (b) Patches; (c) Rings; (d) Cross dipoles [23].

Fig. 3.5 shows some of the most used elements, since simple structures such as square patches to more complex structures like crossed dipoles, both their selection and

their distribution along the reflector depends on the requirements to be met by the antenna, although typically these elements are distributed in a rectangular or circular way.

3.3.2.- Origin and technological development.

The first theoretical definition dates from 1963 [24], where the creation of surfaces with a synthesizable impedance was proposed, which could conform different interference patterns. This theory was demonstrated experimentally from the prototype structure shown in Fig. 3.6: a reflectarray formed from waveguides of different sizes, finished in short-circuit. This design allowed to generate a diagram of directive radiation.

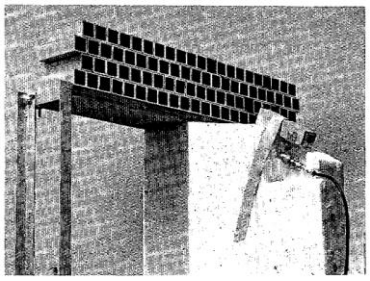

Fig. 3.6. - Waveguide array reflectarray with staggered rows [24].

A priori, it is deduced that these reflector structures are highly heavy and bulky, which is why the development of reflectarray antennas did not undergo a major advance until the arrival of printed circuits or *microstrip* technology (decade of the 80's and early 90's). This allowed the use of radiant elements easily implementable, increasing the interest in this type of antennas.

From this moment, reflectarray designs suitable for numerous applications began to be implemented, as in satellite communications as for example exposed in [25] and [26]. Although as a rule, their use is in beamforming far field diagrams. Reflectarray antennas can also be useful in applications in near field, such as RFID technology [27] or CATR systems, which will be discussed in 3.3.4.

Regarding 5G applications, designs have been proposed at millimetric frequencies as in [28] and [29]. In [30], the design of a reflectarray antenna is proposed for use in the backhaul network in 5G cellular architecture.

There are two important types of reflectarray antennas, based on their ability to modify after manufacturing or not the beam they form. These two types of antennas have undergone a parallel technological development in recent years.

3.3.2.1.- Fixed beam reflectarrays.

Fixed beam reflectarrays have the unique objective of providing a beam, shaped or not, in a direction of space permanently. They have the advantage of being easily implementable antennas because they are completely formed by passive elements.

Assuming the use of a reflectarray formed by simple elements, such as those mentioned in Fig. 3.5, there appear several effects that harm the desired behavior of the antenna, although these can be reduced or even eliminated. This is the case of cross-polar component, for example. In [31] it is proposed a technique that allows to reduce it, decreasing the phase shift in the reflection coefficients for different TE and TM modes. The cross-polar reduction can also be done using optimization methods as [32]-[33].

As mentioned above, one of the desired characteristics of radiant elements is that they can provide enough phase shift, at least 360°, over the incident wave. This fact is not always met as will be seen in chapter 5, which impairs the performance of the antenna. In this sense it is proposed to use several layers of substrate/patch that allows a greater range of phases. Multi-layer designs also permit to perform other features of antennas, such as [34] where each reflector layer is used to provide operability in two frequency bands: Ka and X. However, the use of more than two layers does not significantly improve the design because the substrate losses increase.

Another characteristic of the antennas is the type of polarization to be used. Reflectarray antennas can work in linear or circular polarization, thus adjusting to the requirements of each application. For the most part, antenna designs usually work with linear polarization, since it is very common to use feeds with this type of polarization. However, there are also designs in circular polarization as in [35] where a reflectarray is proposed on which is placed a dielectric layer. This can work in double band at 36 and 19 GHz.

It is possible to create reflectors that allow the conversion between polarizations using more complex elements. In [36] we proposed a reflectarray design formed by double Omega-Shaped resonant elements, which allows the conversion linear to circular polarization. Besides, there are designs that allow working in double polarization as shown in [37].

Generally, reflectarrays are electrically large structure. The maximum size of each element will be less than the wavelength, which means that these antennas are formed by hundreds or thousands of elements. This supposes that the optimization of the elements according to some imposed characteristics is computationally unfeasible in full-wave analysis. Several numerical methods have been proposed, capable of dividing the problem into several parts, reducing as much as possible the computational cost it generates. In

this sense, in [38] several heuristic methods are proposed, such as PSO (*Particle swarm optimization*), GA (*Genetic Algorithms*), SA (*Simulated Annealing*) …

Given the passive nature of the antenna and the requirements normally imposed on it for forming, it is interesting to analyze the use of phase-only synthesis techniques (POS) whose function is to obtain the distribution of phases that the reflector must have to meet the requirements imposed. For the implementation of these techniques are used algorithms such as IA (*Intersection Approach*) and *Levenberg Marquartz* as explained in [39].

Fixed beam reflectarrays can also be used in applications where more than one beam or an electrical scan is needed over a certain area of space. Some studies, bet on the use of several feeds that affect the same reflector, to generate different fixed beams. This is the case of [40], where multiple contiguous beams separated by 0.5° are obtained using 5 feeds. Independently, it is also possible to obtain multibeam diagrams from a single feed as can be seen in [41], where the design of a Ku-band transmit array that generates 4 different beams is proposed.

Finally, reflectarrays can also be arranged on multireflector structures to improve the antenna characteristics, like parabolic reflectors. In [42], it is described the use of reflectarrays as a sub-reflector that dates to the antenna with a wider bandwidth than a simple reflectarray structure and the possibility of beamforming that is not available in multi-reflector parabolic systems.

3.3.2.2.- Reconfigurable beam reflectarrays.

Reconfigurable beam reflectarrays can modify the behavior of their radiation diagram, modifying the direction of the main beam, as can be achieved with array type antennas. In some cases, they could amplify the wave coming to the feeder.

According to reflectarray theory, it is necessary to equip the antenna in some way to modify the phase provided by the radiant elements. This can be achieved by altering the resonant elements, changing the length of the delay lines, using phase shifters or rotating the array elements [43]. Independently, it will be necessary the use of active components that allow to control with tension these changes in the antenna. That said, it is possible to differentiate two subgroups within reconfigurable reflectarrays: those that have a discrete or continuous phase variation.

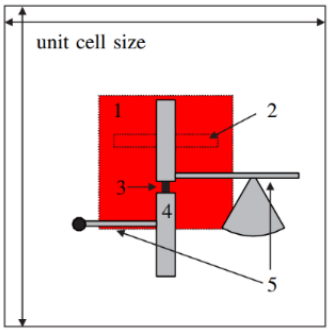

Fig. 3.7. - Final structure for unit cell using PIN diode: 1) patch, 2) slot, 3) diode, 4) open-ended stub and 5) biasing lines+ RF chokes [44].

The reflectarrays with discrete phase variation, have a set of predefined phase shifts on each radiated element, allowing to modify the direction to which the main beam is pointing. As a rule, it is used PIN diodes or MEMS that enable or disable some areas of the radiated element to modify their offset. As an example, [44] shows the design of reflectarray based on couple elements as shown in Fig. 3.7. The PIN diode, point 3, allows to add a delay line on the patch feeding network, obtaining a phase difference on the reflected wave between 48 and 96°.

Nowadays, there is a predominance in the use of *microelectromechanical systems* (MEMS) over PIN diodes. This is due to the better performance of these devices (lower losses and consumption) and their greater ease of manufacture on the reflectors. As an example, [45] shows the design of a reflectarray using simple radiant elements with a 1-bit phase resolution with MEMS switch for imaging applications.

These active devices can also be used to create reflectarray antennas that can work with various polarization modes instead of modifying the polarization phase. In [46] for example, two PIN diodes are used to feed the patches of a reflector and thus generate different modes of propagation in the reradiated wave.

The other group of reconfigurable reflectarrays are those than span a continuous range of phase shift. In this case, a voltage is used that governs or modifies the characteristics of the active element linearly, which allows to change the phase in a continuous way.

In reflectarrays with continuous variation, varacaptor diodes or LC liquid crystals are used. In the case of the first ones, they are usually placed on the radiant element in a similar way to the PIN or MEMS diodes, although a certain polarization voltage is applied to them. As an example, in [47] an integrated board is used in the reflectarrays that controls the polarization of the varacaptor to carry out beam-scanning.

Another option is the use of LC liquid crystal layers, which it is possible to change their electromagnetic properties by applying a certain tension to them. In [48] it is demonstrated how the anisotropic properties of the LC allow to control the phase shift of the unit cell, changing the permittivity of the substrate.

Newer technologies of reconfigurable beam, raise the use of other materials on the cells as ferroelectric materials [49], fluid networks [50], metamaterials [51] or graphene [52]. Although they present interesting characteristics, reconfigurable reflectarrays have a much smaller study in comparison with fixed beam reflectors. However, there is currently and important development of them.

3.3.3.- Advantages and Disadvantages.

Reflectarray antennas focus their main use on the shaping of directive radiation diagrams, or brush type. Traditionally these directive diagrams were obtained using parabolic reflectors or arrays. This type of proposed antennas has certain advantages over traditional structures, which are mentioned above.

Simple reflectarray (fixed beam) have a passive nature, i.e. they do not need any auxiliary feeding way to be distributed along the reflector. This presents a clear advantage over array antennas since there would be fewer losses, especially resistive. In a reflectarray, the Ohmic losses reside in the properties of the dielectric and the shape that these elements have.

The geometry of the parabolic reflectors causes that their implementation is complex, and their limitations come fundamentally from the roughness in the curved surface and the shape in the edges, being critical to high frequencies [18]. The flat nature of reflectarray antennas allows its implementation to be simple and can be performed in highly development manufacturing processes such as the implementation of PCBs or microstrip technology. The reflectarray antennas allow to obtain a high efficiency of opening, like the behavior of the parabolic reflector.

As other advantages with parabolic reflectors, stands out the capacity of shaping and generation of several beams, or the best integration in the structure of the general system. Large parabolic reflectors can be very heavy and require much more complex fixing structures than those needed for a reflectarray.

The main disadvantage of reflectarray is its narrow bandwidth. It is estimated that the operating bandwidth of a reflectarray antenna is 10% of its design frequency. This limitation resides in mainly two factors:

- **Bandwidth of the radiant element.** The elements used in general in reflectarrays antennas, have a reduced bandwidth derived from the sensitivity of these to deviations from the center frequency. As a solution,

more robust radiant elements shapes are used as [53] – [54], or the use of several layers of substrate. These techniques, however, increase the complexity of the element.

- **Differential spatial phase delay.** Due to the difference in paths that a beam reflected in the antenna must travel because the flat structure, an unwanted frequency-dependent phase shift is produced, which limits the bandwidth in electrically large reflectarrays specially. In this sense, there are also techniques that allow to reduce this effect [55] – [57].

3.3.4.- Reflectarray antennas in CATR systems.

Currently, parabolic reflectors used in CATR systems have a high implementation cost and increase exponentially with the size of the reflector itself. The low scalability of the reflectors makes it an arduous and inexpensive task to generate quiet zones similar in size to those of future 5G devices.

Given the advantage of reflectarray antennas over parabolic reflectors, it is interesting to consider the possibly of using these antennas as a substitute for parabolic reflectors in CATR systems.

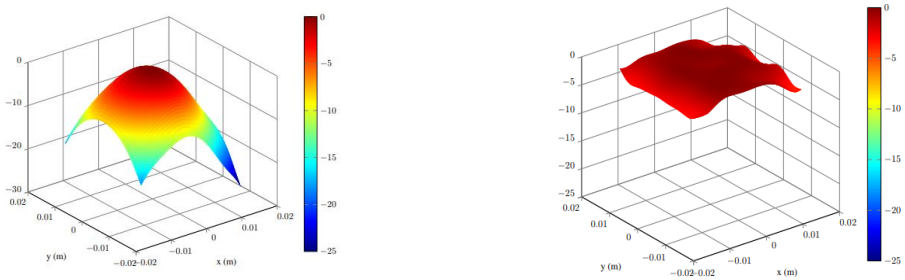

(a) (b)

Fig. 3.8. - Design of reflectarray optimizing its behavior in near field. Flat to 78 mm of the reflector before (a) and after (b) the synthesis of the size of patches [58].

There are currently studies where this topic has been evaluated as in [1], where a parametric study of the quiet zone generated by reflectarray is carried out. Some designs techniques have even been proposed to optimize the near field generated by the reflectarrays [58] as shown in Fig. 3.8, being able to obtain quiet zones of greater sizes, with relations between the size of the reflector and the quiet zone greater than those obtained with the use of parabolic reflectors.

4.- REQUIREMENTS AND DESIGN METHODOLOGY.

4.1.- Introduction.

After contextualizing the project described in this document, the next step will be to detail the electromagnetic targets to be met by the antenna, as well as know what parameters and variables should be considered in the design of the type of antenna chosen: reflectarray antennas.

First, it will be detailed which are going to be the requirements that the electric field generated by the antenna must fulfill, describing qualitatively that it will be considered as a quiet zone as well as the volume that it must have. In this point some basic parameters are also fixed such as the design frequency.

Next, a design methodology is proposed that allows to adjust all the parameters on which the antenna depends so that it generates an electric field adapted to the requirements of the problem. This methodology will be composed by several blocks or stages where it begins by studying individually the elements participating in the structure and then performing an optimization of the antenna as a whole. Finally, other important characteristics of the antenna are studied, such as its in-band behavior.

4.2.- Requirements of the antenna.

Reflectarray designs will be made following a CATR structure at two different frequencies: 1.7 GHz and 28 GHz. Each one of them belongs to sub-bands inside FR1 and FR2 groups.

As previously explained, the aim of CATR systems is to obtain a certain volume of space near the antenna that has a behavior like that which would be had in far field (quiet zone), this means that, theoretically, that the electric field is constant both in amplitude and phase.

Since a flat behavior is not possible in practice, certain conditions are imposed on this electric field. In this project a maximum ripple over the amplitude of the field of 1.5 dB and in phase of 22° will be considered. As a note it is interesting to comment that these impositions are softened in the manufacture and measurement stage.

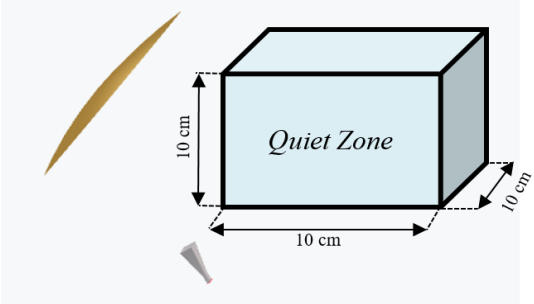

Fig. 4.1. - Requirements of the quiet zone in 28 GHz band.

In relation to the characteristics of the quiet zone, sizes and dimensions are taken as a reference that are expected to have some 5G devices. Zones that are currently achieved using parabolic reflectors. Quiet zone characteristics will depend on the band being worked on. For the 28 GHz band, the aim is to obtain a quiet zone of 10x10x10 cm^3 (see Fig. 4.1). This volume must be enclosed within no more than 50 cm from the reflector.

In the case of the 1.7 GHz band, it is desired to study the ability to best scalability of reflectarrays in search of large quiet zones. Therefore, it is a requirement to look for a 50 cm quiet zone in all axes. Given the limitations of the anechoic chamber in which these systems are to be placed, a maximum distance of 3 m is fixed to the reflector.

Respect to the implementation of the reflector, it is considered materials commonly used in the manufacture of printed circuit boards (PCB) since a standardized process in the manufacture with this material is available. In chapter 5 will detail the materials to be used with their electromagnetic characteristics.

Finally, to make these designs has been imposed as a requirement the use of generic programs available to the company.

4.3.- Methodology.

Based on the requirements imposed, a methodology is defined for the design of reflectarrays based on the use of two commercial programs, such as CST Studio Microware ® and Matlab ®.

In general terms, Matlab codes will be implemented for analytical calculations and processing and representation of measurements, while CST software will be used to obtain the electromagnetic characteristics of the antenna or individually, of the elements that compose it.

The proposed methodology is formed by the 6 blocks exposed in the flowchart of Fig. 4.2 . These blocks are grouped in the following 3 stages:

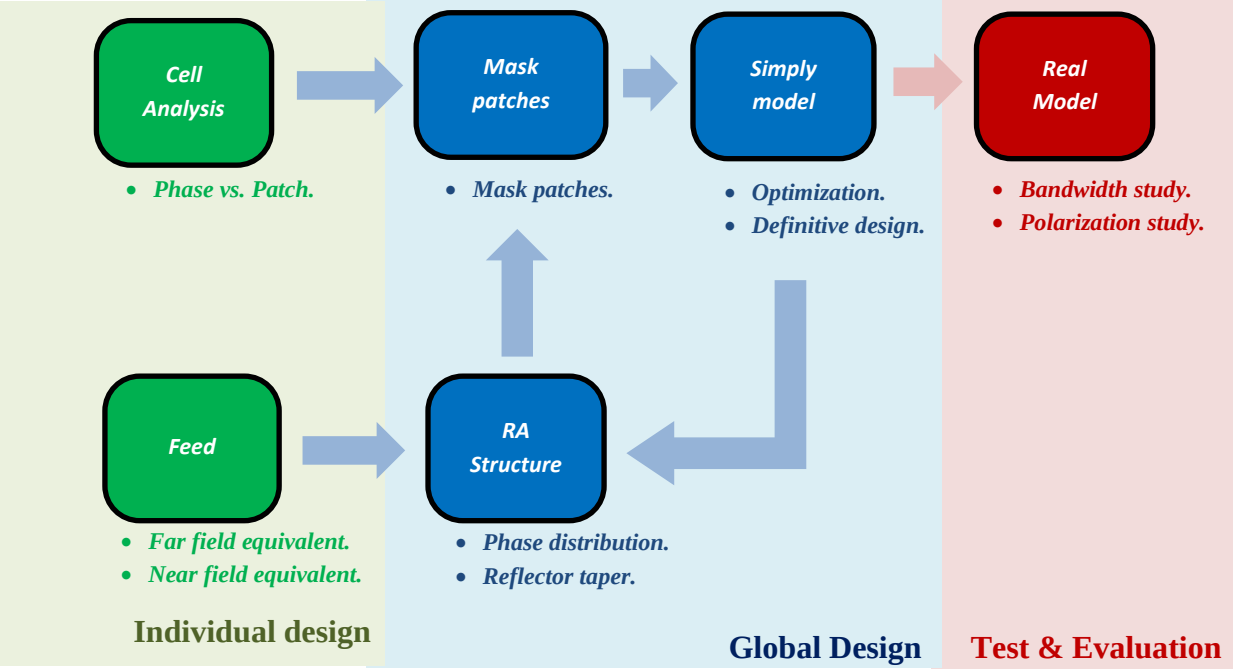

Fig. 4.2. - Methodology to follow for the design of reflectarrays applied to CATR systems.

- **Individual design.** First, the elements that made the structure are studied in an independent way: on the one hand, the isolated behavior of the radiant elements that compose their reflector will be studied and on the other hand, the feeder will be characterized.

- **Global Design.** Next, it will be calculated what phases each patch of the reflector must provide to form the desired electric field of the antenna, defining a starting reflectarray structure.

  One the target phases and the electromagnetic behavior of the unit cell are known; the physical characteristics of each radiant element are calculated (*mask patches*). With this information it is possible to build a CST model of the reflector and analyze its near field.

  In this part of the methodology, an iterative process will be followed where different patch masks and reflectarray structures will be tested. As well as, the parameters that constitute them are altered to improve the performance of the antenna.

- **Test & Evaluation.** Once an optimal reflectarray structure has been designed, a more realistic model of the structure will be constructed, which will be also used to study the behavior of the antenna in frequency.

In the following sections it will be detailed the development and theoretical basis of each of the blocks.

4.3.1.- Cell Analysis.

As mentioned above, the first block in the design of reflectarrays is the study of the electromagnetic behavior of the radiant elements. The aim of this study is to analyze individually the characteristics of the wave reflected in the radiant element based on its physical characteristics.

Of all the existing forms of radiant elements, some of them seen in chapter 3, in this project radiant elements will be used in the form of passive patches (see Fig. 4.3) of a_n x b_n dimensions arranged on one or several layers of substrate of heights h_n and separated from the adjacent patches a distance a and b in each dimension. To simplify the structure, it is assumed that the patches will be square ($a = b$, $a_1 = b_1$, $a_2 = b_2$,…,$a_n = b_n$,….).

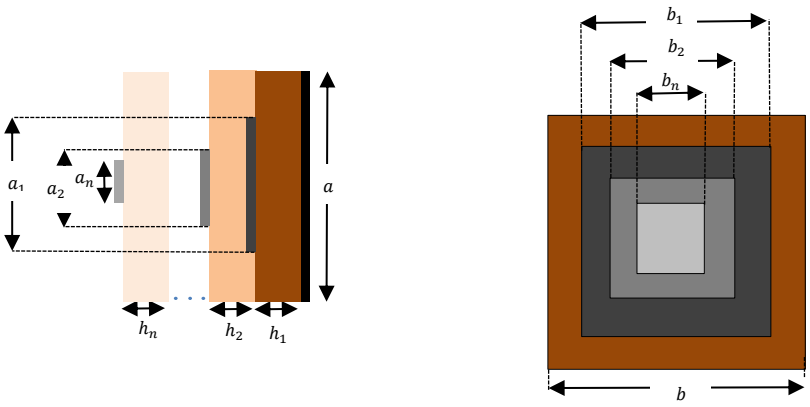

Fig. 4.3. - Generic structure of a reflectarray patch cell. Front face and profile. In grey scale the patches, in color the layers of substrate.

The wave reflected on these elements will be the incident wave with a certain phase shift, depending on the size of the patch (parameters a_n, b_n). This relationship also depends on other design factors such as frequency, distance between patches (periodicity), substrate, etc.

Considering the characteristics of the cells, the first step is to determine the fixed parameters, such as the type of substrate, the height of it and the periodicity of the patches. The aim will be to obtain a proportional (linear) relationship between the size of the patch and the phase introduced. It will also be sought that this linear relationship can provide

the widest possible phase range, trying that the slope is not too high, which would imply that small errors in the size involve substantial differences in phase.

During this design stage, it will be assumed that the wave always reaches the cell perpendicularly. However, it should be note that, according to the structure of the antenna, the wave normally falls obliquely upon the cell. This angle of incidence is represented from the angles that generate their projections on the reference planes according to Fig. 4.4. The range of variation in θ is between 0 and 90° assuming infinite reflectarrays. On the other hand, the range in φ comprises the 360° although for symmetries it is enough to analyses values between 0 and 90°.

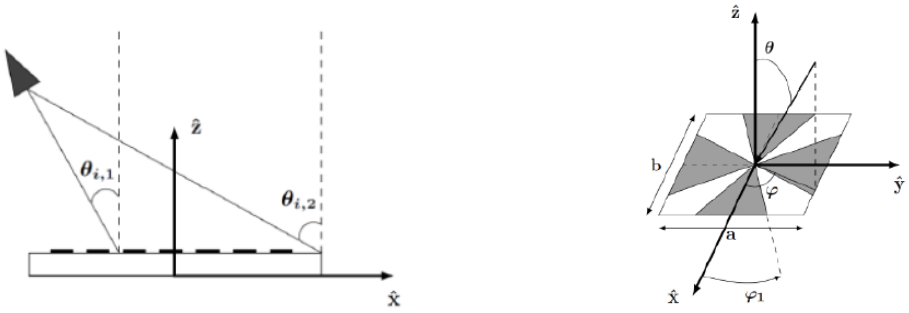

(a) (b)

Fig. 4.4. - Variation of angles of the incidence wave: (a) θ; (b) φ [23].

Based on other cell analysis studies carried out in other reflectarray designs as [1] or [23] it is observed how the angle of incidence on the patch is an important factor that can significantly alter the phase shift, especially in physically large reflectors where these angles will be high. This phenomenon will therefore be considered when designing and creating the mask with the different sizes of patch.

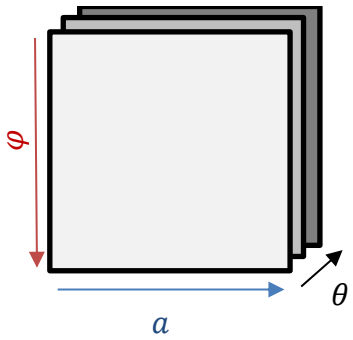

Fig. 4.5. - Design matrix where the cell information is stored.

In this sense, an element called design matrix is created: a 3D matrix where the phase-size curves are stored for different angles of incidence θ and φ. The information of this matrix is ordered according to Fig. 4.5. Design matrix allows a detailed characterization of the independent behavior of each radiant element used.

In each of the mentioned studies, the relationship between phase and patch size will be calculated. To achieve this, a set of tools will be implemented on the above-mentioned programs.

First, a CST model is created where the shape of a single cell is built. This cell is surrounded by a periodical environment of identical cells, separated by a distance called periodicity. An example is shown in Fig. 4.6. The cell under study is assumed to be fed by a plane wave that falls upon with a certain angle defined by θ and φ components.

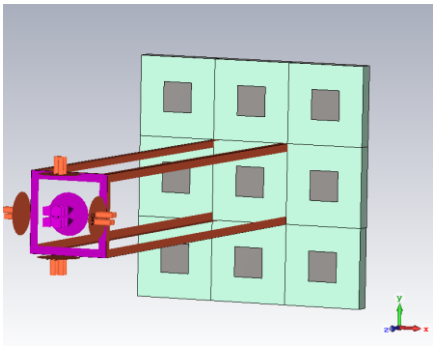

Fig. 4.6. - CST cell analysis model example.

In order to know the phase shift introduced by the patch on the incident wave, it will be necessary then to know its reflection coefficient or parameter S_{11}, which is calculated using *Floquet* modes: solutions of differential equations that define problems on periodical structures [59]. The aim is to calculate the S_{11} parameter on the cell surface, so it will be necessary to define this surface as reference in the model.

After the simulation, CST will provide the phase and amplitude components of this S_{11} over a certain frequency range. Therefore, to obtain the phase-size curve, a parameter sweep of the variable is performed obtaining curves for each cell size. Next, Matlab processes these data, extracting the phase in each curve for the desired frequency. This calculates the target phase-size patch curve. This Matlab processing also includes possible smoothing of the phase curve against atypical data extracted from CST.

4.3.2.- Feed.

The next element to study in the reflectarray structure will be the one in charge of generating the incident wave on the reflector: the feed.

Traditionally, the feeders of the reflector structures are antennas that have a radiation pattern in the shape of brush. This allows to focus most of the energy to be on the reflecting surface and thus reduce the interference caused by the scattering at the edges.

In this step, the feed will be designed based on these premises, creating a CST model of the antenna and extracting its most important characteristics (directivity, gain, radiation pattern, ...). The information extracted from CST will also be processed through Matlab scripts.

With the information extracted from CST, simplified antenna models will be obtained to be used in successive stages.

4.3.3.- Reflectarray structure.

Once the electromagnetic behavior and the characteristics of the antenna elements are known in an independent way, the disposition of these elements in the reflectarray structure will be defined, as well as to obtain that distribution of target phases that will allow the antenna to fulfill the imposed requirements.

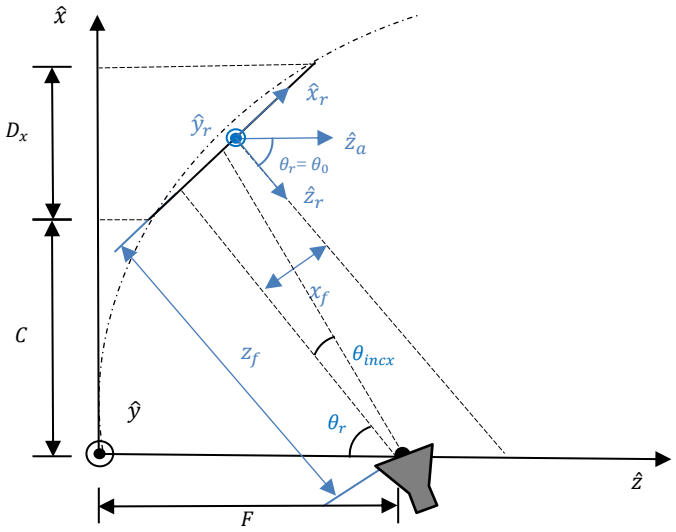

Fig. 4.7. - Coordinates system of RA structure. In black equivalent parabolic reflector. In blue RA coordinate system.

A reflectarray antenna can be geometrically defined following an equivalent parabolic model as shown in Fig. 4.7 placing the reflector on a chordal plane to the parabolic surface. This geometrical structure is fully defined by 3 parameters: the focal distance F, the size of the equivalent aperture D and the clearance C. The θ_{incx} angle is also defined as the inclination of the feed with respect to the normal of reflector. The tilt angle of the feed respect z axe will then the sum of θ_{incx} and θ_r being this the angle of

rotation of the structure so that the main beam points in a direction parallel to the z axis. This θ_r angle coincides theoretically with the radiation angle considered in the design (θ_0), although it will be seen that in simulation there will be discrepancies in this respect.

The reflectarray antenna then follows an offset structure, in this case on the x axis, thus defining two characteristics planes: the xz plane or asymmetrical and the yz plane or symmetrical.

Independently another interesting reference system to use is the one that considers the reflectarray center as the center of the coordinate system ($\hat{x}_r, \hat{y}_r, \hat{z}_r$). Over this system is defined the position of the focus (x_f, y_f, z_f) and the angle that conforms the Z axis to the direction of maximum radiation ($\hat{z}_a$). This system also defines the number of radiant elements that the reflector will have on its axes N_x,N_y respectively and the total number N_t.

Variable	Description	Formula
$\boldsymbol{d_{feedx}}$	*Distance between the feed and the reflector in asymmetric cut.*	$d_{feedx} = \sqrt{{z_f}^2 + {x_f}^2}$
$\boldsymbol{d_{feedy}}$	*Distance between the feed and the reflector in symmetric cut.*	$d_{feedy} = \sqrt{{z_f}^2 + {y_f}^2}$
$\boldsymbol{D_{px}}$	*Diameter of the reflector in Asymmetric cut (only metallization).*	$D_{px} = N_x P_x$
$\boldsymbol{D_{py}}$	*Diameter of the reflector in Symmetric cut (only metallization).*	$D_{py} = N_y P_y$
$\boldsymbol{x_c}$	*X coordinate on the reflector where the feed is pointing.*	$x_c = x_f + z_f tg(\theta_{incx})$
$\boldsymbol{y_c}$	*Y coordinate on the reflector where the feed is pointing.*	$y_c = y_f + z_f tg(\theta_{incx})$
$\boldsymbol{\theta_{in0x}}$	*Tilt of the feed so that it points to the RA center respect X axe*	$\theta_{in0x} = \text{acos}\left(\frac{z_f}{d_{feedx}}\right)$
$\boldsymbol{\theta_{in0y}}$	*Tilt of the feed so that it points to the RA center respect Y axe.*	$\theta_{in0x} = \text{acos}\left(\frac{z_f}{d_{feedy}}\right)$
$\boldsymbol{F}$	*Focal distance*	$F = \frac{z_f[sen^2(\theta_r) + 1]}{cos(\theta_r)}$
$\boldsymbol{c_1}$	*Coefficient for clearance calculus*	$c_1 = \sqrt{\left(x_f + \frac{D_{tx}}{2}\right)^2 + {z_f}^2}$
$\boldsymbol{c_2}$	*Coefficient for clearance calculus*	$c_2 = \frac{D_{tx}}{2}\sin(\theta_r) + \sqrt{{d_{feedx}}^2 - H^2}$
$\boldsymbol{C}$	*Clearance*	$C = \sqrt{{c_1}^2 - {c_2}^2}$
$\boldsymbol{H}$	*Offset of the structure*	$H = d_{feedx}\sin(\theta_r + \theta_{in0x})$
$\boldsymbol{D_x}$	*Equivalent distance of the reflector Asymmetric cut*	$D_x = D_{px}\sin(90 - \theta_r)$
$\boldsymbol{D_y}$	*Equivalent distance of the reflector Symmetric Cut*	$D_y = D_{py}$

Table 4.1. - Reflectarray structure parameters and its formulas.

It will be important to relate these two coordinate systems. For simplicity and by applying trigonometric relations, it is possible to express the parameters of the equivalent parabolic system using the center of the reflector as coordinate's center. It is also possible to define another set of parameters that will be interest during the design. Table 4.1 describes the main geometrical parameters and the formulas that define them. P_x and P_y symbols are considered as the periodicities of the cells obtained in the previous section.

In the design of the structure of the reflectarray two sub processes will be carried out jointly: the calculus of phase distribution on the reflector and the incident field on it.

4.3.3.1.- Phase distribution.

To be able to generate the desired electric field, the aim will be emulating the electromagnetic behavior of a parabolic reflector with a reflectarray antenna. For this reason, it will be sought to design reflectarray antennas that in a far field form a brush type beam in the same way as parabolic reflectors. It is expected that if radiation patterns like parabolic reflectors in far field are obtained, it will be possible to get a similar near field.

A reflectarray antenna be a two-dimensional array. Therefore, to generate a flat wave front in a certain direction of space (θ_0, φ_0) a progressive phase distribution over the surface of the reflector given the formula [1] is required:

$$\phi(x_i, y_i) = -k_0\, sen(\theta_0)\, cos(\varphi_0)\, x_i - k_0\, sen(\theta_0)\, sen(\varphi_0)\, y_i \tag{4.1}$$

Where $k_0 = \frac{2\pi}{\lambda_0}$ is the wavenumber at design frequency; and x_i, y_i the coordinates of the ith patch. For its part, the phase of the field reflected in the flat surface for each patch that comes from the feed is obtained as the sum of the phase shift produced in the propagation from the feed and the phase of the reflection coefficient associated with each element.

$$\phi(x_i, y_i) = -k_0\, d_i + \angle\rho(x_i, y_i) = -k_0 \sqrt{\left(x_i - x_f\right)^2 + \left(y_i - y_f\right)^2 + {z_f}^2} + \angle\rho(x_i, y_i) \tag{4.2}$$

Equalizing both expressions (4.1) - (4.2) and clearing $< \rho(x_i, y_i)$ it is obtained the phase that each one of the patches must have, defined by its x_i, y_i coordinates respect reflectarray system.

$$\angle\rho(x_i, y_i) = k_0(d_i - sen(\theta_0)\, cos(\varphi_0)\, x_i - k_0 en(\theta_0)\, sen(\varphi_0)\, y_i) \tag{4.3}$$

A Matlab script based on the calculation of this expression will be used for the calculation of the phase distribution. In this study it is also consider the phase shift produced in the wave through the substrate and the phase restrictions that obtained in cell analysis stage. These calculated phases are stored in *.dat* file with a pre-applied format for the next stage of the methodology.

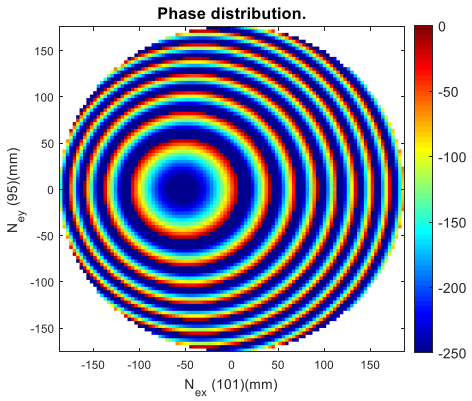

Fig. 4.8. - Example of target phase calculation in the designs of brush beam reflectarrays.

As an example, Fig. 4.8 shows the phase distribution obtained in a 40 GHz elliptic reflectarray design with a periodicity of $\frac{\lambda_0}{2}$ and a total number of elements of 7543 (101 x 95 in their axes respectively). It is assumed a substrate height of 30 mils and a feed position $(x_f, y_f, z_f) = (-153.60, 0.00, 240.00)$ mm. In addition, the reflectarray focuses the electric field in the direction of space $(\theta_0, \varphi_0) = (22.5,0)°$.

4.3.3.2.- Field through the reflector.

In the search of suitable phase distribution, it is also interesting to know how the incident electric field over reflector surface is. As mentioned above, the target phases will depend on the position of the feed respect to reflectarray, a position that also influences the level of the incident electric field in the reflector.

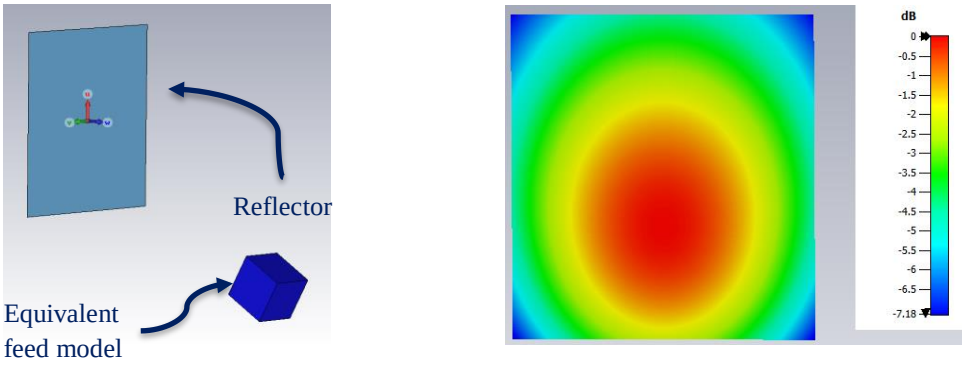

(a) (b)

Fig. 4.9. - Electric field on reflector: (a) CST model; (b) E-Field plane over reflector surface.

Since the feed will generate a brush type diagram pattern, the field level above the reflector will vary. Thus, the determining figure of merit will be the taper: difference in electric field between the point of the reflector to which the feed is pointing and the field at the end of it. The greater or lesser influence of phenomena such as spill-over or field uniformity along the reflector will depend on this taper.

Using an equivalent of the feed, it is possible to create a CST model of the reflectarray structure. In this model the reflector is replaced by a volume of air and the field on its surface is measured as shown in Fig. 4.9. With this tool it can be known if for the position of the feed fixed in the generation of phases, there is a suitable taper on the surface of the reflector. Using formulas detailed in Fig. 4.7 it can be also known the parameters according to equivalent parabolic model (F, C, D_x).

4.3.4.- Mask patches creation.

Known the distribution of the target phases and the relation of these with the size of the patches it prepares to construct the mask of patches that will be arranged on the reflector.

For it, and using Matlab, the files that contain the phase distribution and the matrix of design are read. θ_i, φ_i angles of incidence are also calculated and with them the phase-size curves obtained previously are accessed.

In order to obtain these incidence angles, a third reference system is used, which will be the one that considers as its center of coordinates, the center of each one of the patches. This system will not be more than translations on the surface of the reflector of the reflectarray reference system seen previously. That said, the angles of incidence are calculated according to the following formulas:

$$\theta_i = \begin{cases} \operatorname{atan}\left(\dfrac{\sqrt{{x_{fi}}^2 + {y_{fi}}^2}}{z_{fi}}\right) & z_{fi} > 0 \\ \dfrac{\pi}{2} & z_{fi} = 0 \\ \pi + \operatorname{atan}\left(\dfrac{\sqrt{{x_{fi}}^2 + {y_{fi}}^2}}{z_{fi}}\right) & z_{fi} < 0 \end{cases} \tag{4.4}$$

$$\varphi_i = \begin{cases} \operatorname{atan}\left(\dfrac{y_{fi}}{x_{fi}}\right) & x_{fi} > 0; y_{fi} > 0 \\ \left|\operatorname{atan}\left(\dfrac{y_{fi}}{x_{fi}}\right)\right| & x_{fi} > 0; y_{fi} < 0 \\ \dfrac{\pi}{2} sgn(y_{fi}) & x_{fi} = 0 \\ \left|\operatorname{atan}\left(\dfrac{y_{fi}}{x_{fi}}\right)\right| & x_{fi} < 0 \end{cases} \tag{4.5}$$

Where $(x_{fi}, y_{fi}, z_{fi}) = (|x_i - x_f|, |y_i - y_f|, z_f)$ are the coordinates of the feed respect the reference system of patches. In Fig. 4.10, shows the angles θ_i, φ_i for each patch of the reflector example given in Fig. 4.8.

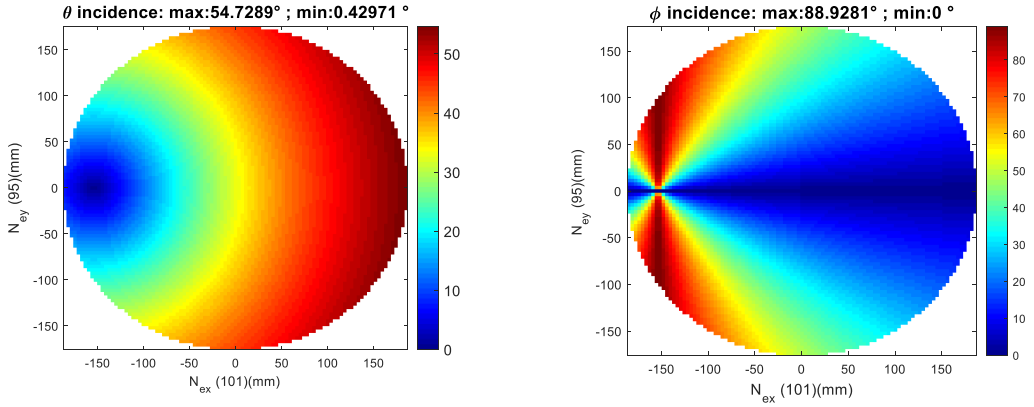

(a) (b)

Fig. 4.10. - Incidence angles in a reflectarray design: (a) Incident θ_i elevation; (c) Azimuth φ_i on each patch.

For each patch, the size of the known phase and its associated phase-size curve is calculated, storing this value in a file. This file will be used to construct the model of reflectarray in CST in the next blocks.

4.3.5.- Simplify model.

Already known all the parameters of the antenna, the next step will be to create the CST model to known what the quiet zone is and where it is in space. Thus, a CST model of the reflectarray structure is created based on the equivalent parabolic system of Fig. 4.7 placing the center of coordinates on the center of the reflectarray.

Using this CST model, it is possible to optimize the characteristics of the quiet zone by modifying the geometrical parameters of the structure (feed position, inclination feed angle …) and, if necessary, the introduction of other elements to the structure, such as for example a blocker on top of the feed.

This stage therefore involves several CST simulations, which implies a high computational cost. Therefore, this model is simplified with respect to the real implementation of the antenna in the following aspects:

- **Feed.** It will be considered that the reflector is in the far field of the feed, therefore and regarding the information extracted in 4.3.2, the feed is replaced by a point source that generates the same far field.

- **Patches and ground plane.** In the model, each one of the patches will be drawn as PEC planes with height 0 of different sizes, as it will be done with the ground plane.

To measure the quiet zone, field monitors are placed along the z axis in a certain range of distances from the reflector. Also, two monitors will be used on the axes x,y in order to study the E-Field of antenna in both cuts (symmetric and asymmetric).

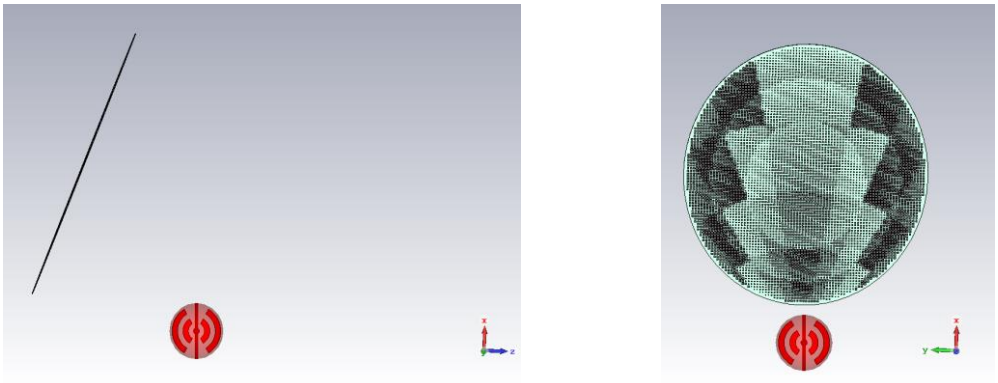

(a) (b)

Fig. 4.11. - Simplify CST model example: (a) Profile view; (b) Front view.

Once the most suitable geometrical parameters for the quiet zone have been determined, the final design will be simulated with more detail for comparison with the real CST model mentioned in the next stage.

4.3.6.- Real model.

To finish the design of the antenna, a CST model is created, more adjusted to the physical characteristics that the prototype will have to manufacture.

The patches and ground plane previously considered as a PEC, will now be metal plates with a certain height and with the requirements imposed during manufacturing. The far field source used, will be replaced by a near field model volume of the feed, identical to the one used in 4.3.3.2. In the case that the design is of several layers, this model will also consider the air o prepreg layer that is used for the union.

On this model it will be calculated in an identical way the E-Field and therefore the characteristics of the quiet zone. These results will be contrasted with those obtained from the simplified model.

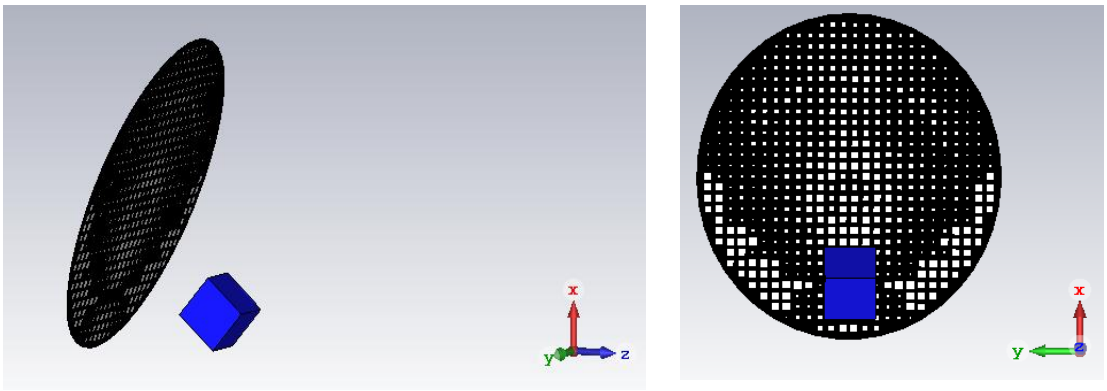

(a) (b)

Fig. 4.12. -Real CST model example: (a) Profile view; (b) Front view.

This CST model also allows to calculate other features of the antenna, such as the quiet zone in the non-optimized polarization and especially the behavior of this at different frequencies, being able to know which the bandwidth of the antenna will be.

4.4.- Conclusions.

From the requirements imposed by the application to be accommodated by the antenna, it is decided to build a methodology for reflectarray designing that follows the line of other methodologies currently used as in [23] but adapted for possible implementation in the software tools available: Matlab © and CST Studio Microware ©.

This methodology begins by characterizing the elements of the antenna independently and then optimizing the geometrical parameters of the structure as a whole in order to improve its performance in the area of the space under study.

After that and using the above-mentioned electromagnetic simulator, it will be studied what effect the practical limitations have on the antenna as well as an exhaustive band study.

5.- REFLECTARRAY DESIGNS.

5.1.- Introduction.

In this chapter, the main results and characteristics of the reflector designs carried out in this project will be presented, putting the methodology described above to the test.

In this project, 3 designs of reflectarray antennas have been made: two at 28 GHz (FR2 sub-band) and one at 1.7 GHz (FR1 sub-band). The difference between the designs at 28 GHz lies in the number of layers that conform the reflector: one or two layers. In the following points it will be detailed the design process for each of the reflectarray designs, which can be summarized in the following points:

- **Step 1 – Cell Analysis.** From the substrates available in each frequency band, the most suitable one will be chosen along with the variables on which each cell depends. From this block will be extracted the relationship between cell-size and introduced offset.
- **Step 2 – Feed analysis**. Working on two different frequencies, two feeds designs will be proposed, both of which correspond to a type of antenna commonly used in CATR systems: Axial Choke Conical Antenna.
- **Step 3 – Reflectarray structure.** An initial point of reflectarray configuration is constructed and the mask of patches is fixed on the reflector. In this block will also be determined the maximum size of these reflectors.
- **Step 4 – Optimization.** From the configurations obtained, the simplified models are constructed and simulated in CST. To improve the initial behavior of the antenna, some parameters of each structure are modified, to finally get an antenna configuration that approaches or meets the requirements set. For simplicity, in this optimization process it will be worked with Y polarization.
- **Step 5 – Real Model**. It will give way to more realistic models of the designs, which will evaluate the effects that can affect these new considerations on the performance of the antenna. These models are also used to perform a study in band or evaluate the polarization not optimized during the process.

5.2.- Cell Analysis.

In the first step of the methodology, the analysis of the radiant elements, it is necessary to know first electrical characteristics of the materials available for the design of the reflector. Materials which, as mentioned in chapter 4, are commonly used in the PCB manufacturing.

For the 28 GHz frequency, a single substrate is available, called Taconic TSM-DS3 [60], thermally stable low loss material with the characteristics shown in Table 5.1. In this material, will be interesting the dielectric constant and the dissipation factor, as well as the different heights of substrate available. The properties of the *prepeg* or bonding material will be considered for multilayer designs.

Characteristic	*Value*
Dielectric constant ($\mathbf{D_k}$)	*3.00 +/- 0.04*
Dissipation factor ($\mathbf{D_f}$)	*0.0011*
Permeability (μ_r)	*1.0*
Height substrate available ($\mathbf{h}$) [mm]	*0.13/0.25/0.51/0.76/1.52/2.29*
Cooper thickness [mm]	*0.035*
Prepeg for layers combination	*fastRise "27*
Dielectric constant of prepeg ($\mathbf{D_{k,s}}$)	*3.0*
Loss tangent of prepeg ($\mathbf{D_{f,s}}$)	*0.0014*

Table 5.1. - Characteristics of Taconic TSM-DS3 [60].

At a frequency of 1.7 GHz, it is also possible to use FR4 [61] as a substrate in the reflector. This material, with a higher dielectric constant, has the characteristics shown in Table 5.2.

Characteristic	*Value*
Dielectric constant ($\mathbf{D_k}$)	*4.7*
Dissipation factor ($\mathbf{D_f}$)	*0.014*
Permeability (μ_r)	*1.0*
Height substrate available ($\mathbf{h}$) [mm]	*0.80/2.0/2.4/3.2*
Cooper thickness [mm]	*0.035*
Prepeg for layers combination	*Uncured FR4*
Dielectric constant of prepeg ($\mathbf{D_{k,s}}$)	*4.7*
Loss tangent of prepeg ($\mathbf{D_{f,s}}$)	*0.0014*

Table 5.2. - Characteristics of FR-4 [61].

In all the cell studies explained below, the first step is to study the behavior of the cell by varying each of its characteristic parameters, considering that the wave strikes perpendicularly $(\theta, \varphi) = (0,0)°$. Once an optimal cell design is obtained, its behavior in band and for different incidence angles is analyzed, which allows to build the previously mentioned design matrix.

All combinations of incidence angles are analyzed, ranging from normal incidence to $(\theta, \varphi) = (80,80)°$. Nine different angles of θ, φ are studied (a 10° step is used), resulting in 81 different combinations of incidence angles.

5.2.1.- Design 28 GHz one-layer.

For the 28 GHz design assuming one-layer substrate, given that the substrate to be used is fixed (Taconic TSM-DS3), the height of the substrate and the periodicity between cells will be studied together. Remember that being square cells, the periodicity in both axes is equal (P_x=P_y).

In reference to Table 5.1, the heights at 0.76 and 1.52 mm are really interesting according to other designs already made in this band [30]. Thus, the phase vs. patch size curves are calculated for a periodicity range, between $\frac{\lambda_0}{4}$ and $\frac{5\lambda_0}{8}$ using $\frac{\lambda_0}{8}$ steps.

Regarding the characteristics of the curves taken from CST, this will have a range of $[0.1, P_x - 0.1]\ mm$ and the distance between two consecutive patch sizes will be 0.1 mm ($0.001\lambda_0$). It is also worth mentioning that in Matlab processing the curves are smoothed over certain atypical phase values taken from CST.

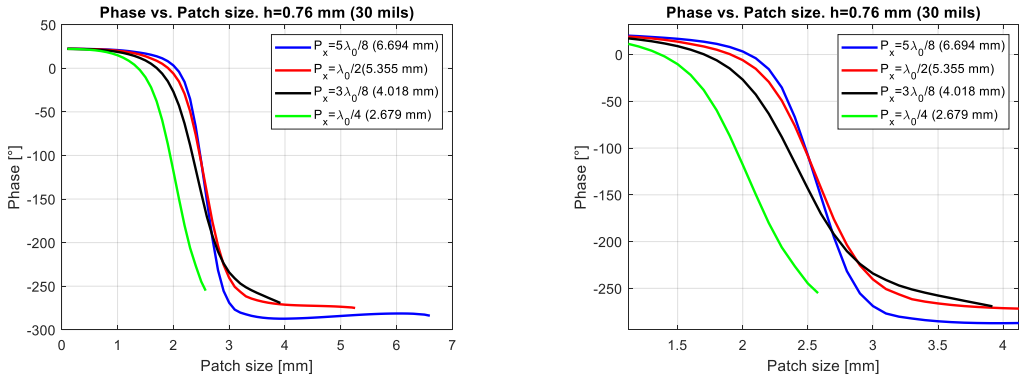

Fig. 5.1. - Design 28 GHz – One-layer. Cell analysis varying the periodicity of the cell. Substrate: Taconic TSM-DS3. Height: 0.76 mm: (a) Comparison between periodicities; (b) Linear zone detail.

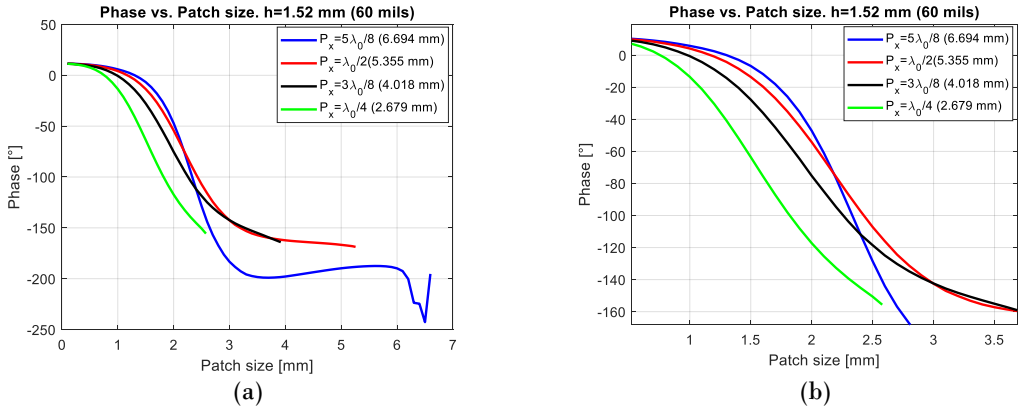

Fig. 5.2. - Design 28 GHz – One-layer. Cell analysis varying the periodicity of the cell. Substrate: Taconic TSM-DS3. Height: 1.52 mm: (a) Comparison between periodicities; (b) Linear zone detail.

In view of Fig. 5.1 and Fig. 5.2, it is possible to discard both the extreme periodicities $\left(\frac{\lambda_0}{4}, \frac{5\lambda_0}{8}\right)$. For $P_x = \frac{\lambda_0}{4}$ the curve has a small phase range, while for $P_x = \frac{5\lambda_0}{8}$ it has the largest phase range in the linear zone at the expense of a steep slope. Furthermore, in the case of $h = 1.52\ mm$, atypical curve behaviors appear.

This leaves in both cases two candidates' curves, the periodicity curves $\frac{\lambda_0}{2}$ and $\frac{3\lambda_0}{8}$. It is observed that in both figures, these two curves have a very similar range of phases in their linear zone, although the curve for $P_x = \frac{3\lambda_0}{8}$ has a smoother slope. That is why this configuration is chosen for both substrate heights.

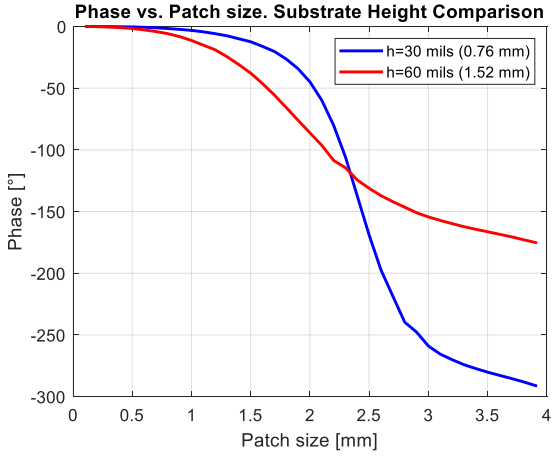

Fig. 5.3. - Design 28 GHz – One-layer. Cell analysis height comparison. Substrate: Taconic TSM-DS3. Periodicity: $\frac{3\lambda_0}{8}$ (4.018 mm).

In the comparison between the heights of the Fig. 5.3, it is observed that the phase range of the curve with lower height is clearly greater. Therefore, it is concluded that the

best combination of parameters will be using $P_x = \frac{3\lambda_0}{8}$ with a $h = 0.76\ mm$. In Fig. 5.4 it is shown the curved selected.

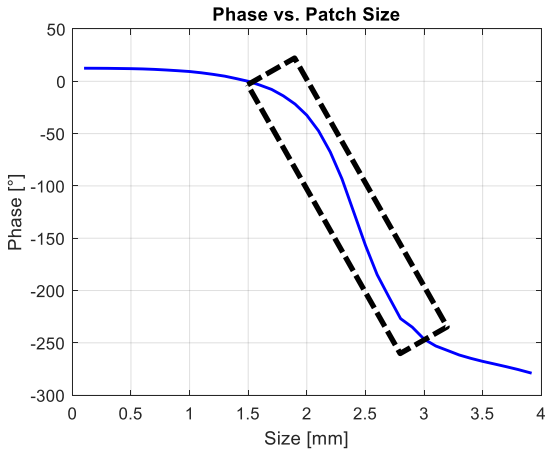

Fig. 5.4. - Design 28 GHz – One-layer. Configuration selected. Substrate: Taconic TSM-DS3. Periodicity: $\frac{3\lambda_0}{8}$ (4.018 mm). Height: 0.76 mm.

An offset of 108.8° is applied to this curve to make the 0 coincidence with the beginning of the linear zone, in such a way that it has a phase range of 250°, locating the linear zone between 1.5 and 3.0 mm of patch size. The curve has 39 points of which 15 form its linear zone.

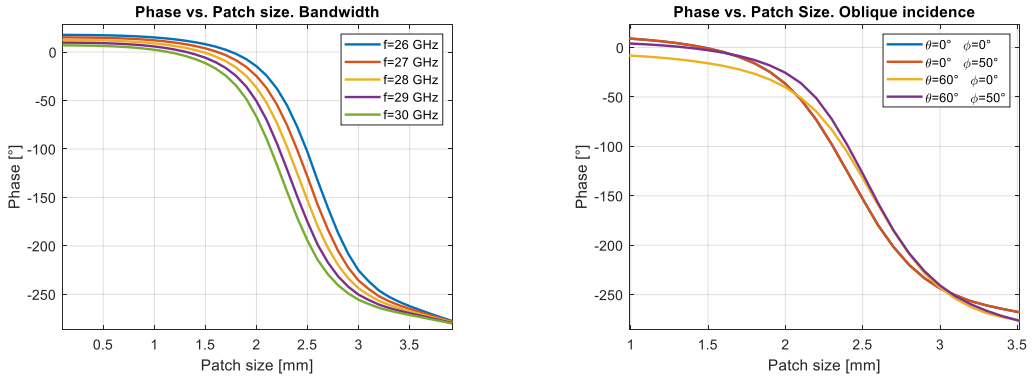

Fig. 5.5. - Design 28 GHz – One-layer. In-band (a) and Multi-angle (b) incidence cell studies.

Once the cell parameters have been set, a band study is carried out and its behavior is evaluated for different angles of incidence. In the first case, the Fig. 5.5 (a) shows that the curve suffer an increase in its slope and a slight increase in the phase range as the frequency increases. For frequencies lower than the design frequency, the slope and phase range decrease.

In the case of the angle of incidence (Fig. 5.6 (b)), it is observed that the linear zone is altered when considering high incidence angles, especially the elevation angles.

Another detail observed is that incidences with high φ angles affect the curve when, in addition, high elevation angles are also present. Despite this, in general terms the curve is robust against the oblique incidence.

5.2.2.- Design 28 GHz two-layer.

In the two-layer design, it is necessary to introduce into the cell study two new variables that will be the second layer height substrate (h_2) and the ratio between the patches of both layers **(**α).

When introducing a new substrate layer and taking as reference the substrate heights of the previous design, 4 different combinations of substrate heights appear: $(h_1, h_2) = [\,(0.72,0.72);\ (0.72,1.52);\ (1.52,0.72);\ (1.52,1.52)]\ mm$. Having said this, the first analysis to be carried out in the double layer design aims to fix the substrate heights h_1 and h_2. It will maintain a fixed periodicity of $\frac{3\lambda_0}{8}$ and a α =0.5. As it also a 28 GHz, the characteristics of the curve will be identical to the single layer design.

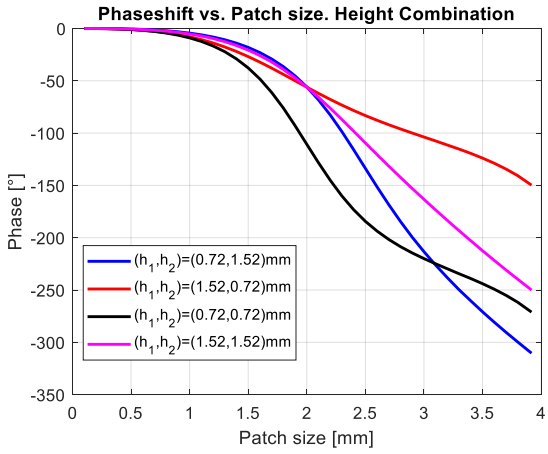

Fig. 5.6. - Design 28 GHz – Two-layer. Cell analysis height combinations. Substrate: Taconic TSM-DS3. Periodicity: $\frac{3\lambda_0}{8}$ (4.018 mm). Relation α=0.5.

The curves resulting from this study are shown in Fig. 5.6. From the 4 combinations it is observed that the curve with heights $(h_1, h_2) = (0.72,1.52)\ mm$ achieves a better performance both on slopes and in the range of phases with respect to the rest of the curves. This will be therefore the configuration of heights of chosen substrate.

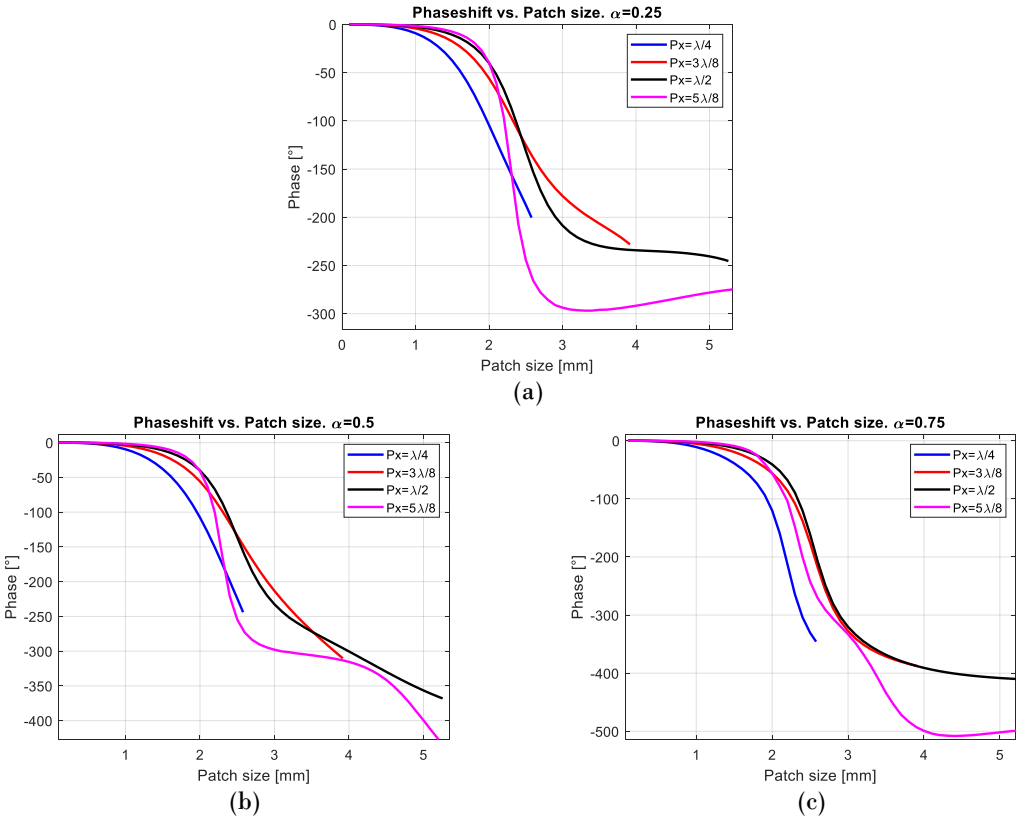

Fig. 5.7. - Design 28 GHz – Two-layer. Cell analysis varying the periodicity of the cell for different α ratios. Substrate: Taconic TSM-DS3. Height: 0.76 mm: (a) $\alpha = 0.25$; (b) $\alpha = 0.50$; (c) $\alpha = 0.75$

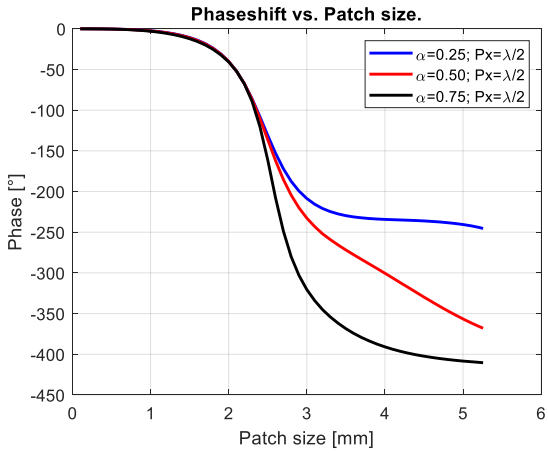

Fig. 5.8. - Design 28 GHz – Two-layer. Cell analysis α ratio comparison. Substrate: Taconic TSM-DS3. Periodicity: $\frac{\lambda_0}{2}$ (5.400 mm).

The next step will be to decide which periodicity and α ratio is most suitable for the cell design. Fig. 5.7 shows the comparison of curves for different periodicities and relationships between layers. For all of them, curves with $P_x = \frac{\lambda_0}{2}$ are those that acquire a better compromise between phase range and slope. If these three best curves are compared

(Fig. 5.8), a layer ratio of 0.75 provides a curve with a higher phase range than $\alpha = 0.25$ curve and a more linear behavior than the curve with $\alpha = 0.5$. Although it has a steeper slope than the rest, in this case the range of phases it has prevails, almost twice as much as in the case of lesser α.

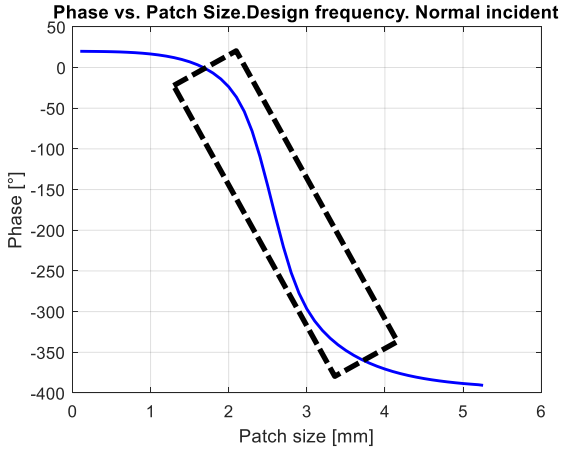

Fig. 5.9. - Design 28 GHz – Two-layer. Configuration selected. Substrate: Taconic TSM-DS3. $(h_1, h_2) = (0.72,1.52)$ mm. $\alpha = 0.75$. Periodicity: $\frac{\lambda_0}{2}$ (5.400 mm).

That said, the cell considered in the design is made up of two layers with heights $(h_1, h_2) = (0.72,1.52)$ mm, with a relation between patches $\alpha = \frac{h_2}{h_1} = 0.75$ and a periodicity $P_x = P_y = \frac{\lambda_0}{2}$.

An offset of 136.4° is applied to the phase curve, making its linear zone (Fig. 5.9) comprise a phase range greater than 360° for cell sizes between 1.7 and 3.8 mm. The curve has a resolution of patch size analogous to the design with one layer (0.1 mm), so it will be formed by 53 points of which 22 belong to the linear zone. The two layers design the allows to eliminate the phase restriction seen in the previous design and therefore to eliminate the effects caused by this.

The in-band behavior of this design (Fig. 5.10(a)) is very similar to the one seen below. However, a slight displacement of the curves can be highlighted, a greater variation of the offset, in the edge of the curves.

For the study of oblique incidence (Fig. 5.10(b)), greater discrepancies between designs are observed. For high theta elevation angles, the linear zone is strongly distorted and displaced over the phase axis, which indicates that the multilayer design will have a greater distortion than one-layer design in those areas of the reflector with a high elevation angle.

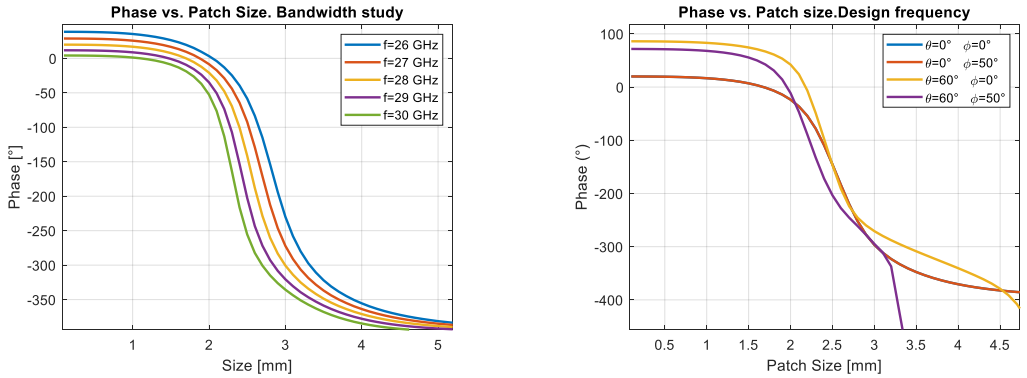

(a) (b)

Fig. 5.10. - Design 28 GHz – Two-layer. In-band (a) and Multi-angle (b) incidence cell studies.

5.2.3.- Design 1.7 GHz one-layer.

A similar reasoning will be followed for the design at 1.7 GHz, although in this case, it will be possible to use it as FR-4 substrate, therefore, prior to the adjustment of periodicity and height, it is necessary to decide which type of substrate to use.

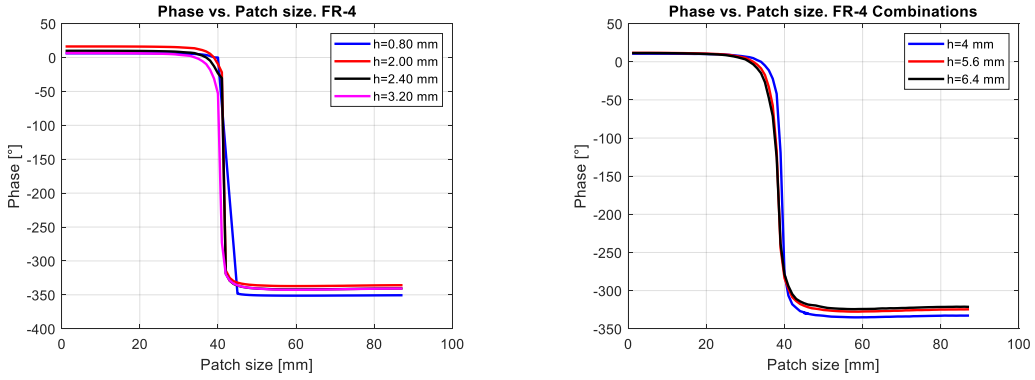

(a) (b)

Fig. 5.11. - Design 1.7 GHz – One-layer. Cell analysis varying the substrate height. Substrate: FR-4. $P_x = \frac{\lambda_0}{2}$: (a) Available standard heights; (b) Heights formed by 2 substrate layers.

Therefore, the phase vs. patch size curve with normal incidence is calculated for the different substrate sizes available. Fig. 5.11 and Fig. 5.12 show the cell study considering a $\frac{\lambda_0}{2}$ (88.235 mm) periodicity and the different substrate heights available in FR-4 and Taconic TSM-DS3. The size range will be from 0.5 to P_x-1 mm with a step width of 1 mm.

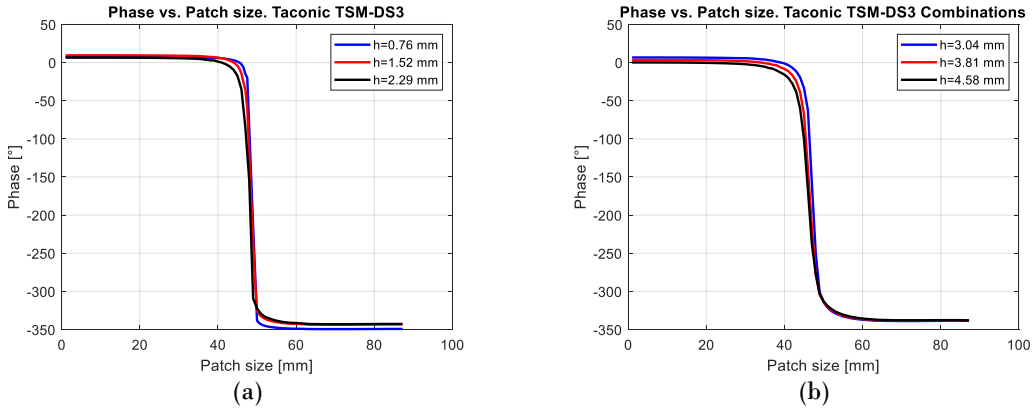

Fig. 5.12. - Design 1.7 GHz – One-layer. Cell analysis varying the substrate height. Substrate: Taconic TSM-DS3. $P_x = \frac{\lambda_0}{2}$: (a) Available standard heights; (b) Heights formed by 2 substrate layers.

Both figures show that the curves for the available substrate heights have a very high slope, which would require high cell size resolution. Therefore, the possibility of using combinations of several layers of substrate of standardized heights is considered. Thus, a cell study is performed with FR-4 assuming heights of $4\ mm$ $(2 \cdot 2\ mm)$, $5.6\ mm$ $(2.4 + 3.2\ mm)$ and $6.4\ mm$ $(2 \cdot 3.2\ mm)$. In the same way, the cell is analyzed with the Taconic TSM-DS3 substrate for heights of $3.04\ mm$ $(1.52 + 0.76\ mm)$, $3.81\ mm$ $(1.52 + 2.29\ mm)$, $4.58\ mm$ $(2 \cdot 2.29\ mm)$. A greater number of layers is not considered as this would considerably increase the losses in the substrate.

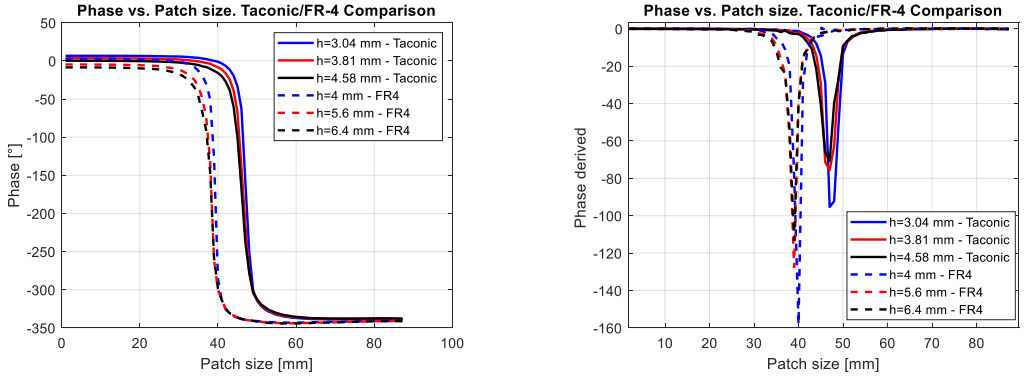

Fig. 5.13. - Design 1.7 GHz – One-layer. Cell analysis varying the substrate height. Material Comparison. $P_x = \frac{\lambda_0}{2}$: (a) Phase vs. Patch size; (b) Derivative respect size.

It should be noted that for the realization of this model of two layers of substrate, in CST it will leave a gap of 35 µm (height of patches marked in manufacture) that simulates the *prepreg* that joins both layers of substrate.

In Fig. 5.13 a comparison is made between materials for the different candidate heights. To better visualize the differences between materials the different curves, the derivative respect size is also represented.

It is observed that the curves using Taconic TSM-DS3 present a better behavior and less slope than those using FR-4. Based on this, Taconic TSM-DS3 will be chosen as the substrate of the reflectarray.

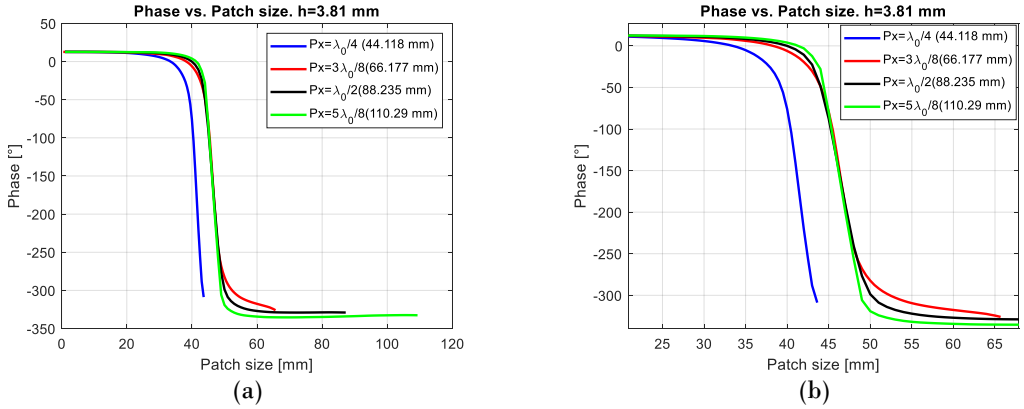

Fig. 5.14. - Design 1.7 GHz – One-layer. Cell analysis varying the periodicity of the cell. Substrate: Taconic TSM-DS3. Height: 3.81 mm. One layer: (a) Comparison between periodicities; (b) Linear zone detail.

After this step, the most suitable periodicity will be evaluated. In Fig. 5.13 it is possible to remain with two substrate heights of the Taconic due to its lower slope: 3.81- and 4.58-mm heights substrate. Following the same process as in 28 GHz designs, the curve is calculated for different cell periodicities at the two substrate heights. The result of this study is shown in Fig. 5.14 and Fig. 5.15.

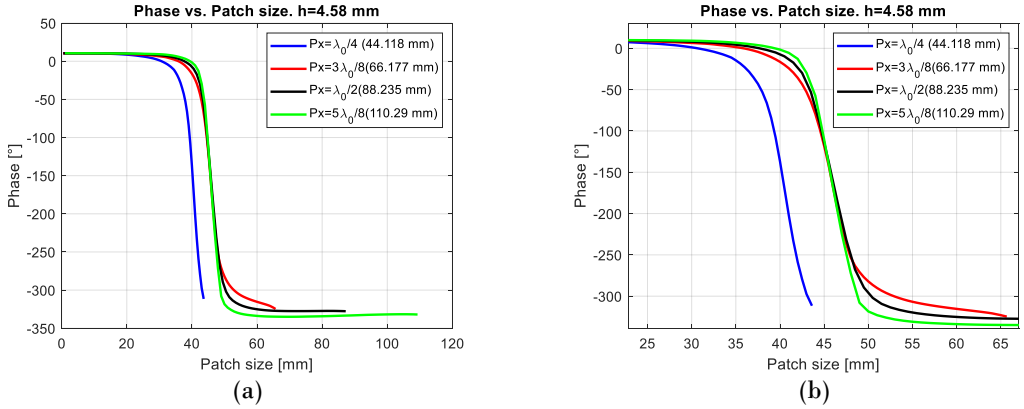

Fig. 5.15. - Design 1.7 GHz – One-layer. Cell analysis varying the periodicity of the cell. Substrate: Taconic TSM-DS3. Height: 4.58 mm. One layer: (a) Comparison between periodicities; (b) Linear zone detail.

As in the previous point, it is possible to discard for both heights the $\frac{\lambda_0}{4}$ periodicity as it has the smallest range of phases. Therefore, the curves with the three largest periodicities remain. Curves are very similar to each other, although it can be observed that for $P_x = \frac{3\lambda_0}{8}$ the slope and phase range is the lowest, while for $\frac{5\lambda_0}{8}$ is the opposite.

Therefore, it will be decided to choose the curve for $P_x = \frac{\lambda_0}{2}$ as it has an intermediate behavior (higher range than $\frac{3\lambda_0}{8}$ and lower slope than $\frac{5\lambda_0}{8}$). This decision is identical for both heights.

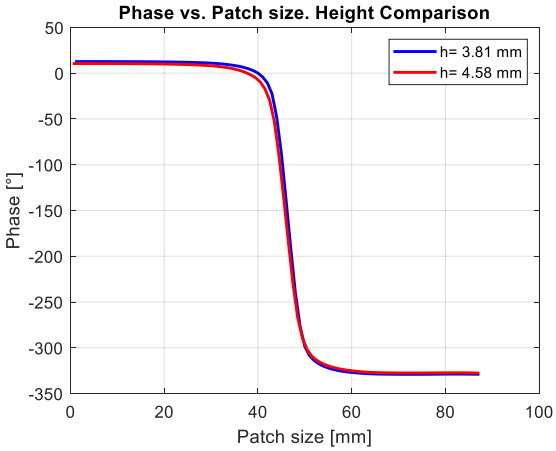

Fig. 5.16. - Design 1.7 GHz – One Layer. Cell analysis height comparison. Substrate: Taconic TSM-DS3. Periodicity: $\frac{\lambda_0}{2}$ (88.235 mm).

The comparison of heights is represented in Fig. 5.16. Both curves are practically identical, although the substrate with height 4.58 mm will present greater losses. Based on this, the cell configuration is chosen: $P_x = Py = \frac{\lambda_0}{2}$ and $h = 3.81$ mm.

Fig. 5.17 shows the phase vs. patch size curve for the chosen configuration assuming normal incidence. An offset of 152.4° is applied to this curve, making its linear zone have a phase range of 324.9°. The linear zone is located between 40 and 56 mm.

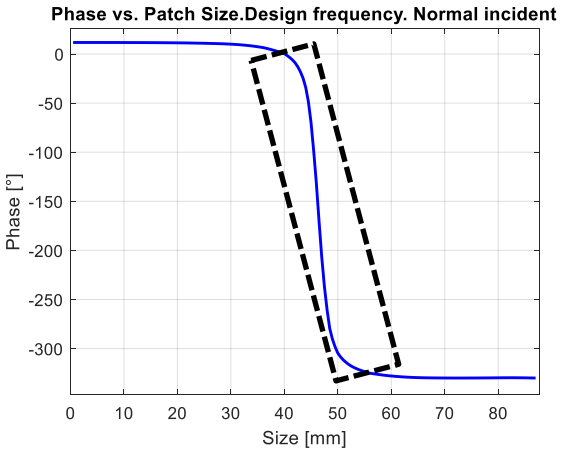

Fig. 5.17. - Design 1.7 GHz - One layer. Configuration selected. Substrate: Taconic TSM-DS3. Periodicity: $\frac{\lambda_0}{2}$ (88.235 mm). Height: 3.81 mm. Normal incidence.

Since this configuration has a steeper slope, it is necessary to store a larger number of points comparing to 28 GHz design. Each curve of this configuration will have 104 points, distributed with an irregular mesh, of which 33 points belong to the linear zone.

Finally, in the study in band of this configuration (Fig. 5.18(a)), it is observed that the curve has a behavior very similar to that seen in 28 GHz design, with an increase of the slope to reason of the frequency. The proposed configuration also presents a good rousted against different types of incidence (Fig. 5.18(b)) which is favorable because it implies less harmful effects generated by the antenna.

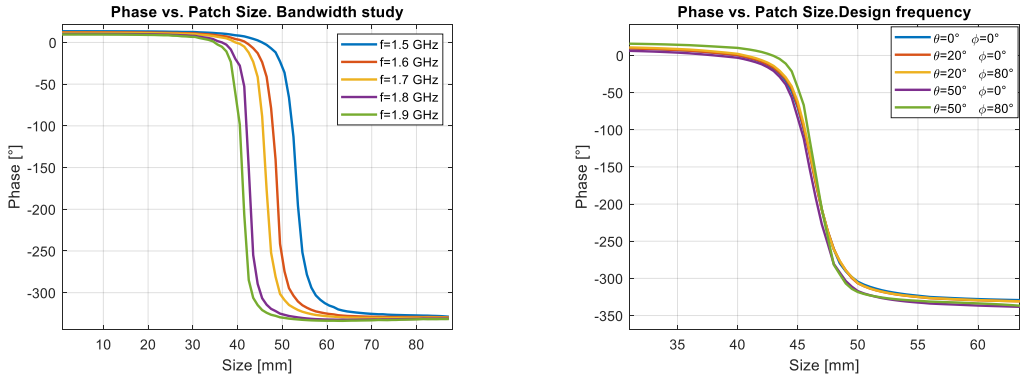

(a) (b)

Fig. 5.18. - Design 1.7 GHz – One Layer. In-band (a) and multi-angle (b) incidence cell studies.

5.3.- Feed Design.

The type of antenna chosen as feed in the designs receives the name of Axial-Choke Conical Horn. It consists of a conical horn formed by corrugations on its opening according to Fig. 5.19. This antenna can be used for both circular and linear polarizations. In this case the linear mode will be used (X and Y components).

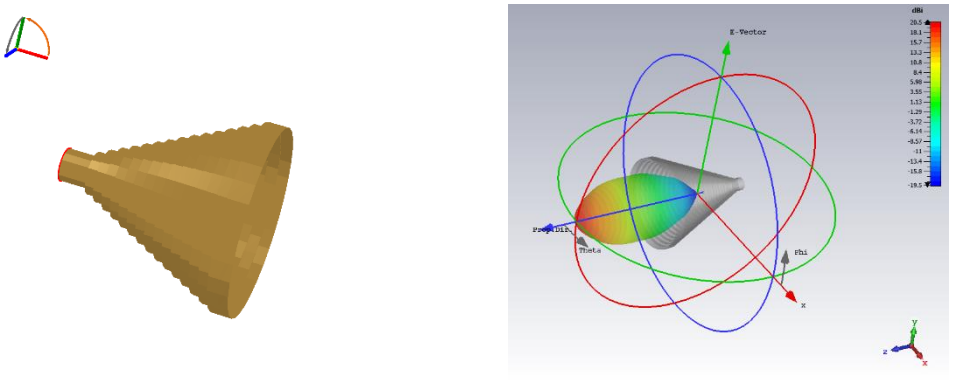

(a) (b)

Fig. 5.19. - Axial-Choke Conical Horn: (a) 3D Model example [62]; (b) Diagram Pattern example.

In Table 5.3, the main electromagnetic characteristics are shown. These antennas are electrically large $\left(>\frac{\lambda_0}{2}\right)$ and, like any other horn antenna, form a radiation beam with a reduced secondary lobe level. Compared to conventional horns, these antennas have a reduced cross-polar level thanks to their corrugated surfaces, arranged concentrically on their Z-axis.

Variable	Typical	Minimum	Maximum
Polarization	Linear	Dual-linear	Circular
Radiation pattern	Symetrical axial beam		
Gain	15 dBi	10 dBi	20 dBi
Complexity	Medium		
Ballum	None required		
SLL (Side-lobe level)	-30 dB		

Table 5.3. - Electromagnetic characteristics of Axial-Choke Conical Horn [62].

Fig. 5.20 shows the physical parameters on which the horn depends. It is necessary to highlight especially three parameters in this design that substantially affect the characteristics of the antenna of the following form:

- *The antenna dimensions decrease/increase as frequency f_0 increase/decrease.*
- *The gain increases/decreases as the flare angle θ increases/decreases or as the number of chokes N increase/decrease.*
- *The beam flatness increases/decreases as the number of chokes N increases/decreases.*

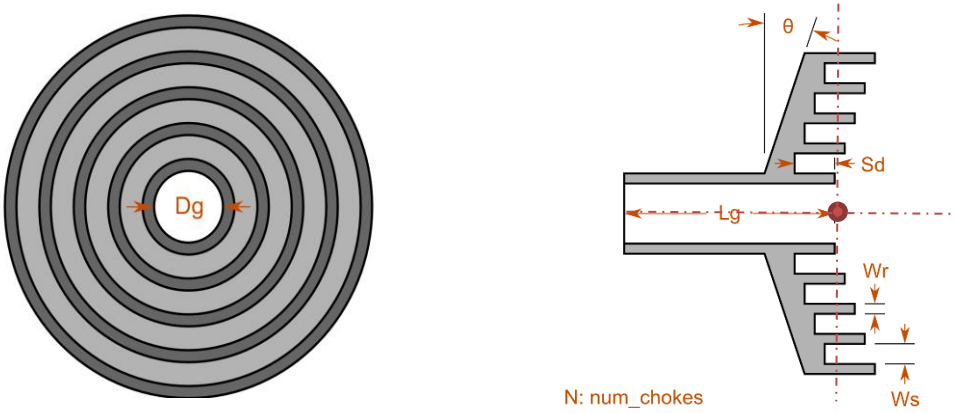

Fig. 5.20. - Feed physical parameters: (a) Front view; (b) Profile view [62]. The point red represents the center for which the phase center is calculated.

Regarding the rest of the parameters, these are fixed based on the central frequency. The diameter and length of the waveguide (L_g, D_g) will have the order of λ_0. With respect to the parameters of each choke (S_d, W_r, W_s), these will be the order of a quarter of the wavelength, although these will serve to refine the radiation pattern, especially in its broad-side direction.

The phase center (PC) of this horn, calculated considered both planes, will always be located on the direction of propagation, at a distance from the center of coordinates shown in Fig. 5.20, which will be the point where the wave guide ends.

That said, two horn designs will be made, each of them adjusted to the frequencies covered by this project: 28 GHz and 1.7 GHz.

5.3.1.- Design 28 GHz.

Since this is a reflectarray structure and based on some directivity and quiet zone studies such as [1], it is estimated that reflectarray antennas require a high taper in the reflector to achieve an acceptable quiet zone. This taper or difference of E-field level on the reflector, depends on the position of the feed in the structure (which will be optimized in the following points) and the gain of the feed itself. The gain, and therefore the radiation pattern of the antenna, are variables that are kept fixed in the process of optimization of the antenna.

Physical dimensions		*Diagram pattern – Electric characteristics.*	
Waveguide length - L_g [mm]	*10.707*	***Design frequency [GHz]***	*28.000*
Waveguide diameter - D_g [mm]	*9.058*	***Farfield [mm]***	*260.224*
Flare angle – θ [°]	*66.25*	***Main lobe magnitude - G_0 [dBi]***	*20.52*
Number of chokes - N	*20*	***Side lobe level (SLL) [dB]***	*-37.50*
Slot depth - S_d [mm]	*2.677*	***Main lobe direction [°]***	*0.00*
Choke ridge width - W_r [mm]	*0.236*	***Angular width (3 dB) [°]***	*15.3*
Chokes slot width - W_s [mm]	*1.178*	***PC – Position [mm]***	*7.164*
Device X-dimension [mm]	*33.031*	***PC – phase variation (δ)***	*10.35*
Device Y-dimension [mm]	*33.031*	***PC – Distance to aperture [mm]***	*57.076*

Table 5.4. - Axial Choke antenna design at 28 GHz. Physical and electric characteristics.

Having said this, in the design at 28 GHz it will be looked for a horn to provide the maximum gain as possible, considering that its physical dimensions are not too large, as this increases its distance from far field as well as could increase the blockage on the field reflected on the reflectarray. The diagram should also be as flat as possible in its maximum radiation area, although the target gain prevails over this. Table 5.4 shows the characteristics of this antenna for the 28 GHz design.

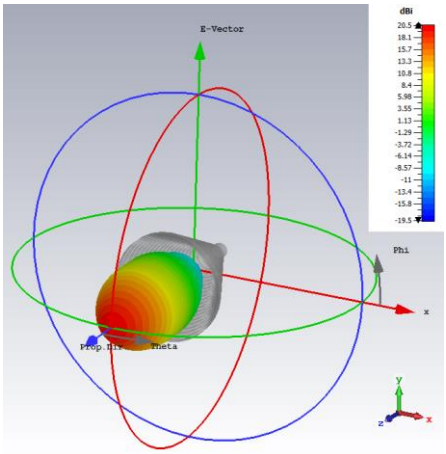

(a)

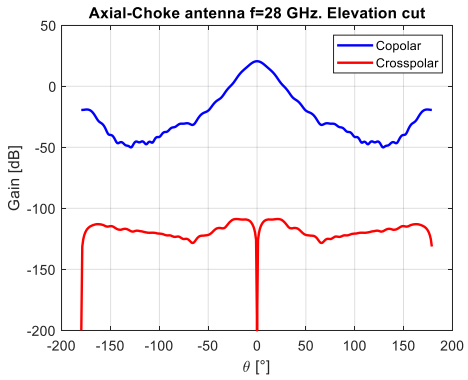

(b)

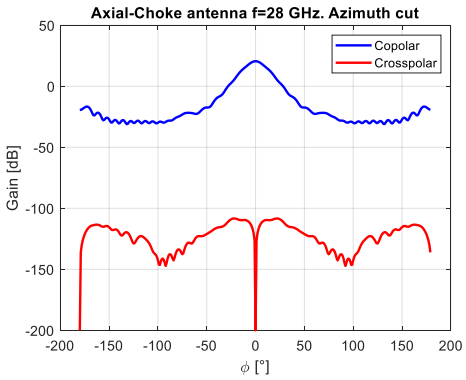

(c)

Fig. 5.21. - Axial Choke antenna design at 28 GHz – Diagram pattern: (a) 3D view; (b) Elevation principal cut; (c) Azimuth principal cut.

With this design it is possible to reach the maximum gain that the antenna can provide (20 dBi). For this, it requires a high number of chokes (20) and a pronounced flare angle (66.25°) which slightly increases the complexity in manufacturing. However, a compact antenna (66 mm aperture) is achieved, which gives a small distance to the far field (260.224 mm).

Fig. 5.21 shows the far field obtained from this antenna. The horn generates a radiation pattern with a reduced cross-polar level. In its copolar component it can be seen how the side lobes are much reduced (hence the SLL level in Table 5.4) respect a conventional horn antenna. The symmetry existing in both cuts (Fig. 5.22) of the diagram pattern is clearly observed, as can be expected from antennas of this type.

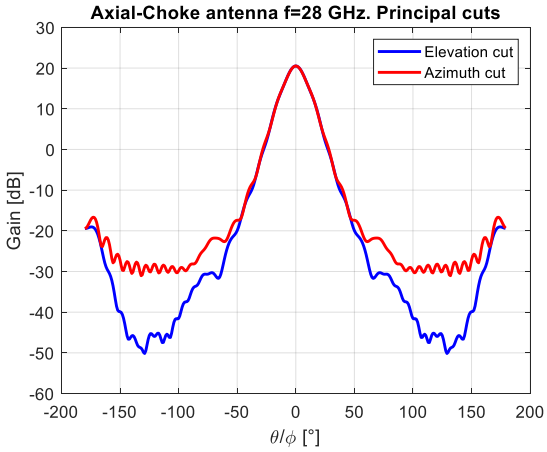

Fig. 5.22. - Axial Choke antenna design at 28 GHz – Diagram pattern: Principal Cut's comparison.

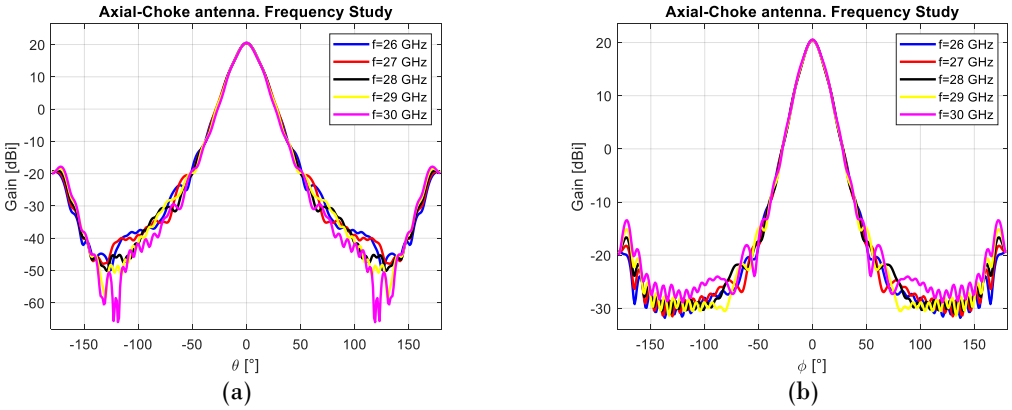

Fig. 5.23. - Axial Choke antenna design at 28 GHz – Bandwidth study: (a) Elevation cut; (b) Azimuth cut.

With respect to its behavior in band (Fig. 5.23), it is observed that in both cuts there is an excellent stability in frequency, at least 4 GHz around the central frequency. These data predict that the limitations in band will be derived from the behavior of the patches that make up the reflector fundamentally. Fig. 5.22 also shows the reflection coefficient

(S_{11}) at the frequencies under study. A good performance in band is observed in this sense, since this coefficient is below -10 dB.

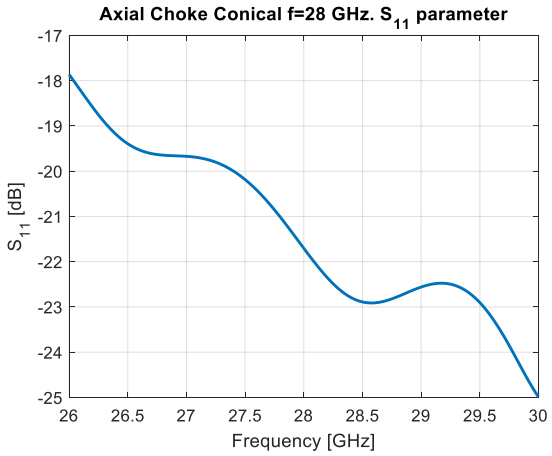

Fig. 5.24. - Axial Choke antenna design at 28 GHz – S_{11} parameter over the band study.

5.3.2.- Design 1.7 GHz.

At 1.7 GHz, the proposed design should generate a large quiet zone, which implies working with large reflectors (between 1 or 2 meters). In a large reflector it is possible to achieve a high taper with a lower gain feed. This aspect is especially interesting because at the frequency of 1.7 GHz, the dimensions of the feed will be physically large, which translates into a higher manufacturing cost and possible increase in blockage. If the gain restriction is lower, it is possible to make more compact feed designs.

Physical dimensions		*Diagram pattern – Electric characteristics.*	
Waveguide length - L_g [mm]	*176.349*	***Design frequency [GHz]***	*1.700*
Waveguide diameter - D_g [mm]	*149.192*	***Farfield [mm]***	*430.65*
Flare angle – θ [°]	*62.76*	***Main lobe magnitude - G_0 [dBi]***	*15.10*
Number of chokes - N	*5*	***Side lobe level (SLL) [dB]***	*-30.60*
Slot depth - S_d [mm]	*44.087*	***Main lobe direction [°]***	*0.00*
Choke ridge width - W_r [mm]	*3.880*	***Angular width (3 dB) [°]***	*31.80*
Chokes slot width - W_s [mm]	*19.398*	***PC – Position [mm]***	*143.175*
Device X-dimension [mm]	*194.865*	***PC – phase variation (δ)***	*22.106*
Device Y-dimension [mm]	*194.865*	***PC – Distance to aperture [mm]***	*82.918*

Table 5.5. - Axial Choke antenna design at 1.7 GHz. Physical and electric characteristics.

In this case, it is sought that the feed offers a gain of 15 dBi, typical gain of this antennas according to Table 5.3.Table 5.5 shows the physical parameters of the designed antenna. It is observed that when reducing the gain requirements, the antenna design is clearly simplified in comparison with the 28 GHz design (the number of chokes is reduced from 20 to 5). Note also the difference of physical magnitudes in both designs, derived mainly by change of frequency.

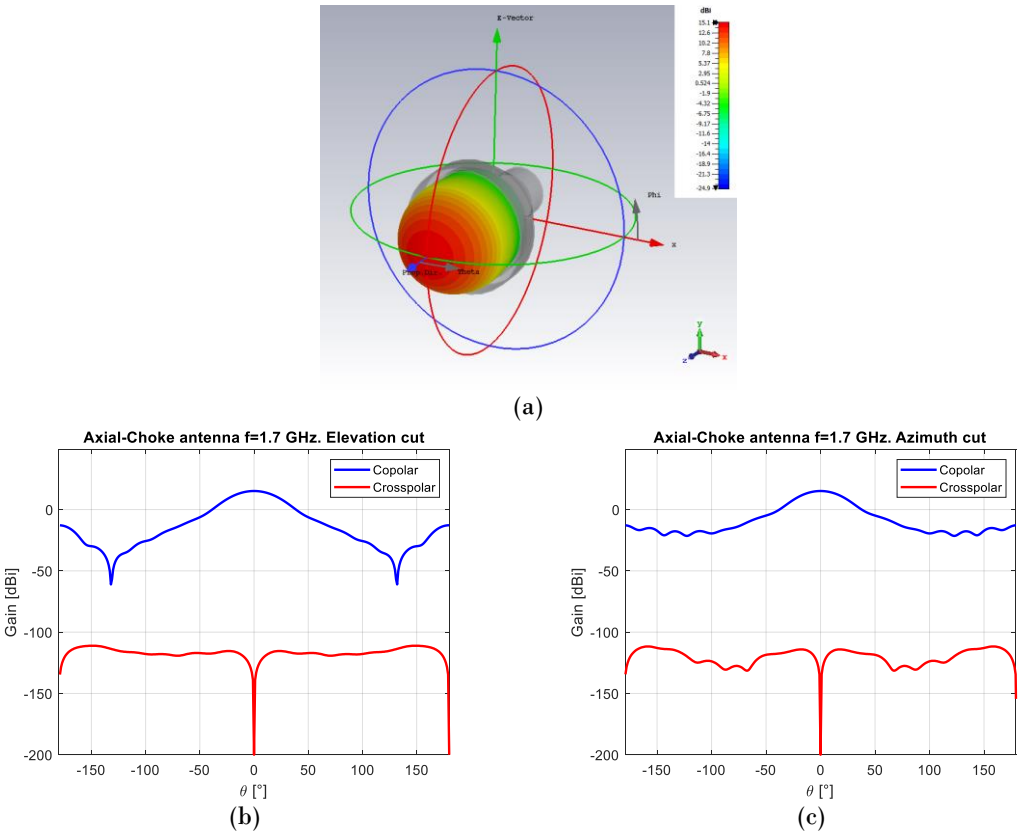

Fig. 5.25. - Axial Choke antenna design at 1.7 GHz – Diagram pattern: (a) 3D view; (b) Elevation principal cut; (c) Azimuth principal cut.

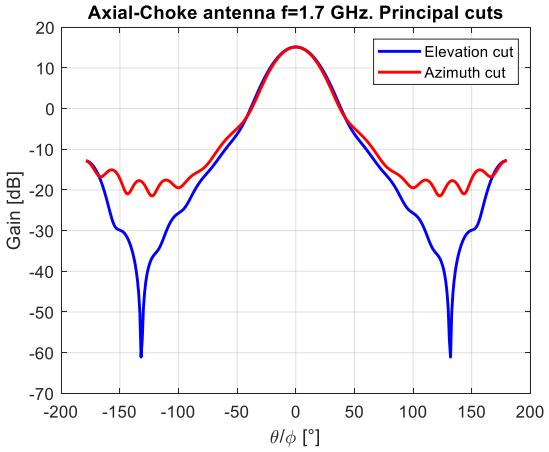

Fig. 5.26. - Axial Choke antenna design at 1.7 GHz – Diagram pattern: Principal Cut's comparison.

Fig. 5.25 and Fig. 5.26 shows the radiation pattern of this antenna. Its behavior in terms of SLL and cross-polar is very similar to the antenna at 28 GHz, thanks to the features mentioned above. The symmetry of both cuts is also another characteristic that

can be seen in this antenna. Analogous to the previous point, the radiation pattern of this antenna will be very stable in band as shown in Fig. 5.27.

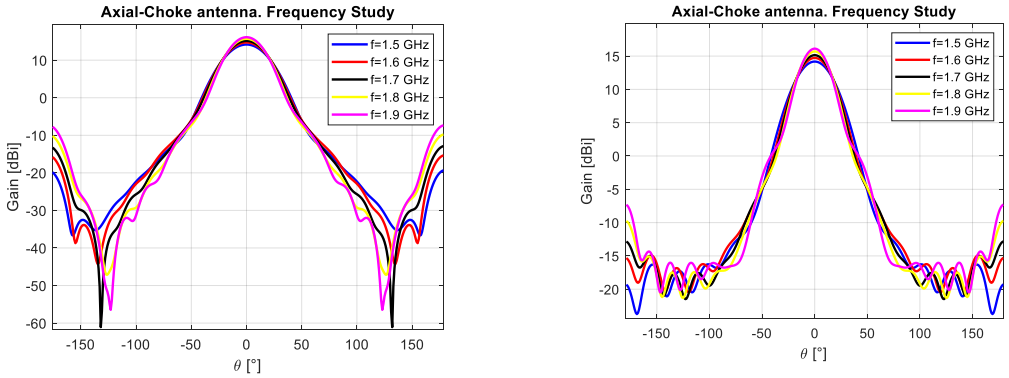

Fig. 5.27. - Axial Choke antenna design at 1.7 GHz – Bandwidth study: (a) Elevation cut; (b) Azimuth cut.

In the same way, an S_{11} parameter (Fig. 5.28) below -10 dB around 400 MHz respect to the design frequency is achieved. This translates into reduced reflection losses in the supply of the structure as it also happens in 28 GHz design.

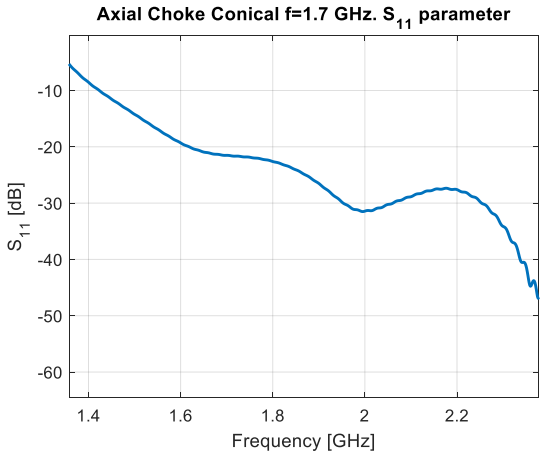

Fig. 5.28. - Axial Choke antenna design at 1.7 GHz – S_{11} parameter over the band study.

5.4.- Reflectarray Structure.

For the design of the reflector, and therefore the mask of patches, the formulas described in the previous chapter will be applied to obtain an adequate phase distribution. As it was commented previously, this distribution is translated later in the mask of patches to place in the model CST on the following stage.

In the cell study, the independent analysis of each patch is considered that its adjacent cells were formed by patches of periodicity and size identical to the cell under study, i.e., the cell study is based on a full wave analysis based on local periodicity. This then implies that the linear behavior seen above is conditioned to the neighboring cells having a size similar or equal to the patch under study.

The phase of the incidence field caused by the chosen feed (horn antenna) is conform by a concentric circles' distribution. That said, one of the targets of this stage is to achieve a phase distribution made up of concentric circles, where the target phase of adjacent cells is similar, which will imply in the manufacturing mask similar patch sizes.

In (4.3) seen in the previous chapter, it is observed that there are several factors that determine these phases: the position of the feed (x_f, y_f, z_f) and the angle of maximum radiation (θ_0). This feed position will be also decisive to the taper in the reflector, so it should be considered the incident E-Field on the reflector. According to [1], to get a suitable starting point, this taper must be between 6 and 10 dB for both cuts.

Regarding some preliminary designs, the circular or elliptical reflectors are the ones that present better characteristics since they present less critical scattering points, as it happens with square or rectangular reflectors. Regarding the size, it is possible to make a first estimation of the size, starting from the quiet zone target. In [1] it is estimated that a reflector can obtain a quiet zone size of 30% of its diameter.

Having said this, it will be started with a design whose approximate size generates the desired quiet zone. Then, an adequate phase distribution will be adjusted by varying the number of elements on each axis (N_x,N_y) the radiation angle (θ_0) and the position of the feed (x_f, y_f, z_f). Finally, from the CST model the incident E-Field on the reflector is obtained and the taper in both cuts is calculated. If this fits to the described premises, the associated patch mask will be calculated, otherwise, the position of the feed will be refined in the phase distribution calculation.

In the following sub-sections, there are the characteristics of the reflectarray structure of the proposed designs.

5.4.1.- Design 28 GHz One-Layer.

For 28 GHz designs, the target is to obtain a quiet zone of 10 by 10 cm^2 taking into account what has been said before, it will be start from considering a 34 x 34 cm^2 circular reflector, which translates into a number of elements in both axes of $N_x = N_y = \frac{340}{P_x} = 84{,}62 \rightarrow 85$. To reduce the blockage that could be generated by the feed in the structure of the antenna, a radiation angle of 20° is assumed as the starting point. The position of

the feed is first chosen arbitrary. Fig. 5.29 shows the phase distribution obtained with these parameters.

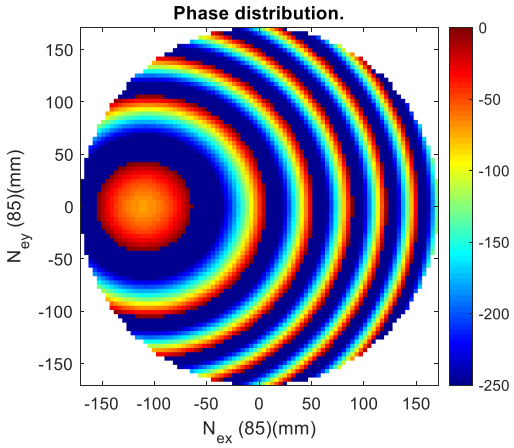

Fig. 5.29. - Design 28 GHz one-layer structure: starting point. $(x_f, y_f, z_f) = (-256, 0, 400), \theta_0 = 20.0°, N_x = N_y = 85.$

It is observed how this point is far from the conditions marked for good phase distribution. Note also that the phase is delimited by the restriction calculated in the cell analysis stage (250°) as it will be the maximum phase shift that the patches can provide.

After carrying out several iterations where the parameters on which this distribution depends vary, it is obtained the one shown in Fig. 5.30 (a) and whose characteristics are detailed in Fig. 5.6.

Structure Characteristics	
Number of patches X - N_x	*96*
Number of patches Y - N_y	*82*
Total number of patches - N_t	*6188*
Radiation angle – θ_0 [°]	*30.5*
Feed position - (x_f, z_f) [mm]	*(-256,400)*
Phase restriction [°]	*250*

Table 5.6. - Reflectarray structure 28 GHz One-Layer. Starting point characteristics.

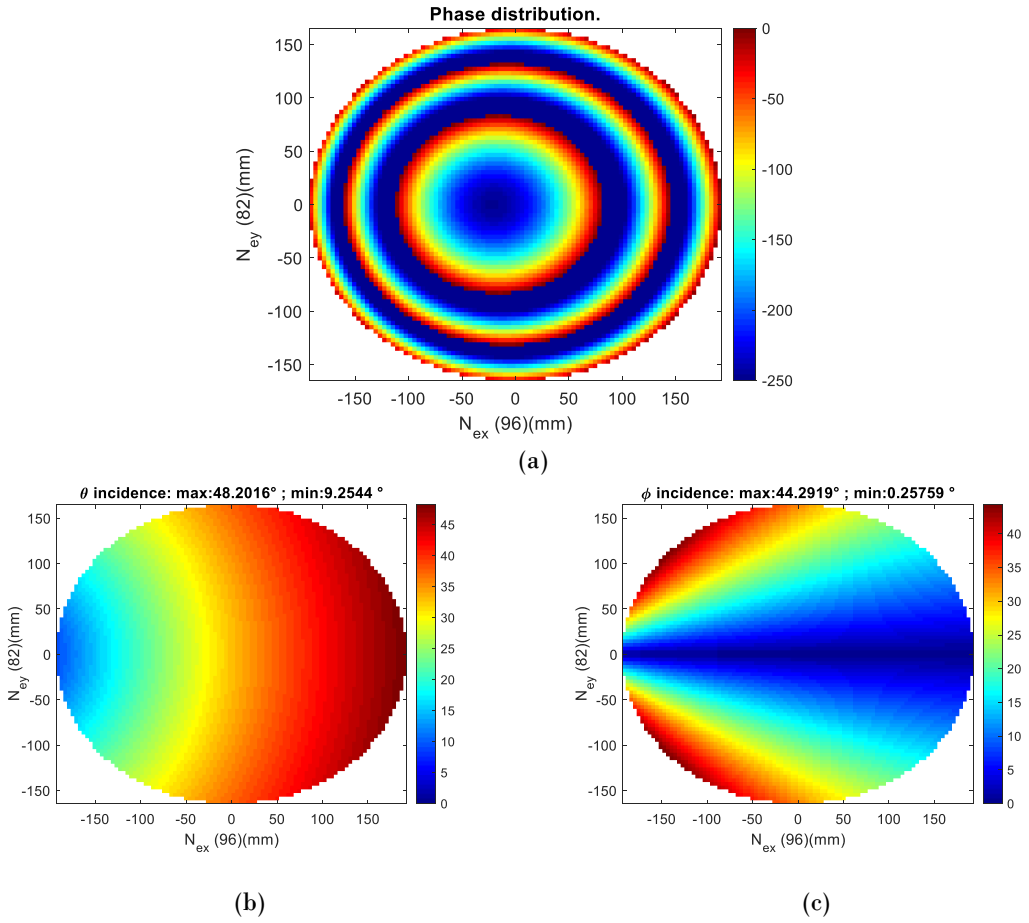

Fig. 5.30. - Design 1.7 GHz. Starting point structure: (a) Phase distribution; (b) Elevation (θ) wave incidence; (c) Azimuth (φ) wave incidence.

As the radiation angle increases, the phase distribution forms concentric ellipses with a greater eccentricity. To obtain similar phases at the edges, the shape of the reflectarray is adjusted so that it is also elliptical (different N_x and N_y).

Evaluating the angles of oblique incidence (θ, φ) it is observed that high elevations are reached (close to 50°) located in the zone of the reflector furthest from the feed. It can also be concluded that the angles in azimuth φ are high in those areas where θ is low. Based on the cell analysis seen above, the high φ angles of the incidence wave will not significantly affect the behavior of the cell.

Regarding the taper on the reflectarray surface, Fig. 5.31 shows that the E-Field at the edges of the reflector reaches a difference of at least 10 dB from its maximum value, which indicates a good taper for the position that has been fixed feed.

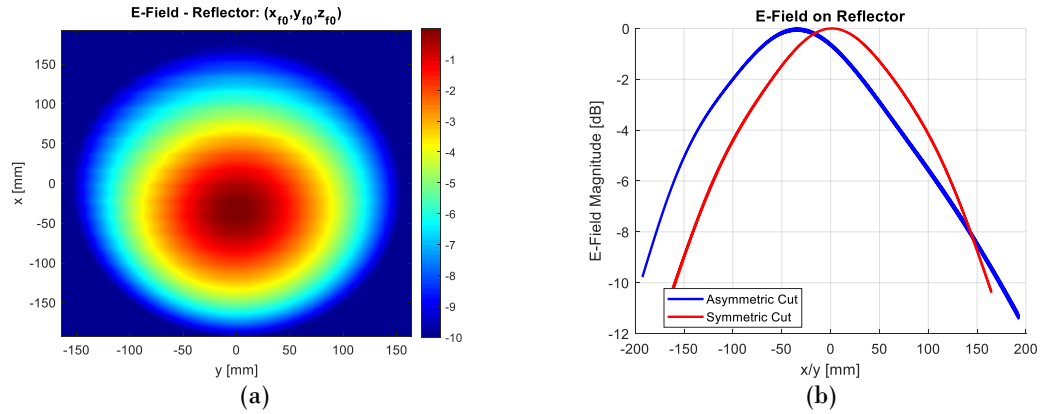

(a) (b)

Fig. 5.31. - E-Field on the reflectarray: (a) 2-D view; (b) Principal Cuts.

5.4.2.- Design 28 GHz Two-Layers.

For the 28 GHz design, the starting point is the initial configuration of the design to a layer as shown in Table 5.7, since both designs share the antenna requirements. However, the fact that the selected periodicity is slightly higher ($\lambda_0/2$ versus $3\lambda_0/8$) will reduce the total number of patches if a similar total reflector size is to be maintained.

Structure Characteristics	
Number of patches X - N_x	*72*
Number of patches Y - N_y	*62*
Total number of patches - N_t	*3504*
Radiation angle – θ_0 [°]	*30.5*
Feed position - (x_f, z_f) [mm]	*(-256,400)*
Phase restriction [°]	*No*

Table 5.7. - Reflectarray structure 28 GHz Two-layer. Starting point characteristics.

The target phase distribution is shown in Fig. 5.32(a). The main difference observed in comparison with one-layer design is the greater range of phases covered by this distribution, caused mainly by not having a phase restriction as if it occurred in the previous case. By not modifying the position of the feed, it is also corroborated that the angles of incidence (Fig. 5.32(b) and (c)) remain very similar.

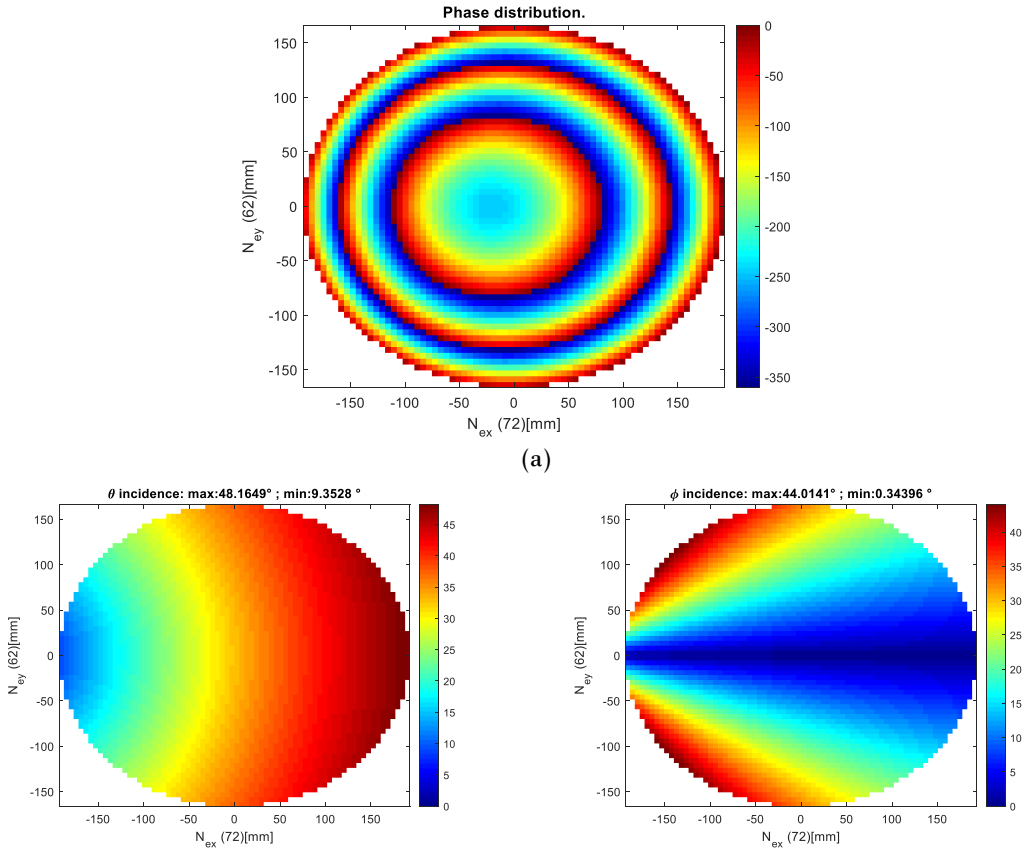

Fig. 5.32. - Design 28 GHz Two layers. Starting point structure: (a) Phase distribution; (b) Elevation (θ) wave incidence; (c) Azimuth (φ) wave incidence.

Despite the reduction in the number of elements, the size of the reflector increases slightly, which makes the taper on the reflector also do as shown in Fig. 5.33. The increase in the taper reduces the contribution of the reflector areas with a higher angle of incidence and therefore benefit, a priori, the behavior of the E-Field.

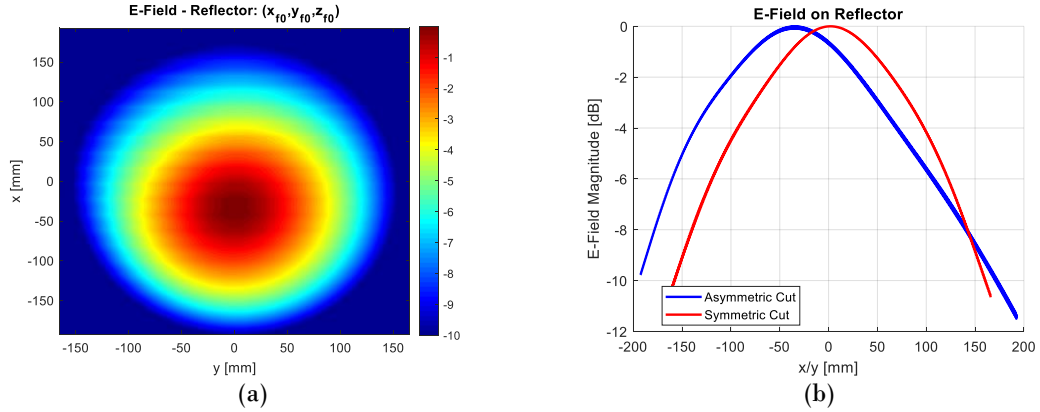

Fig. 5.33. - E-Field on the reflectarray: (a) 2-D view; (b) Principal Cuts.

5.4.3.- Design 1.7 GHz One-Layer.

For the 1.7 GHz design, a quiet zone of 50 cm was mentioned above. Following the reasoning described above, it will begin by considering a circular reflector of 1.5x1.5 m, that is, a reflectarray formed by $\frac{1500}{P_x} = 17.007 \rightarrow 18$ elements in its axes. A radiation angle of 20° is also assumed. In this case, the position of the feed is chosen by scaling the position of the feed fixed in the 28 GHz design. Fig. 5.34 shows the phase distribution of this initial point. As 28 GHz one-layer desing, there is also a slight phase restriction because as observed in section 5.2.3 the maximum phase shift provided by the cell is 324.9°.

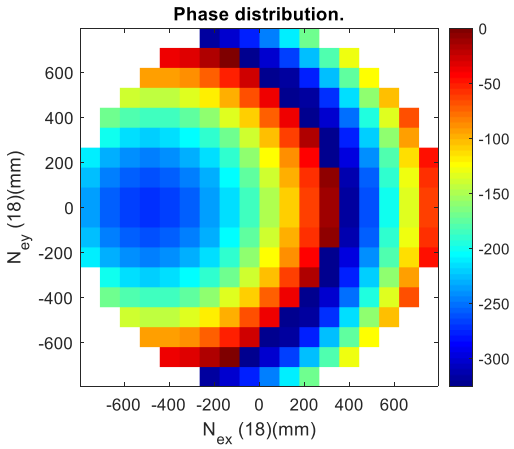

Fig. 5.34. - Design 1.7 GHz Structure. $(x_f, y_f, z_f) = (-1126, 0, 1760)\ mm$, $\theta_0 = 20.0°, N_x = N_y = 18.$

By modifying the variables on which the phase distribution depends, it is possible to obtain a $\phi(x_i, y_i)$ as shown in Fig. 5.35. The fixed reflectarray parameters considered as starting point are shown in Table 5.8.

Structure Characteristics	
Number of patches X - N_x	*20*
Number of patches Y - N_y	*19*
Total number of patches - N_t	*300*
Radiation angle – θ_0 [°]	*30*
Feed position - (x_f, z_f) [cm]	*(-102.4,160)*
Phase restriction [°]	*324.9°*

Table 5.8. - Reflectarray structure 1.7 GHz One-Layer. Starting point characteristics.

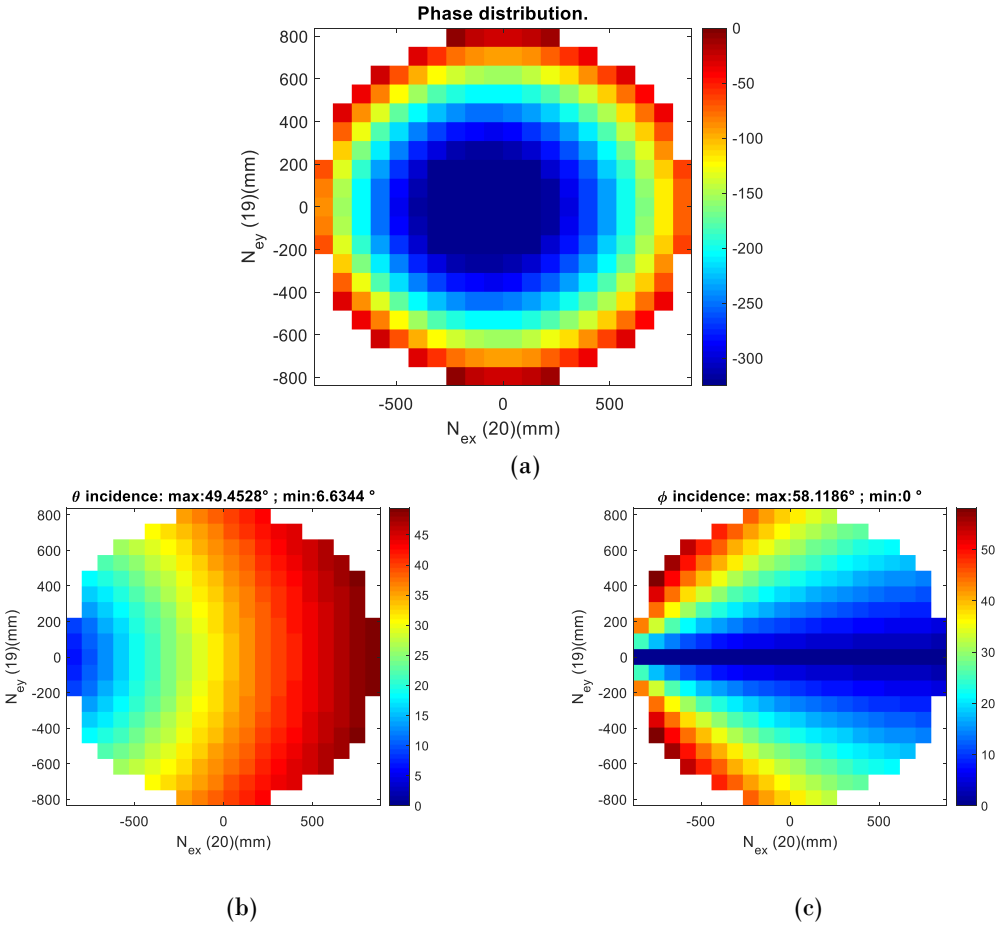

Fig. 5.35. - Design 1.7 GHz. Starting point structure: (a) Phase distribution; (b) Elevation (θ) wave incidence; (c) Azimuth (φ) wave incidence.

In this case, the elliptical shape of the reflector has a lower eccentricity than 28 GHz design and a greater variety of phases is available, mainly derived from the lower restriction in the phase range. On the other hand, a much smaller number of elements (patches) is obtained due to the frequency at which it is designed.

The angles of incidence (θ, φ) on the reflector are similar, since the position of the feed in this design is like a scaled version of the position (x_f, y_f, z_f) fixed in the design at 28 GHz.

Finally, for the fixed feed position, the taper generated on the reflector surface (Fig. 5.36) reaches 6 to 8 dB. This taper is slightly smaller than in the 28 GHz design, although it is still a suitable taper as a starting point.

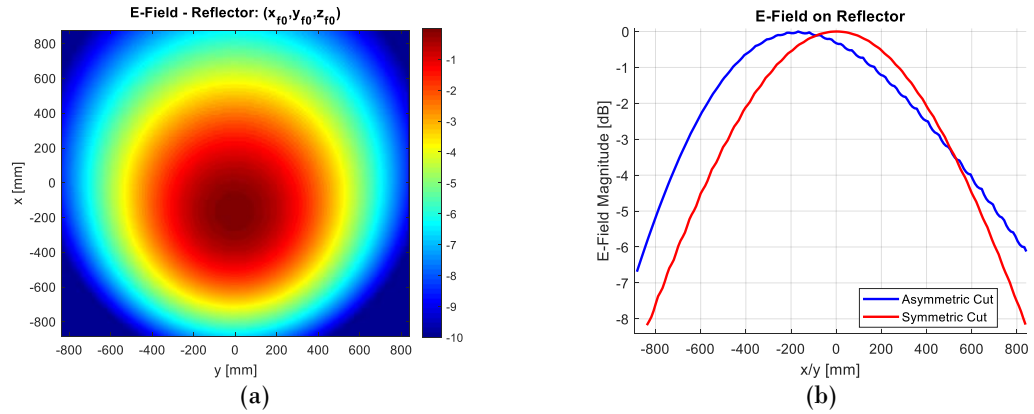

(a) (b)

Fig. 5.36. - E-Field on the reflectarray – Y-Polarization: (a) 2-D view; (b) Principal Cuts.

5.5.- Simplify model. Optimization.

Fixed an initial point in the designs and obtained the sizes of each patch from the cell analysis and the structure of the reflectarray. The optimization process then begins to obtain a reflectarray structure that generates the best possible quiet zone.

At this point, the geometrical parameters of the antenna will be used as variables, mainly expressed in the position of the feed with respect to the RA system (x_f, y_f, z_f) and the inclination of this respect to the perpendicular of the reflector θ_{incx} (see Fig. 4.7) Apart from these variables it is possible to introduce elements or structures to the antenna, in order to study if this could benefit or not to the quiet zone obtained.

In each of the designs described below, studies will be carried out where one of the main geometrical parameters is taken as a variable, leaving the rest of the parameter's constant. Based on the results obtained, the parameter under study is set and the next variable is studied.

As mentioned above, the quiet zone is measured from the electric field in the surrounding area of the antenna. The physical dimensions of this area were $D_x\ x\ D_y\ x\ D_z$, where D_x and D_y are the equivalent diameters obtained following the formulas in Table 4.1. The dimension along Z axe (D_z) and the resolution inside the area (step) will depend on each of the designs.

Since the quiet zone will be a volume centered on the maximum radiation direction of the reflectarray, it is necessary to measure it using different perspectives.

On the one hand, for initial and definitive geometrical configurations, the E-Field will be measured over the cut in the X and Y axis, symmetric and asymmetric cut. At the same time, the field will be measured in planes arranged on the Z axis and centered in the direction that passes through the center of the RA. Finally, and as a third point of view,

the information obtained from the electric field in each plane on the Z axis translates into quiet zone sizes according to requirements marked in point 4.1.

On each one of the planes on the Z axis, 4 different measures of quiet zone will be obtained: measure of the E-Field in amplitude and phase for its main cuts (symmetric and asymmetric cut). The measurement procedure is shown in Fig. 5.37. For the magnitude of the field, the point will be searched and measured on the point where the x/y axis level of the field is 1.5 dB lower. In the case of the phase, an area is searched where this is delimited between 22°.

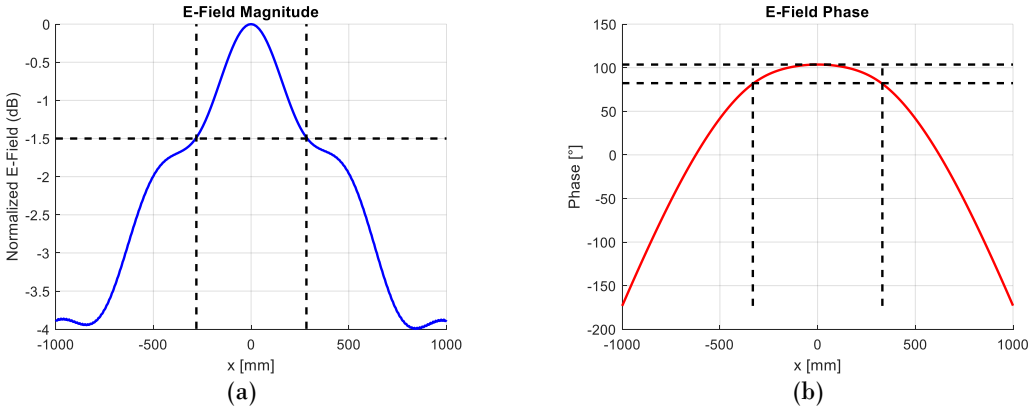

Fig. 5.37. - Procedure for calculating the quiet zone: (a) Magnitude of the E-Field; (b) Phase of the E-Field.

When measuring on several planes, this gives rise to 4 curves of quiet zone size: two for amplitude and two for phase. In some cases, these curves can be quite different from each other, which can make it difficult in some cases to compare configurations. Therefore, certain operations are carried out with these curves, calculating the approximate area of the quiet zone by multiplying the magnitude and phase curves between them.

Since it is sought to generate quiet zones with sizes in both similar axes (like square or circle shapes) in the comparisons where one parameter is varied and with the quiet zone sizes calculated for each cut, the minimum size measured is chosen for each Z plane. The minimum quiet zone size will be calculated independently for amplitude and for phase in the optimization process. Also, some cuts will be represented on the Z axis in order to provide more data when deciding which value is the most suitable for each variable to optimize.

Once a definitive design is available, the quiet zone curves will be calculated in the same way as in the optimization process. From these, the minimum distance to the reflector at which the quiet zone complies with the requirements imposed on the XY plane will be calculated.

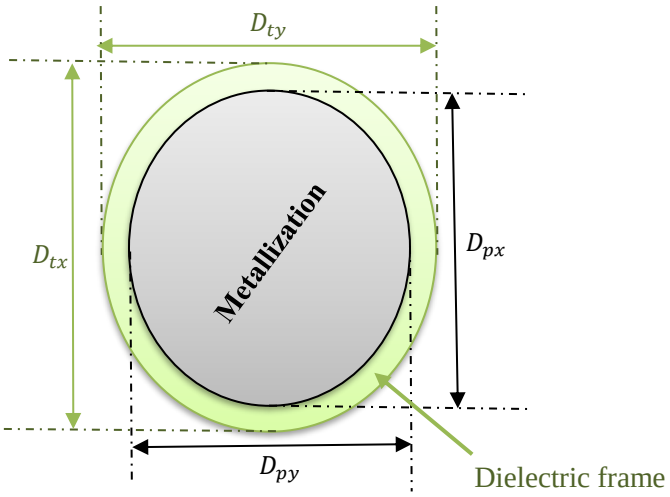

Fig. 5.38. - Diameters and dimensions of reflectarray.

In all the models to be used in this stage is convenient to know the different parameters of the reflectarray. The reflector to be drawn on the CST model is composed of a large area where the previously calculated patches will be placed (metallization area). An area whose size depends on the periodicity and number of patches in both cuts. In addition, at the end of this zone will be left a ring excess substrate or dielectric frame, to facilitate the integration of this on the structure of the antenna. The nomenclature that will be used to characterize the reflectarray is shown in Fig. 5.38.

Note that the reflector characteristics will remain fixed throughout the optimization process.

5.5.1.- Design 28 GHz One-Layer.

Before studying the model, it is necessary to calculate the dimensions of the reflector. Based on the data obtained in point 5.4.1, the diameters that characterize the reflectarray are shown in Table 5.9. In this case, a cell periodicity (4.018 mm) is used as the dielectric frame. Note that the characteristics of the reflector will remain fixed throughout the optimization process.

Reflector characteristics	
Diameter of the reflector in Asymmetric cut - $\boldsymbol{D_{px}}$ [mm]	*385.714*
Diameter of the reflector in Symmetric cut - $\boldsymbol{D_{py}}$ [mm]	*329.464*
Total diameter of the reflector in Asymmetric cut - $\boldsymbol{D_{tx}}$ [mm]	*393.750*
Total diameter of the reflector in Asymmetric cut - $\boldsymbol{D_{ty}}$ [mm]	*337.500*
Equivalent diameter of the reflector in Asymmetric cut - $\boldsymbol{D_x}$ [mm]	*339.266*
Equivalent diameter of the reflector in Asymmetric cut - $\boldsymbol{D_y}$ [mm]	*337.500*

Table 5.9. - Design 28 GHz One-Layer. Diameter and dimensions of the reflector.

With these data, it is possible to study the quiet zone generated by the reflector antenna and according to the geometry from which starts. For this design, the study area of the quiet zone will range from the center of the reflector to one meter. The planes on the z axis is arranged every 50 mm at a distance between 300 and 1000 mm from the center of the reflectarray. According to some studies such as [63], it is assumed to consider an angle $\theta_{incx} = \theta_r = \theta_0$. This condition allows to minimize the deviation of the main beam with the frequency, which is an interesting angle as a starting point.

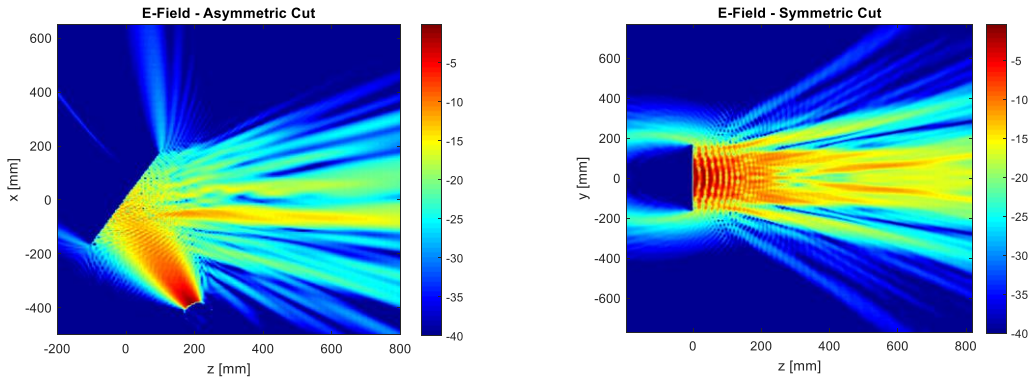

(a) (b)

Fig. 5.39. - Design 28 GHz One-Layer – Starting point. E-Field Magnitude. Y-Polarization: (a) Asymmetric Cut; (b) Symmetric Cut.

Fig. 5.39 shows the results of the reflectarray design before optimization. It is observed that the E-Field is very scattered in both cuts and that there is a high dispersion at the edges of the reflector. A narrow beam can be distinguished almost parallel to the z axis. This beam can be seen more clearly in z cuts shown in Fig. 5.40**.** Although it is verified that its size increases as it propagates along the z axe, and therefore the quiet zone increases, the shape it has I not the desired one, since it does not resemble any simple shape such as a circle or ellipse.

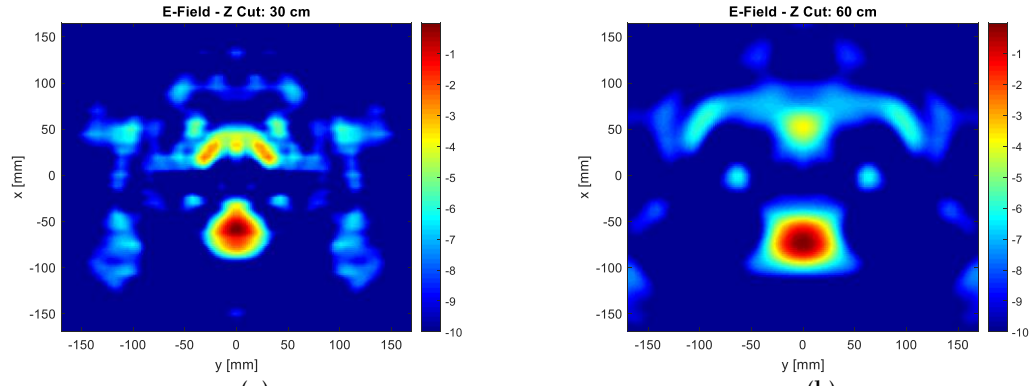

(a) (b)

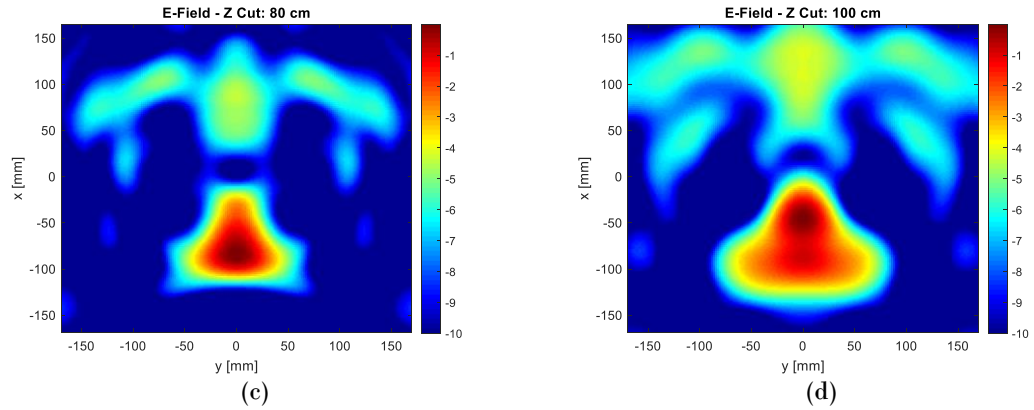

Fig. 5.40. - Design 28 GHz One-Layer – Starting point. E-Field Magnitude – Z Cuts. Y-Polarization: (a) z=30 cm; (b) z=60 cm; (c) z=80 mm; (d) z=100 cm.

For its part, the phase does not have a behavior as desired (Fig. 5.41), although in the area where the quiet zone in magnitude, it can be distinguished how the phase remains constant in some cuts.

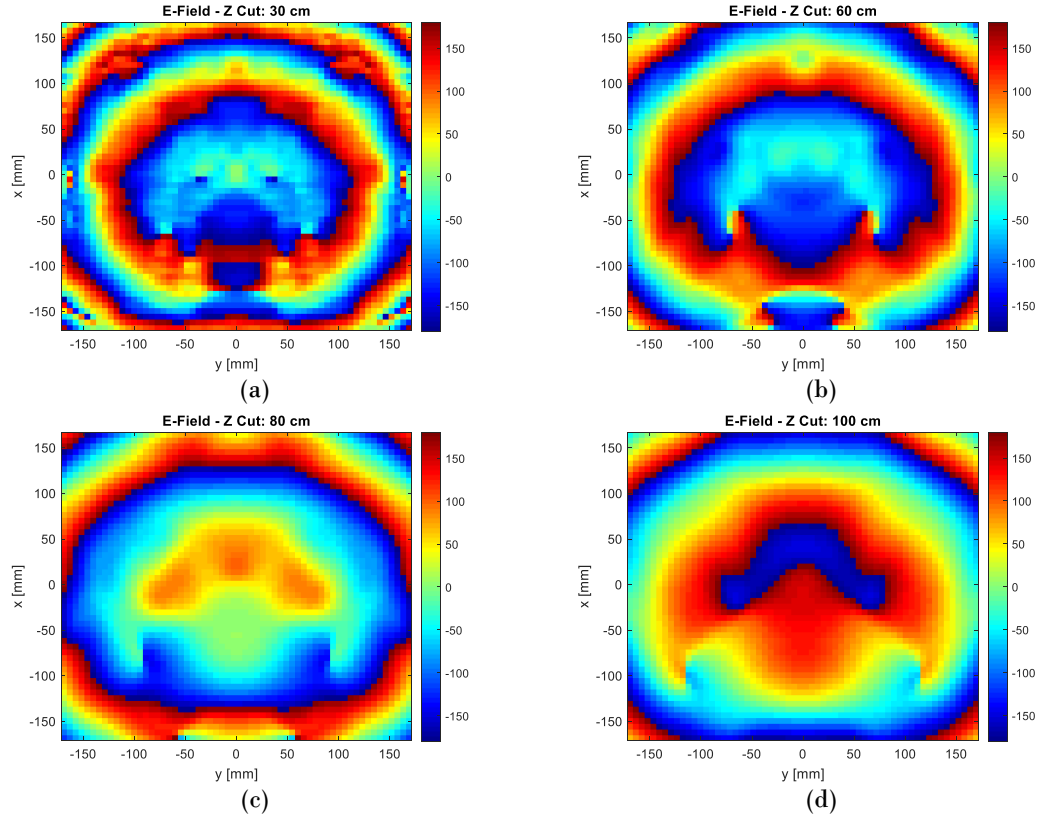

Fig. 5.41. - Design 28 GHz One-Layer – Starting point. E-Field Phase – Z Cuts. Y-Polarization: (a) z=30 cm; (b) z=60 cm; (c) z=80 mm; (d) z=100 cm.

Another detail observed in these figures is that is a displacement of the beam. Theoretically, in the planes shown in Fig. 5.40 the main beam should be at the center of each plane. However, it is observed how the beam heels slightly downwards, which

means that as it moves away from the reflector, the quiet zone moves to negative positions in x. It is possible to readjust this beam by calculating the drift angle (θ_d) and rotating the structure (reflector and feed) at the ratio of this angle. The following optimization stages will alter this drift angle, so this readjustment is made once a definitive antenna model is available.

Finally, the size of the quiet zone along z axis is shown in Fig. 5.42. It is observed that it is not possible to obtain a quiet zone size at least 10 cm in any of the magnitude and phase cuts. On the surface, it is also far from reaching the 100 cm^2 target.

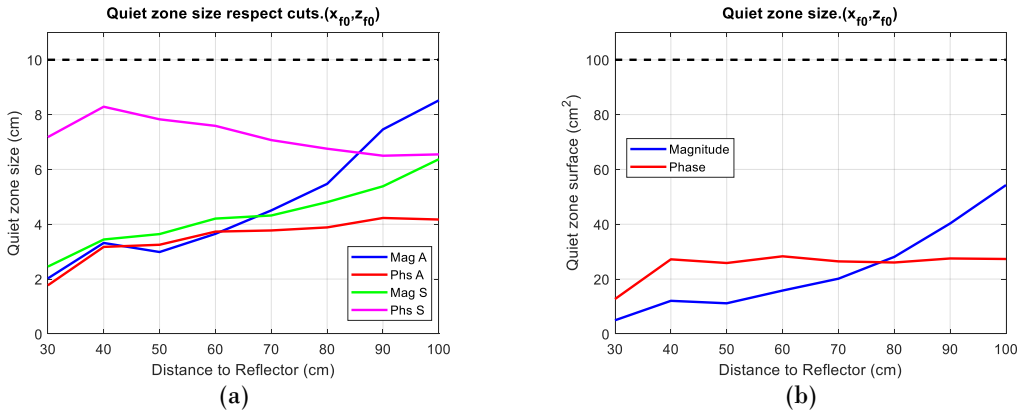

Fig. 5.42. - Design 28 GHz One-Layer – Starting point. Quiet zone size (a) and approximate surface (b).

5.5.1.1.- Feed Position.

To improve the results obtained so far, the first step is to optimize the position of the horn in relation with the reflector.

The increase and decrease of the distance between feed and reflector fundamentally affects the taper on the reflector surface, which then allows to provide a higher or lower level of E-Field to certain areas of the reflector. Since it is known that two important harmful effects for the E-Field are the dispersion in the edges and the distorted contribution in certain zones derived from high angles of incidence, it is important that these taper increases and therefore that the distance between feed and reflector is reduced.

However, it is necessary to consider another important factor to bring the feed closer. The phase distribution calculated in 5.4.1 is affected by this change in position, which may introduce additional distortion to the E-Field. Based on this, the position of the horn antenna will be modified by scaling the coordinates of the initial feed $(x_{f,0}, y_{f,0}, z_{f,0})$ making displacements on the normal straight line to the reflector that passes through the initial point. This allows to maintain the concentric form of the distribution of phases and therefore to minimize this distortion.

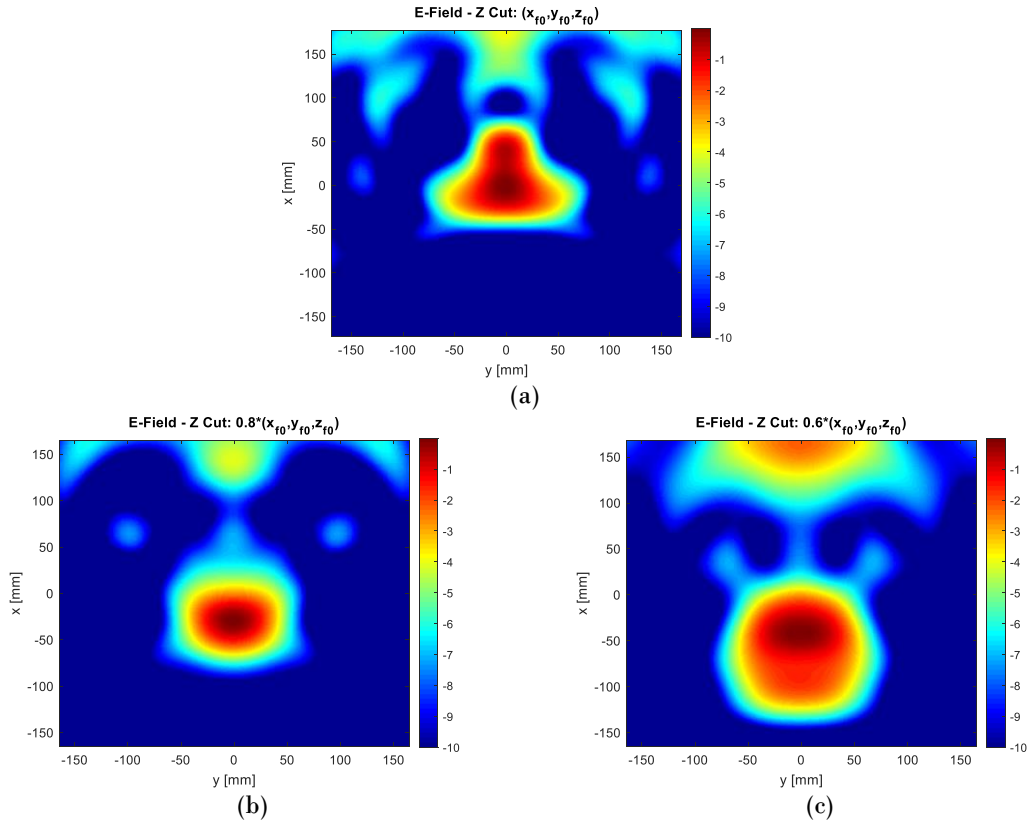

Fig. 5.43. - Design 28 GHz One layer – Feed position. E-Field Magnitude at z=90 cm: (a) Initial position (b) 80 % of initial position (c) 60 % of initial position;

Fig. 5.43, shows the behavior of the electric field at 90 cm from the reflector reducing by 20 and 40% the distance between feed and reflector. The angular condition $\theta_{incx} = \theta_0$ is maintained but θ_r is reduced to 25.5° so that the main beam is contained in the study area for all configurations.

It is clearly observed how the quiet zone acquires a more circular shape and therefore more adjusted to the requirements. In phase, also a slight improvement is observed with respect to the initial configuration.

This improvement also translates into an increase in the size of the quiet zone as shown in Fig. 5.44. Reducing the distance by 40 %, a quiet zone of at least 7 cm is achieved in both phase and amplitude cuts.

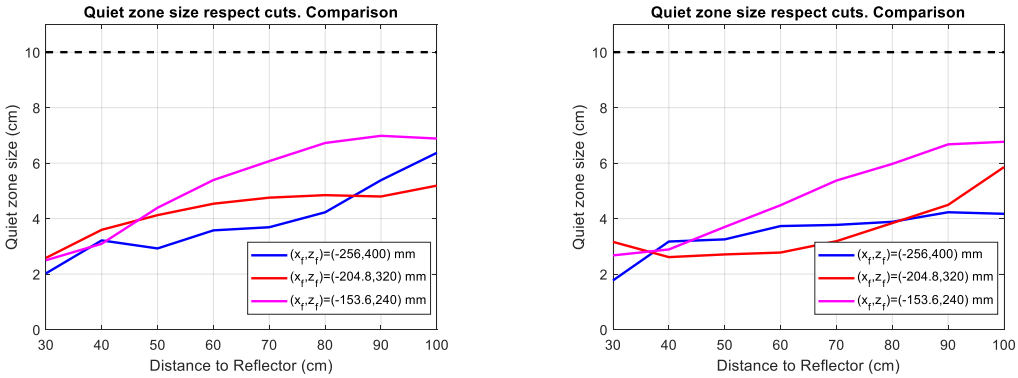

Fig. 5.44. - Design 28 GHz One layer – Feed position comparison. Minimum Quiet zone size in magnitude (a) and in phase (b).

Although everything seems to indicate that reducing the distance even more could achieve a better quiet zone, in this design appears a minimum limit that will be the far field distance of the horn. According to the feed study, the minimum distance to assume far field is 260 mm and placing the reflector in the near field of the horn could lead to a significant increase in the cross-polar and possible contamination in the quiet zone.

Having said this, the position of the feed will then be set to $(x_f, y_f, z_f) = (-153.6, 0.0, 240.0)$ mm. At this position the minimum distance to the reflector z_f is less than the farfield distance but very close to this limit, which indicates that the effect will be not relevant. However, this behavior will be studied in greater detail in the real model.

5.5.1.2.- Incidence Feed Angle (θ_{incx}).

In order to approach the 10 cm condition in quiet zone size, another characteristic parameter of the configuration is being optimized, in this case the angle θ_{incx} defined above. The E-Field is simulated in the study area, for horn inclination angles above and below the initial condition ($\theta_{incx} = \theta_0$). The results are shown in Fig. 5.45.

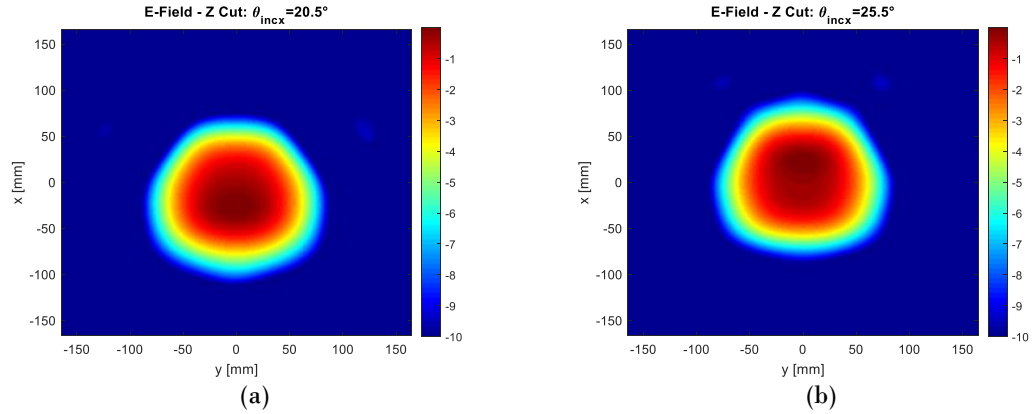

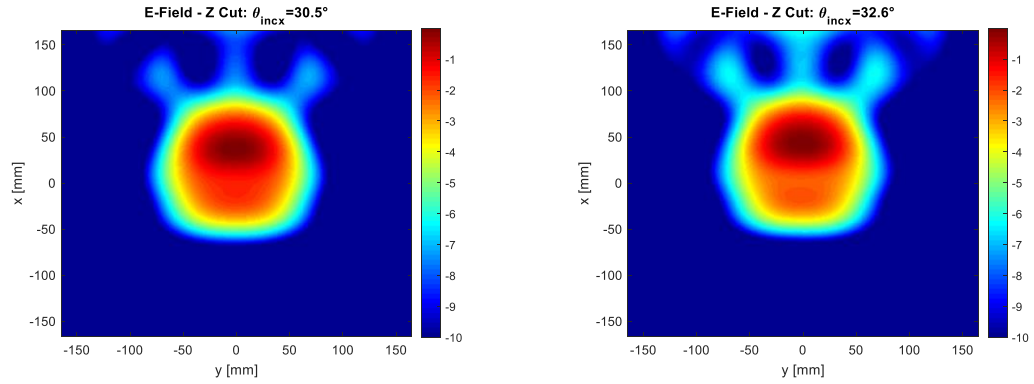

Fig. 5.45. - Design 28 GHz One layer – Incidence Feed Angle. E-Field Magnitude at z=90 cm. Y-Polarization: (a) $\theta_{incx} = \theta_0 - 10 = 20.5°$; (b) $\theta_{incx} = \theta_0 - 5 = 25.5°$; (c) $\theta_{incx} = \theta_0 = 30.5°$; (d) $\theta_{incx} = \theta_{in0x} = 32.6°$;

It is observed how the quiet zone has more uniform field level for smaller angles, i.e. if the horn points to lower areas of the reflector. This makes sense because by reducing the θ_{incx} angle, the E-Field level on the surface affects patches with lower angles of incidence, and therefore with a behavior more similar to that of the design curve with normal incidence. In addition to this, it allows concentrating more energy in the beam, thus reducing the field level outside the principal beam.

The size of the quiet zone also benefits for low angles as shown in Fig. 5.46. For a $\theta_{incx} = 20.5°$ the best quiet zone result is achieved, where the threshold of 10 cm in amplitude exceeded, and a size of at least 8 cm is reached in both components from 80 cm of the reflector.

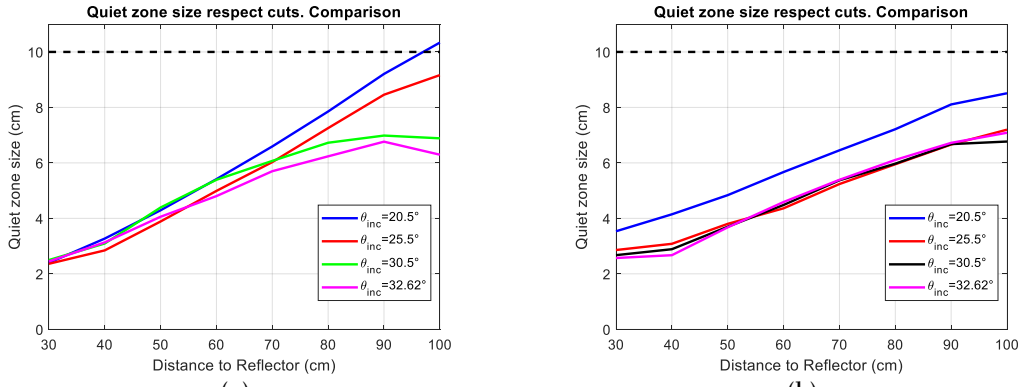

Fig. 5.46. - Design 28 GHz One layer – Incidence Feed Angle. Minimum Quiet zone size in magnitude (a) and in phase (b).

5.5.1.3.- Other optimization studies.

In the 28 GHz design, additional quiet zone studies have also been carried out, introducing elements to the reflectarray structure of modifying in block certain parameters in order to look for a better performance configuration.

After the optimization of the angle of incidence, the E-Field in its asymmetric cut of the configuration has an aspect as shown in Fig. 5.47 It is observed how the quiet zone near the reflector is small due, in part, to the influence that the E-Field of the feed relies on this zone. This effect is common in offset systems as mentioned above, since the combination of incident and reflected wave can generate an interference pattern that affects the near field and therefore the quiet zone.

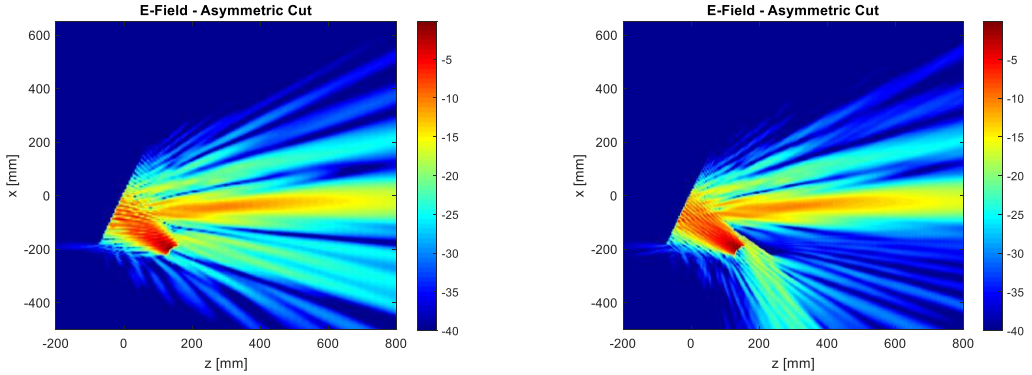

(a) (b)

Fig. 5.47. - Design 28 GHz One layer – Use of the PEC as a block: $(x_f, y_f, z_f) = (-153.6, 0.0, 240.0)\ mm.\theta_{incx} = 20.5°$. Asymmetric Cut: (a) Normal design; (b) Considering block.

From the point of view of the CST model, one of the solutions adopted consists of placing on the feed a PEC plane that reflects those incident waves that may affect the quiet zone, in addition to eliminating the dispersion on the lower part of the reflector. In parabolic reflector systems, the feed is not a limiting element in the distance from the reflector to the quiet zone.

Having said this, the PEC surface will be placed on a plane parallel to the feed and its size will increase towards the reflector. Fig. 5.48 shows the minimum quiet zone measured for amplitude and phase and different blocker sizes.

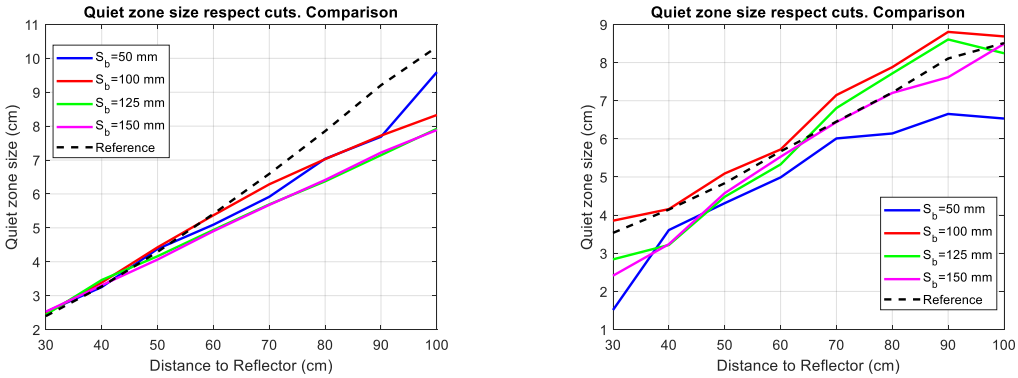

Fig. 5.48. - Design 28 GHz One layer – Blocker size. Minimum Quiet zone size in magnitude (a) and in phase (b).

Despite blocking the harmful field, this blocker fails to increase the size of the quiet zone as expected. In fact, as the size of the block increases, the waves reflected in the blocker generate an interference pattern that narrows the main beam of the field and thus the size of the quiet zone. In phase, there is also no substantial improvement in the size of the quiet zone.

Another possible option to increase the quiet zone is to place the feed in a position that does not generate any kind of blockage on the field reflected in reflector. Thus, a set of configurations is simulated where the x_f coordinate will be reduced towards more negative values, keeping the other two coordinates (z_f, y_f). Due to this displacement, the θ_{incx} angle will also vary in such a way that the feed maintains the pointing on the same zone of the reflector. This will not increase the dispersion at the bottom of the reflector.

Simulations of these configurations are made with and without a blocker on top of the feed, of a fixed size $S_b = 100$ mm. In Fig. 5.49 the results of the quiet zone measured both in amplitude and phase of study are measured.

It is observed how the still zone in all the designs is stagnant in a maximum size of 7 cm, far from the 10 cm that are obtained with the configuration after the study of θ_{incx} angle. The size of the quiet zone at a distance close to the reflector is like that achieved in the previous point, which does not imply an improvement over the design. However, it is worth mentioning that the use or not of blocker in these cases does not modify the behavior of the quiet zone.

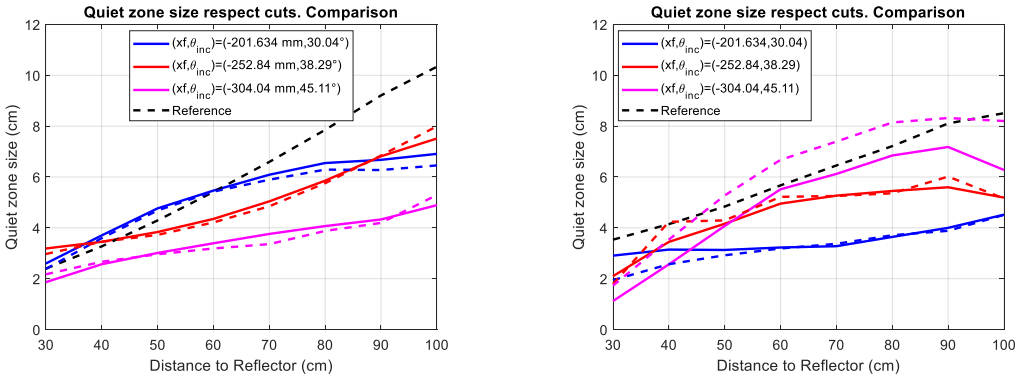

Fig. 5.49. - Design 28 GHz One layer – x_f modifying. Minimum Quiet zone size in magnitude (a) and in phase (b). In solid color, the designs with blocker($S_b = 100$ mm). Dotted, the designs without blocker.

On the basis of the results seen in both studies, they do not provide a significant improvement in the quiet zone behavior, therefore, the design resulting from the study analyzed in point 5.5.1.2.- is maintained as the optimum design.

5.5.1.4.- Definitive Design.

To finish with the optimization stage, the following point summarizes the characteristics of the final design, making a more detail study to those made in previous points. Table 5.10 shows an overview regarding the physical parameters in reflectarray structure.

In this point, it is intended to solve a previously mentioned effect: the deviation of the main beam. It has been seen that in the initial configuration, the main beam suffers both angular deviation and the point where it is generated.

In order to correct these effects, two new variables are defined in reflectarray structure shown in Fig. 5.50**.** First the rotation angle of the structure θ_r will be the design angle θ_0 plus a certain drift angle θ_d calculated as:

$$\theta_{\mathrm{d}} = \operatorname{asin}\left(\frac{E_{zmax} - E_{zmin}}{Z_{max}}\right) \tag{5.1}$$

Where E_{zmax} and E_{zmin} are the positions of maximum radiation point respect to the center in the E-Field planes at a distance Z_{max} and Z_{min} from the reflector respectively.

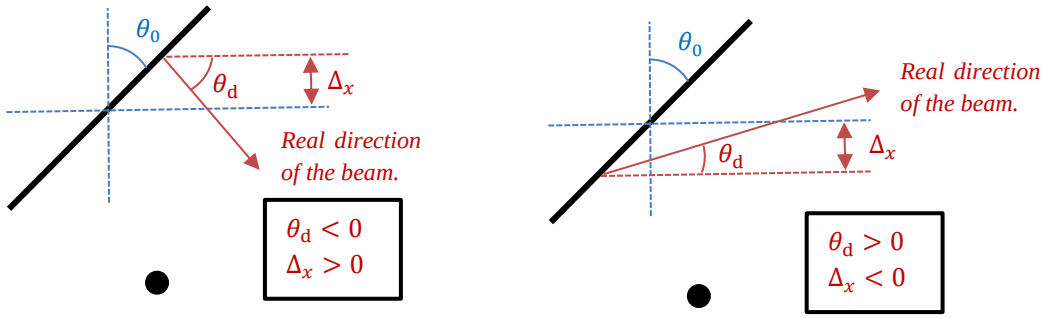

(a) (b)

Fig. 5.50. – Deviation of the main beam from the theoretical design. Possible cases of deviation: towards the upper (a) or lower (b) part of the reflector.

28 GHz Design One-Layer. Physical characteristics.		
Symbol	*Name/Units*	*Value*
f_0	*Desing frequency [GHz]*	*28.000*
λ_0	*Wavelength at design frequency [mm]*	*10.714*
P_x/P_y	*Periodicity of the cells in both axes [mm]*	*4.018*
h	*Height of the substrate [mm]*	*0.760*
N_x	*Number of cells in asymmetric cut*	*96*
N_y	*Number of cells in symmetric cut*	*82*
D_{tx}	*Total diameter of the reflector in Asymmetric cut [cm]*	*39.375*
D_{ty}	*Total diameter of the reflector in Asymmetric cut [cm]*	*33.750*
θ_r	*Real angle of radiation. Tilt to rotate the structure [º]*	*22.82*
Δ_x	*Deviation of the direction of maximum radiation on the Asymmetric Cut [mm]*	*-52.855*
(x_f, y_f, z_f)	*Coordinates of the feed respect the reflector [mm]*	*(153.6,0.0,240.0)*
D_x	*Equivalent diameter of the reflector in Asymmetric cut [cm]*	*33.927*
D_y	*Equivalent diameter of the reflector in Asymmetric cut [cm]*	*33.750*
F	*Focal distance [cm]*	*29.955*
C	*Clearance [mm]*	*53.193*
F/D_{tx}	*Relation between focal distance and size of the reflector*	*0.761*
$(\theta_{incx}, \theta_{incy})$	*Angles of inclination feed [º]*	(20.5,0.0)
(x_c, y_c)	*Coord. of the point in reflector where the feed is pointing [º]*	(−63.87,0.00)

Table 5.10. - Design 28 GHz One-Layer. Physical characteristics review.

On the other hand, the variable Δ_x is defined as the deviation in position of the main beam from the center of the reflector. Z_{min} distant plane will be the one closest to the reflector in margin of study, so it is possible to apply the approximation.

Regarding Z_{max} plane, this is chosen based on which distance the E-Field meets the requirements considered as quiet zone. Thus, in this design, $Z_{min} = 40\ cm$ and $Z_{max} = 90\ cm$ will taken to calculate θ_r and Δ_x show in Table 5.10.

In Table 5.10 also shows the characteristics of the structure expressed according to the equivalent parabolic model, where it is worth mentioning that the F/D_{tx} relation

obtained is close to the unit, unlike the designs using parabolic reflectors, which tend to have F/D_{tx} ratios of less than 0.5. The main reason for this lies in the vulnerability of the reflectarray as incidence angles with respect to the high feed.

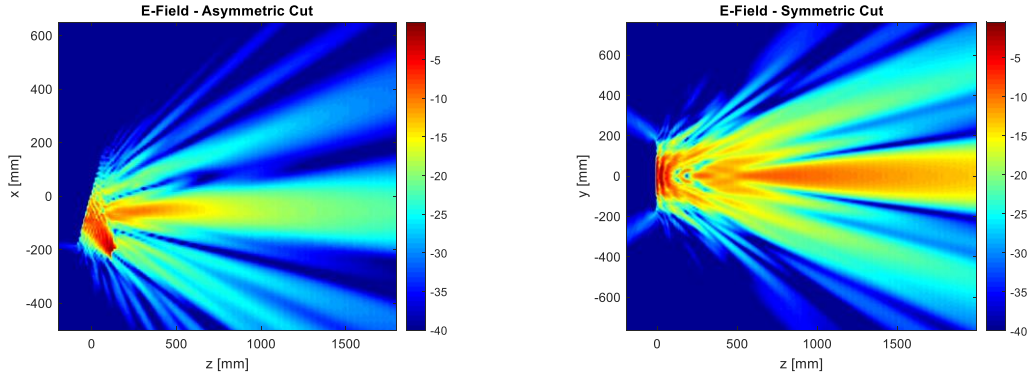

(a) (b)

Fig. 5.51. - Design 28 GHz One-Layer – Definitive Design. E-Field Magnitude. Y-Polarization: (a) Asymmetric Cut; (b) Symmetric Cut.

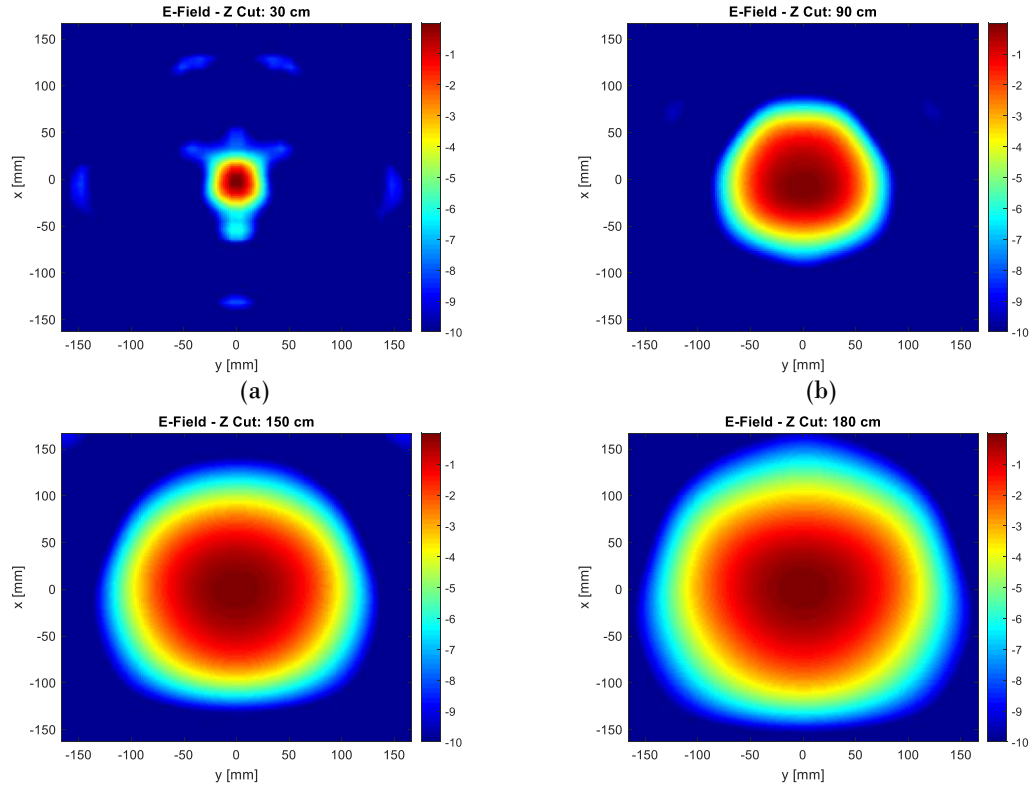

(a) (b) (c) (d)

Fig. 5.52. - Design 28 GHz One-Layer – Definitive Design. E-Field Magnitude – Z Cuts. Y-Polarization: (a) z=30 cm; (b) z=90 cm; (c) z=150 mm; (d) z=180 cm.

Fig. 5.51 shows the cuts in the final design. Making a comparison with the initial configuration, it is observed how the distortion on the edges is considerably reduced and it is obtained a main beam that increases its sizes when moving away from the reflector as corroborated in Fig. 5.52. Both in amplitude and phase (Fig. 5.53) can concentrate the E-Field on a quasi-circular zone.

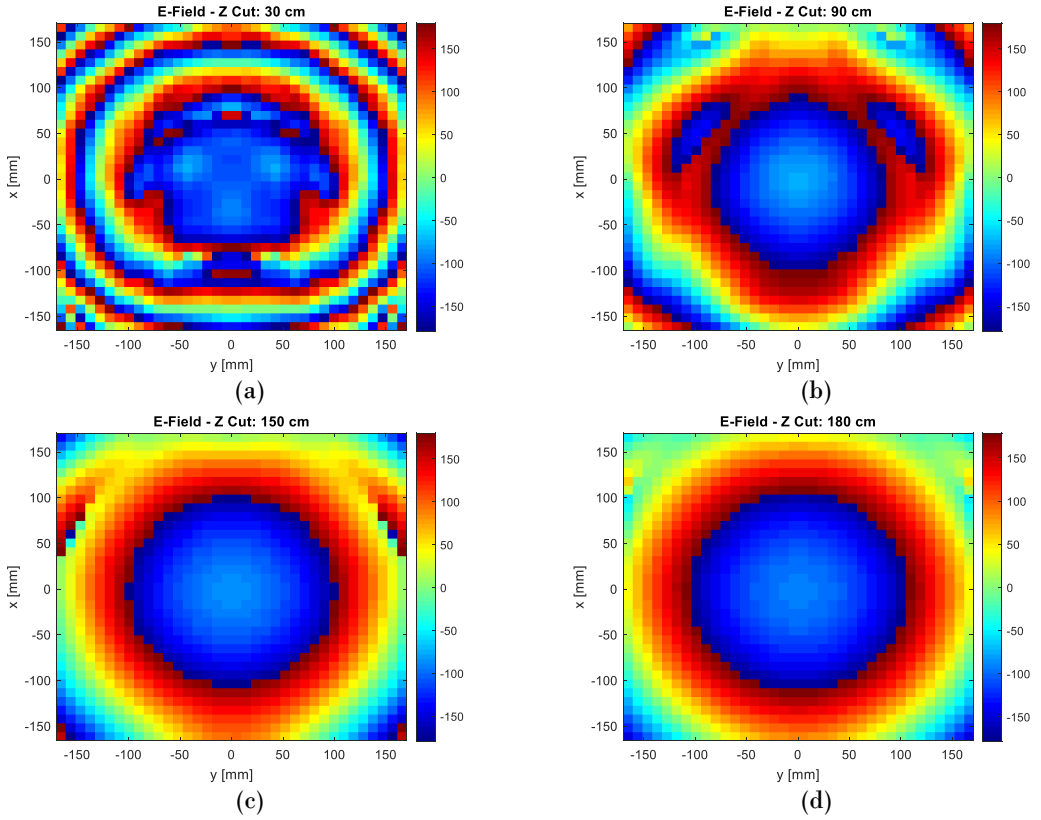

Fig. 5.53. - Design 28 GHz One-Layer – Definitive Design. E-Field Magnitude – Z Cuts. Y-Polarization: (a) z=30 cm; (b) z=90 cm; (c) z=150 mm; (d) z=180 cm.

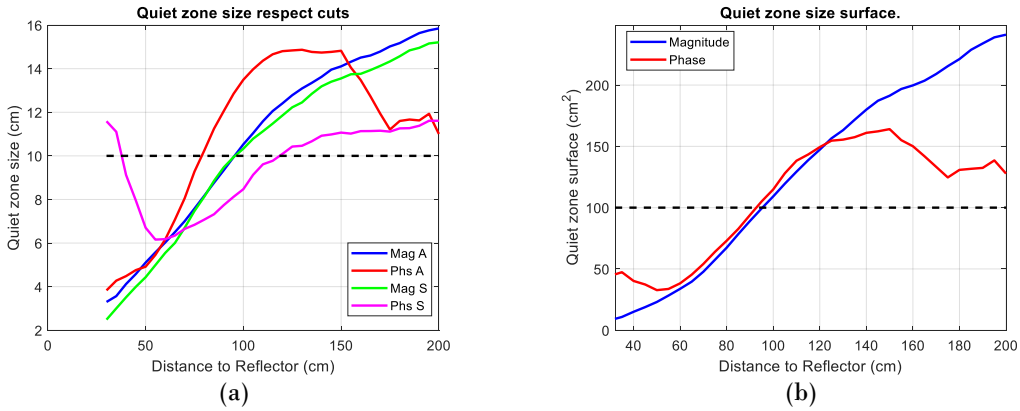

Fig. 5.54. - Design 28 GHz One-Layer – Starting point. Quiet zone size (a) and approximate surface (b).

According to Fig. 5.54, it is possible to calculate the distance at which a quiet zone adjusted to the requirements is obtained, for both components and assuming the measured size or approximate surface. These characteristics are reflected in Table 5.11**.** In addition to this, from 140 cm the quiet zone area has a minimum size of 11 cm in all cuts.

In view of these results, it is corroborated that it is possible to obtain a quiet zone adjusted to the requirements on the X and Y axes, but not so on the distance to the reflector that will be greater than the 500 mm marked as initial requirement.

	Amplitude	*Phase*
QZ Measured [cm]	*[90,100]*	*[110,120]*
Ap. Surface [cm^2]	*[90,100]*	*[90,100]*

Table 5.11. - Design 28 GHz One-Layer. Location of the quiet zone respect the center of the reflector.

5.5.2.- Design 28 GHz Two-Layer.

Regarding the multilayer design of this project, Table 5.12 describes the different diameters that characterize the reflector, according to Fig. 5.38 having taken as reference the characteristics of the design one layer, it is observed how the diameters are very similar respect to the previous design.

Reflector characteristics	
Diameter of the reflector in Asymmetric cut - $\boldsymbol{D_{px}}$ [mm]	*385.714*
Diameter of the reflector in Symmetric cut - $\boldsymbol{D_{py}}$ [mm]	*332.143*
Total diameter of the reflector in Asymmetric cut - $\boldsymbol{D_{tx}}$ [mm]	*396.429*
Total diameter of the reflector in Asymmetric cut - $\boldsymbol{D_{ty}}$ [mm]	*342.857*
Equivalent diameter of the reflector in Asymmetric cut - $\boldsymbol{D_x}$ [mm]	*341.574*
Equivalent diameter of the reflector in Asymmetric cut - $\boldsymbol{D_y}$ [mm]	*342.857*

Table 5.12. - Design 28 GHz Two-layer. Diameter and dimensions of the reflector.

However, certain discrepancies will be observed with respect to the behavior of the initial configuration. In Fig. 5.55 it is observed that the E-Field in both cuts is dispersed more than the one-layer design. As in the previous case, the distance from the feed causes a strong component at the edges of the reflector and therefore greater dispersion.

The quiet zone can be seen more clearly in the cuts on the Z axis, where a very deformed quiet zone is clearly observed both in amplitude (Fig. 5.56) and in phase (Fig. 5.57), although in the latter a certain improvement can be perceived regarding the design of one layer. In this design also appears a slight drift angle, which will be corrected in the final design.

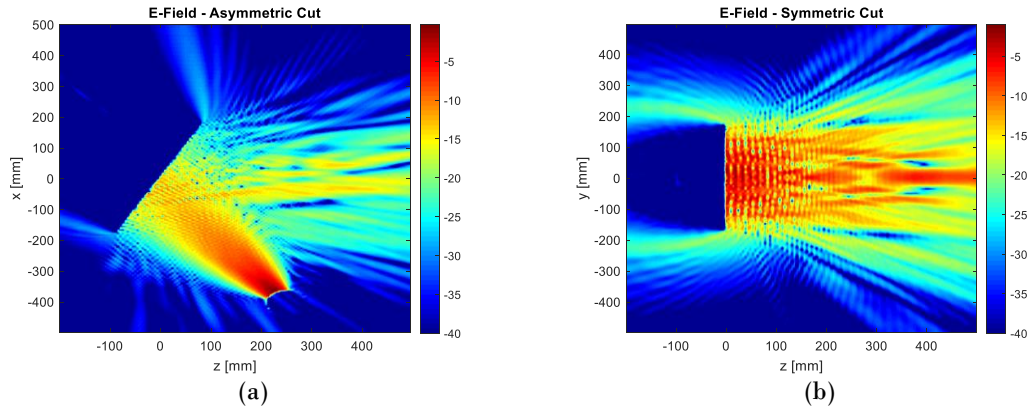

(a) (b)

Fig. 5.55. - Design 28 GHz Two-layer – Starting point. E-Field Magnitude. Y-Polarization: (a) Asymmetric Cut; (b) Symmetric Cut.

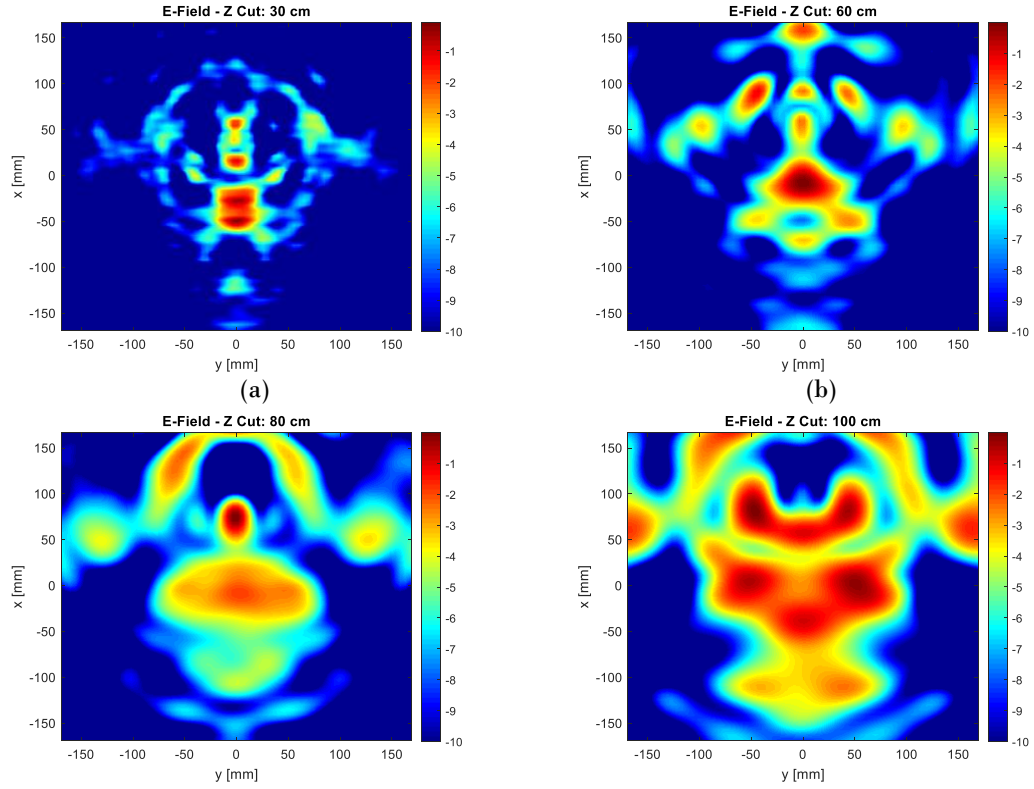

(a) (b) (c) (d)

Fig. 5.56. - Design 28 GHz Two-layer – Starting point. E-Field Magnitude – Z Cuts. Y-Polarization: (a) z=30 cm; (b) z=60 cm; (c) z=80 mm; (d) z=100 cm.

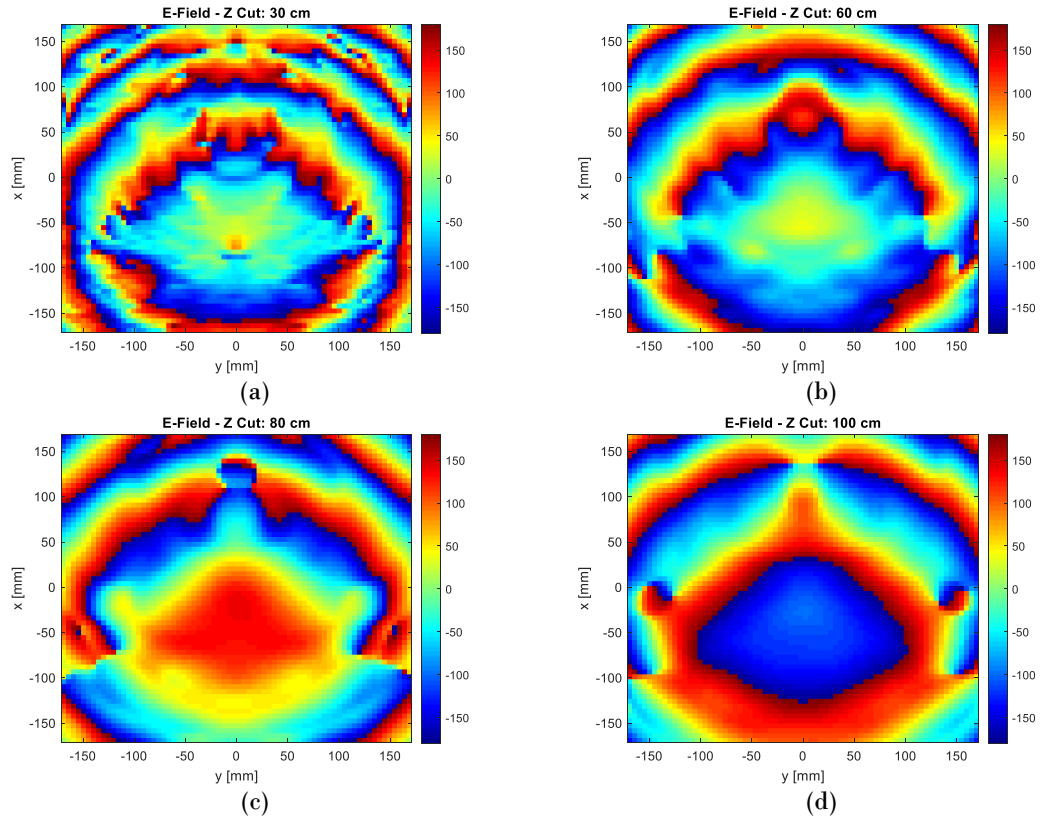

Fig. 5.57. - Design 28 GHz Two-layer – Starting point. E-Field Phase – Z Cuts. Y-Polarization: (a) z=30 cm; (b) z=60 cm; (c) z=80 mm; (d) z=100 cm.

Despite it, regarding the quiet zone size (Fig. 5.58(a)), it can be observed as for distances near to 1 meter, a size of quiet zone near to the 10 cm requirement is obtained in some cuts. Based on the shape of the electric field seen above, this measurement is unrepresentative, so it is inherent in drawing the relevant conclusions. The equivalent Surface however (Fig. 5.58(b)) follows the line seen in the previous figures, showing a small quiet zone Surface in all cuts.

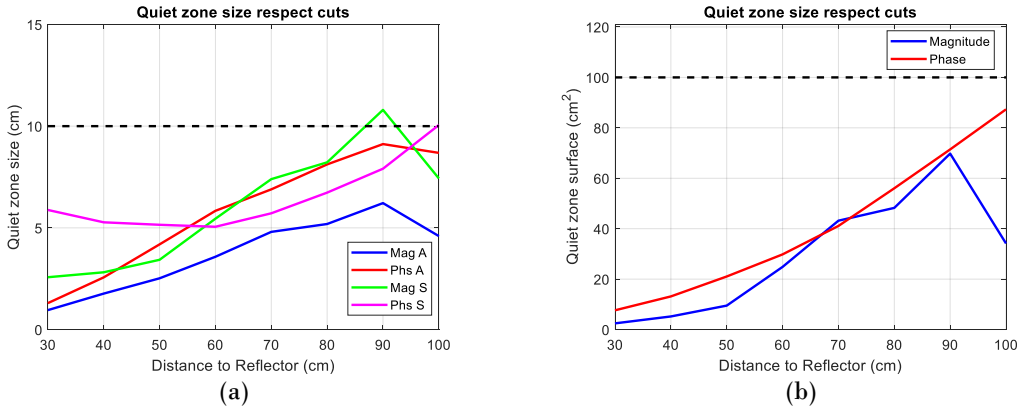

Fig. 5.58. - Design 28 GHz Two-layer – Starting point. Quiet zone size (a) and approximate surface (b).

5.5.2.1.- Feed Position.

In order to improve the design, the distance between feed and reflector will be modified following a process analogous to the previous case. As it happens with the design one layer, when reducing this distance, the quiet zone acquires a more regular size. In comparison with the previous design, it is appreciated a higher level of E-Field outside the studied quiet zone, which a priori will not suppose any problem.

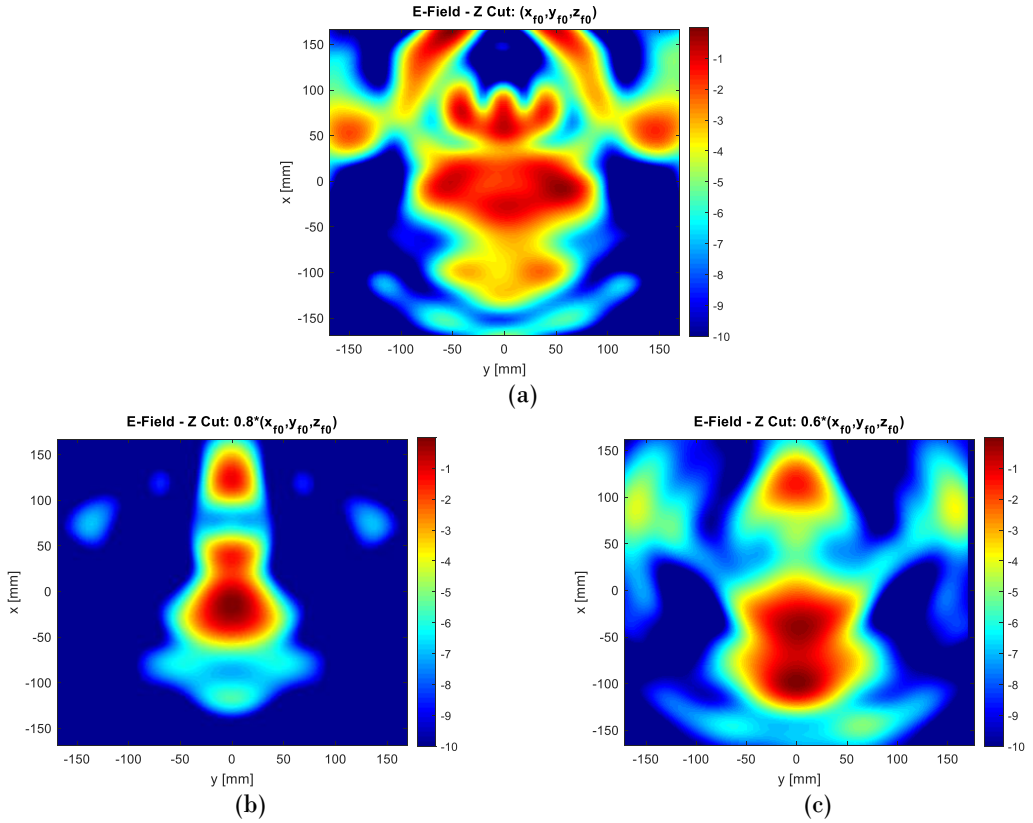

Fig. 5.59. - Design 28 GHz Two layer – Feed position. E-Field Magnitude at z=90 cm: (a) Initial position (b) 80 % of initial position (c) 60 % of initial position;

As far the size in the Fig. 5.60 is observed that from 90 cm a quiet zone at least 8 cm is obtained in both components. In comparison with the design to a layer, it supposes an improvement, especially in the phase of this electric field.

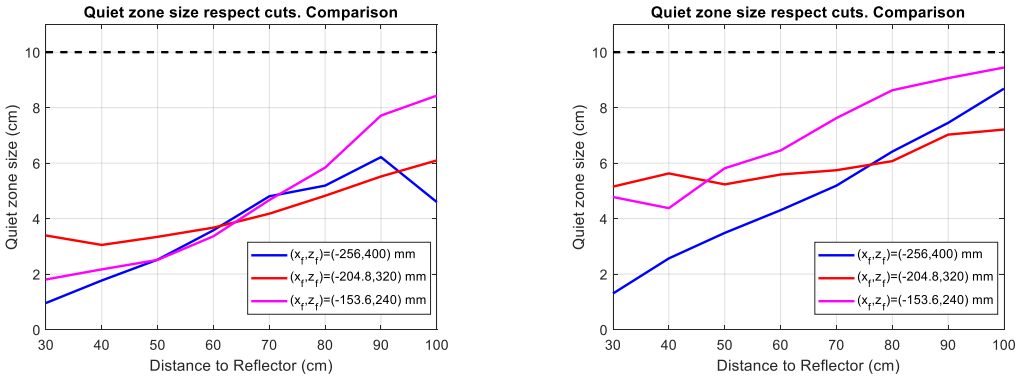

Fig. 5.60. - Design 28 GHz Two layer – Feed position comparison. Minimum Quiet zone size in magnitude (a) and in phase (b).

Everything also indicates that by reducing the distance between the feed and the reflector, the quiet zone improves, however in this case again appears the farfield limit mentioned above. This is because the minimum possible distance between both elements will be $(x_f, y_f, z_f) = (-153.6, 0.0, 240.0)$.

5.5.2.2.- Incidence Feed Angle (θ_{incx}).

As was done in the previous designs, in the next point is intended to vary the angle of inclination θ_{incx} to improve the behavior of the quiet zone. Fig. 5.61 shows the E-Field cuts at z=90 mm for four different angles chosen in an analogous way to the previous design.

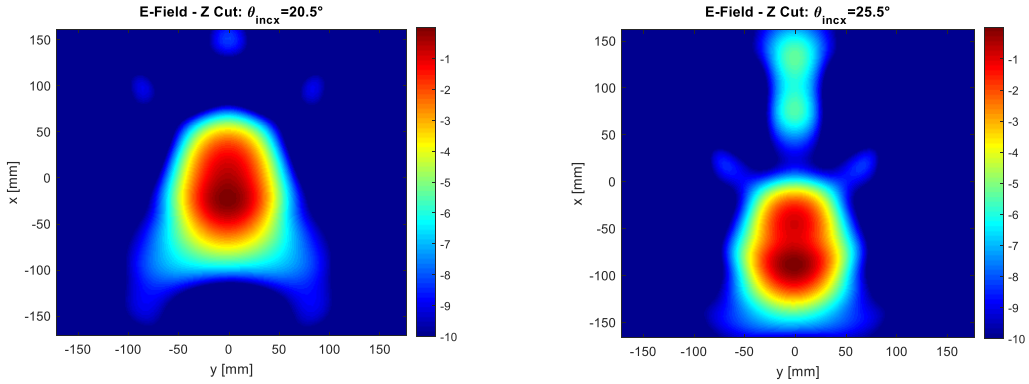

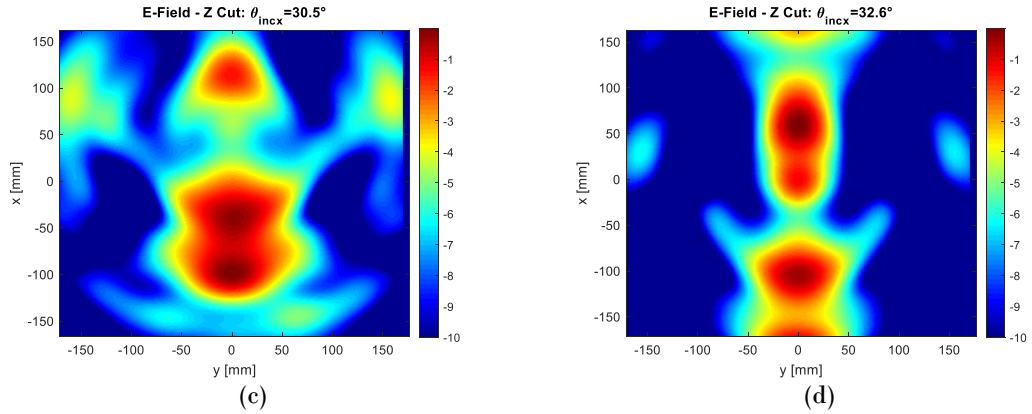

Fig. 5.61. - Design 28 GHz Two layer – Incidence Feed Angle. E-Field Magnitude at z=90 cm. Y-Polarization: (a) $\theta_{incx} = \theta_0 - 10 = 20.5°$; (b) $\theta_{incx} = \theta_0 - 5 = 25.5°$; (c) $\theta_{incx} = \theta_0 = 30.5°$; (d) $\theta_{incx} = \theta_{in0x} = 32.6°$;

For the two smaller angles, the quiet zone takes on a more elliptic shape and has a lower field level outside of it. In contrast, for upper angles, the quiet zone increases in size although pollution will also increase in its surroundings. In fact, when the horn points exactly at the center of the reflector (θ_{in0x}), the E-Field beam is strongly deformed.

A priori it might be interesting to choose a low angle of inclination because there is a sharper quiet zone. However, in order to make such a decision it is necessary to know what size of quiet zone the minimum for these angles is (Fig. 5.62).

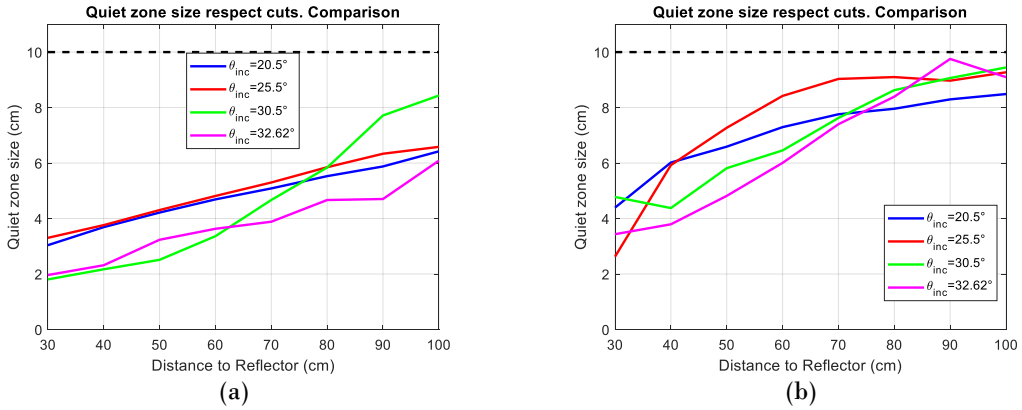

Fig. 5.62. - Design 28 GHz Two layer – Incidence Feed Angle. Minimum Quiet zone size in magnitude (a) and in phase (b).

In amplitude, it is observed a considerable loss of quiet zone (approximately half) in comparison with the initial configuration ($\theta_{incx} = 30.5$) in the distances of greater size. The fact of considering small angles slightly improves the characteristics in phase, although they do not allow to satisfy the requirements in size.

It is concluded that both for angles above and below the initial condition, improve the size of the quiet zone for the phased component in exchange for significantly reducing

the size in amplitude. Therefore, for the final design $\theta_{incx} = 30.5$ will be considered as the optimum angle.

After studying the angle of inclination of the horn, in the area under study it is possible to reach a quiet zone of at least 8 cm between 90 cm from the reflector, a value that is not enough to comply with the requirements. Given that the use of blockers or abrupt modifications of the feed position are not effective (see point 5.5.1.3), this configuration will be taken as a definitive design. In the next point, an exhaustive study of the same will be carried out.

5.5.2.3.- Definitive Design.

With the variables considered at this stage fixed, it is ready to summarize the characteristics of the design, shown in Table 5.13. It is observed how the parameters obtained are very similar to the design of a layer given the initial premises marked in reflectarray structure, as well as the results obtained in this stage.

28 GHz Design Two-Layer. Physical characteristics.		
Symbol	*Name/Units*	*Value*
f_0	*Desing frequency [GHz]*	*28.000*
λ_0	*Wavelength at design frequency [mm]*	*10.714*
P_x/P_y	*Periodicity of the cells in both axes [mm]*	*5.357*
h_1	*Height of the substrate - First layer [mm]*	*0.760*
h_2	*Height of the substrate - Second layer [mm]*	*1.560*
N_x	*Number of cells in asymmetric cut*	*72*
N_y	*Number of cells in symmetric cut*	*62*
D_{tx}	*Total diameter of the reflector in Asymmetric cut [cm]*	*39.643*
D_{ty}/D_y	*Total diameter of the reflector in Asymmetric cut [cm]*	*34.286*
θ_r	*Real angle of radiation. Tilt to rotate the structure [º]*	*26.19*
Δ_x	*Deviation of the direction of maximum radiation on the Asymmetric Cut [mm]*	*-40.496*
(x_f, y_f, z_f)	*Coordinates of the feed respect the reflector [mm]*	*(153.6,0.0,240.0)*
D_x	*Equivalent diameter of the reflector in Asymmetric cut [cm]*	*35.574*
F	*Focal distance [cm]*	*31.953*
C	*Clearance [mm]*	*65.873*
F/D_{tx}	*Relation between focal distance and size of the reflector*	*0.806*
$(\theta_{incx}, \theta_{incy})$	*Angles of inclination feed [º]*	(30.5,0.0)
(x_c, y_c)	*Coord. of the point in reflector where the feed is pointing [º]*	(−12.23,0.00)

Table 5.13. - Design 28 GHz Two layer. Physical characteristics overview.

One of the aspects that have been described is that the size of the Quiet zone increases due to the distance to the reflector, although it does not reach 10 cm in the first 100 cm. That is why at this point the study is extended to 2 meters in order to calculate the minimum distance to the reflector to meet the requirements of the quiet zone.

The main cuts of this design are shown in Fig. 5.63. Notice a greater dispersion of the electric field compared to the final design at a layer, slightly larger in its symmetrical

cut. This fact can be corroborated in the cuts on the Z axis (Fig. 5.64) where it is observed how it is necessary to move away from the reflector distances above a meter so that the quiet zone has an acceptable shape. Regarding phase (Fig. 5.65), it is possible to generate a quiet zone with a more acceptable shape at 90 cm from the reflector.

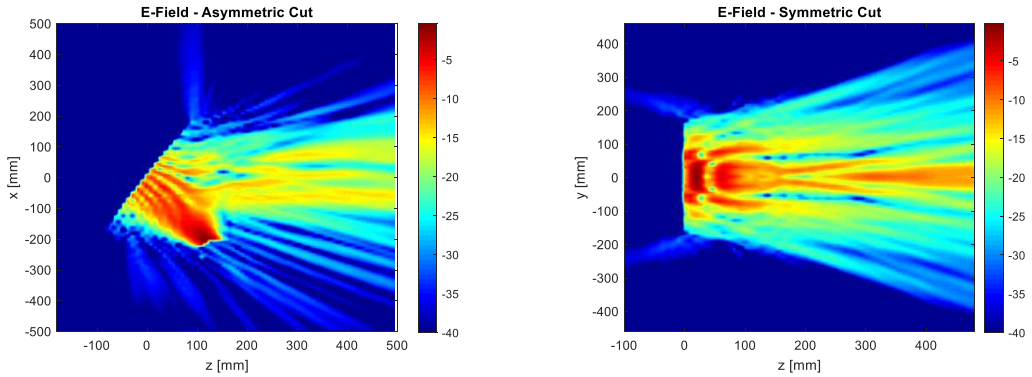

(a) (b)

Fig. 5.63. - Design 28 GHz Two layer– Definitive Design. E-Field Magnitude. Y-Polarization: (a) Asymmetric Cut; (b) Symmetric Cut.

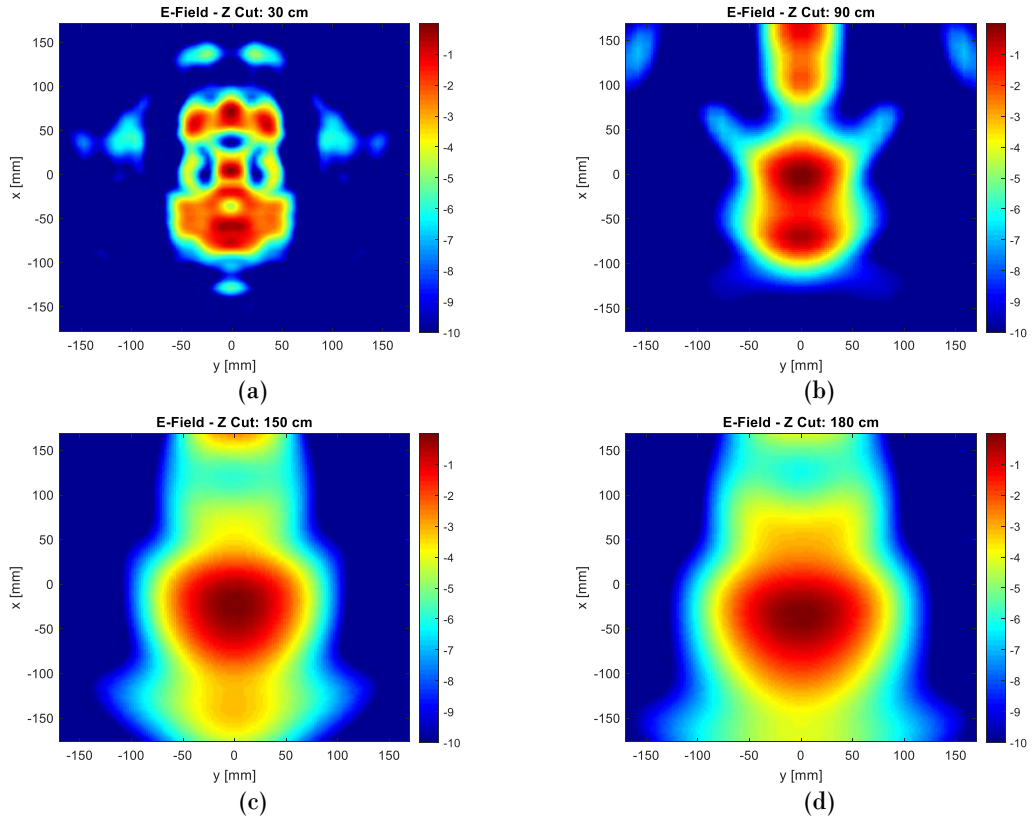

(a) (b) (c) (d)

Fig. 5.64. - Design 28 GHz Two layers – Definitive Design. E-Field Magnitude – Z Cuts. Y-Polarization: (a) z=30 cm; (b) z=90 cm; (c) z=150 mm; (d) z=180 cm.

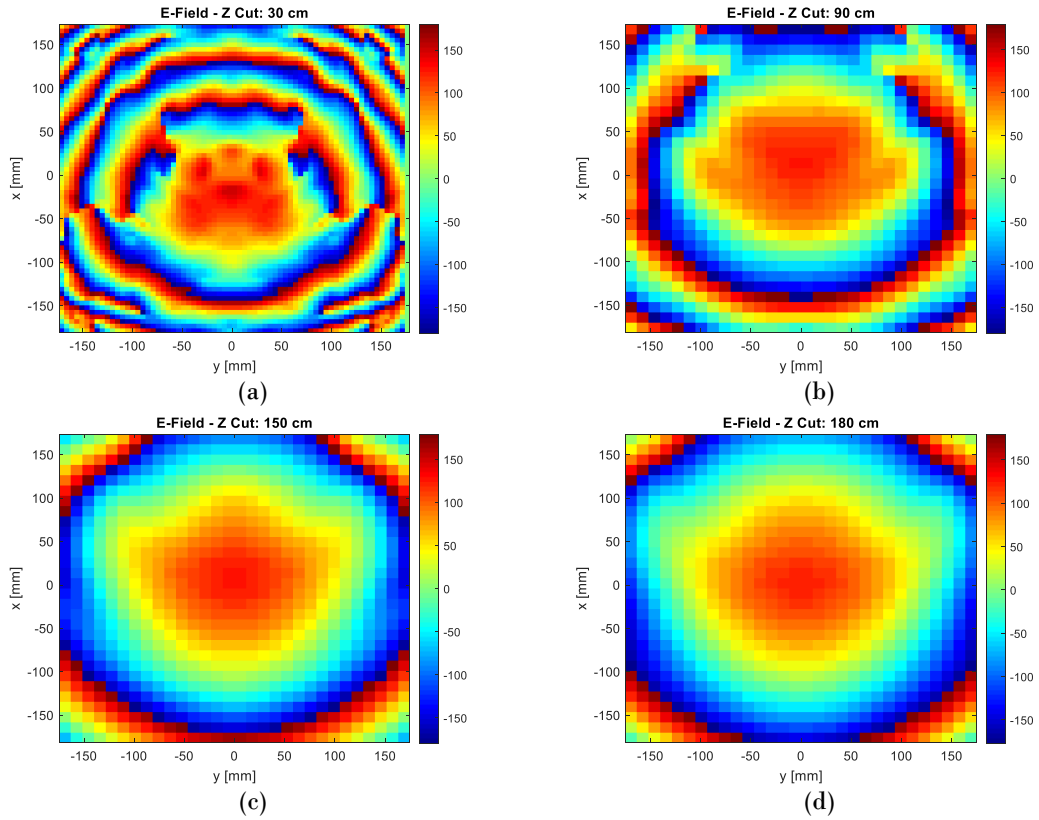

Fig. 5.65. - Design 28 GHz Two layer – Definitive Design. E-Field Magnitude – Z Cuts. Y-Polarization: (a) z=30 cm; (b) z=90 cm; (c) z=150 mm; (d) z=180 cm.

Concerning the size of the calculated quiet zone (Fig. 5.66), it is observed that in amplitude the main cuts have a very uneven size up to distances above the meter. Somewhat predictable due to the elliptical shape than could be seen in Fig. 5.64. In phase, a better behavior is achieved, being able to comply with the characteristics at distances below one meter. As in the previous case, on approximate surface these minimum distances will be slightly reduced. For distances above 2 meters, both in phase and amplitude, the quiet zone continues to increase in symmetrical cut and stagnates in asymmetrical cut.

Table 5.11 will detail the position of the quiet zone according to these requirements. Making a comparison with the one-layer design, it is observed how the quiet zone in phase approaches the reflector while in amplitude it moves considerably away.

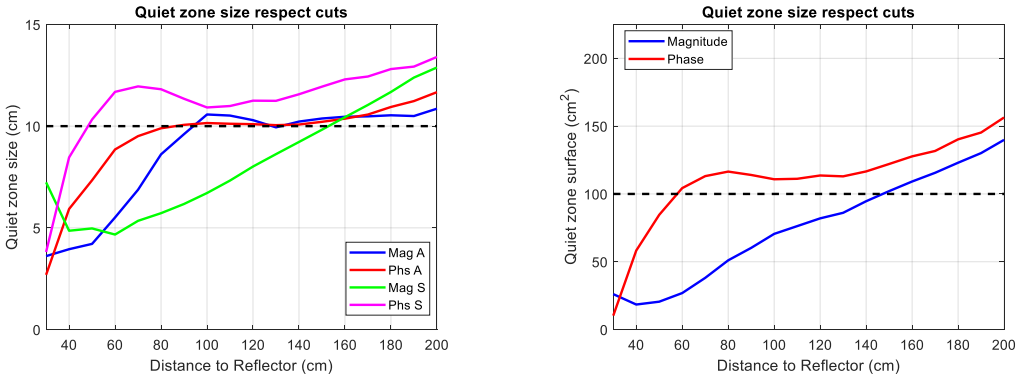

Fig. 5.66. - Design 28 GHz two-layers – Starting point. Quiet zone size (a) and approximate surface (b).

	Amplitude	*Phase*
QZ Measured [cm]	*[150,160]*	*[80,90]*
Ap. Surface [cm²]	*[150,160]*	*[60,70]*

Table 5.14. - Design 28 GHz two-layers. Location of the quiet zone respect the center of the reflector.

5.5.3.- Design 1.7 GHz.

For the 1.7 GHz design, the characteristic reflector diameters are shown in Table 5.15.When working with higher wavelength (176.47 mm) it will be enough to leave a dielectric frame of a half the periodicity (44.117 mm). This can slightly reduce the overall reflector dimensions, as well as its effect on the generated field. Regarding the area under study, it will be between 1 and 3 meters, placing E-Field monitors every 20 cm. As with the previous designs, an angle of inclination $\theta_{incx} = \theta_0$ will be used first.

Reflector characteristics	
Diameter of the reflector in Asymmetric cut - $\boldsymbol{D_{px}}$ *[cm]*	*176.471*
Diameter of the reflector in Symmetric cut - $\boldsymbol{D_{py}}$ *[cm]*	*167.647*
Total diameter of the reflector in Asymmetric cut - $\boldsymbol{D_{tx}}$ *[cm]*	*185.294*
Total diameter of the reflector in Asymmetric cut - $\boldsymbol{D_{ty}}$ *[cm]*	*176.471*
Equivalent diameter of the reflector in Asymmetric cut - $\boldsymbol{D_x}$ *[cm]*	*174.120*
Equivalent diameter of the reflector in Asymmetric cut - $\boldsymbol{D_y}$ *[cm]*	*176.471*

Table 5.15. - Design 1.7 GHz One-Layer. Diameter and dimensions of the reflector.

In relation to the E-Field obtained by this initial configuration in its asymmetric and symmetric cuts (Fig. 5.67), a high dispersion in the edges of the reflector is observed as it happened in previous designs. Although in this case, already in the initial point it can be seen how the field is more focused on the area under study.

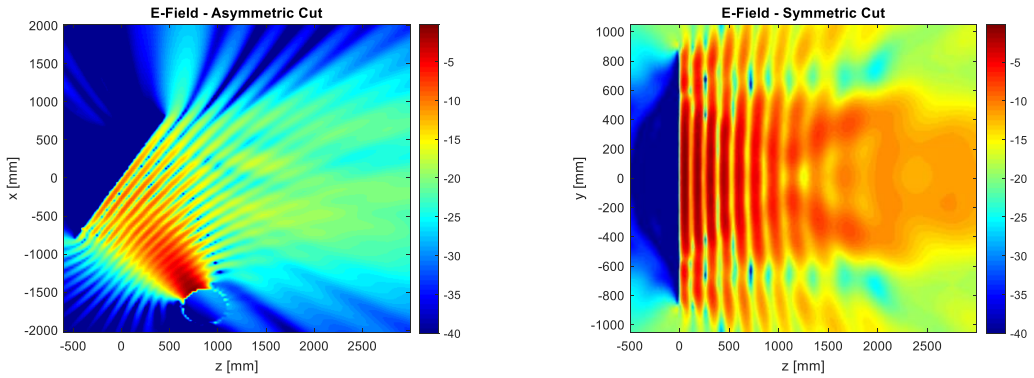

(a) (b)

Fig. 5.67. - Design 1.7 GHz One-Layer – Starting point. E-Field Magnitude. Y-Polarization: (a) Asymmetric Cut; (b) Symmetric Cut.

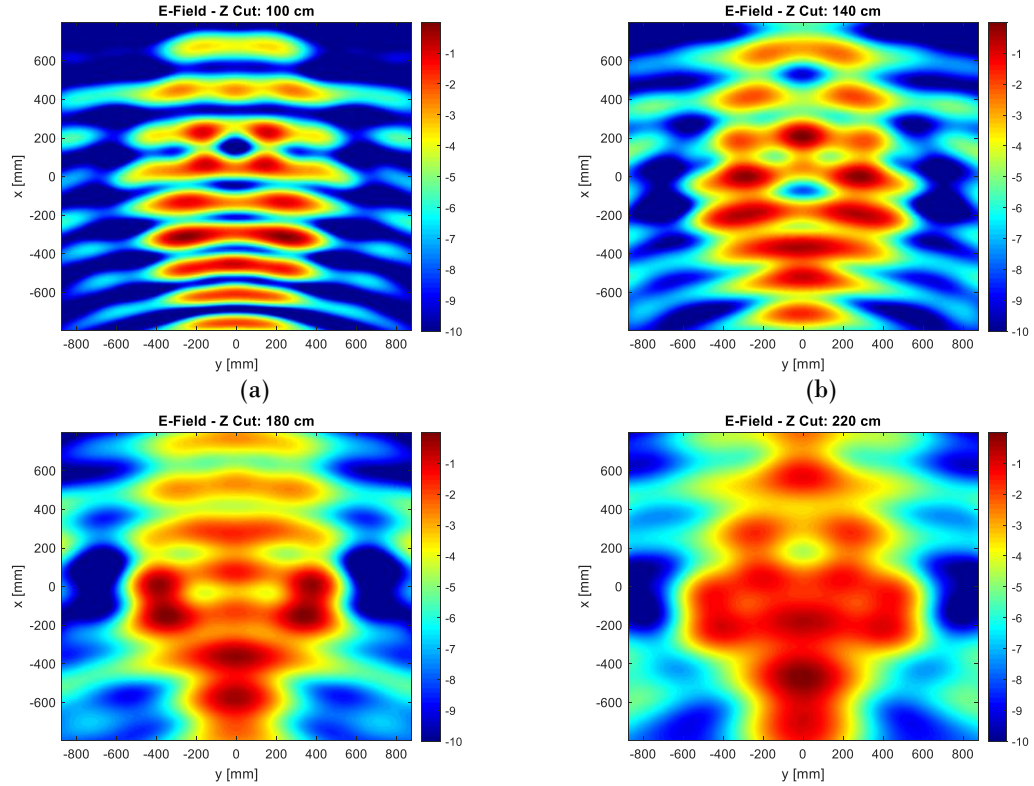

(a) (b)

(c) (d)

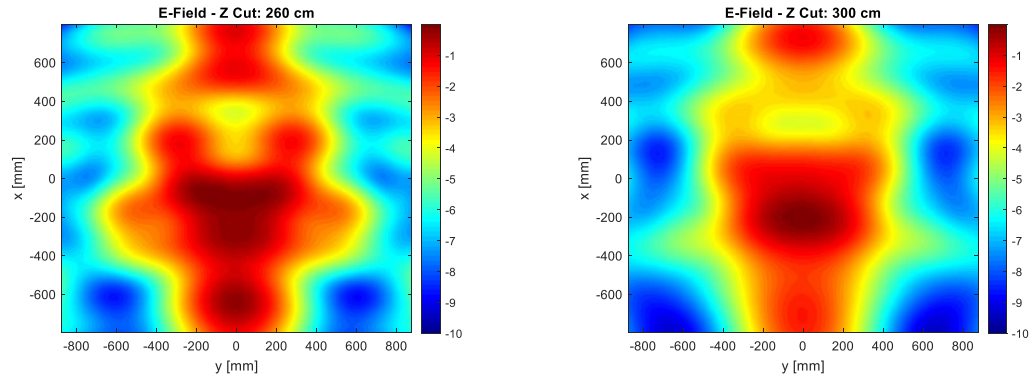

(e) (f)

Fig. 5.68. - Design 1.7 GHz One-Layer – Starting point. E-Field Magnitude – Z Cuts. Y-Polarization: (a) z=100 cm (b) z=140 cm (c) z=180 cm; (d) z=220 cm; (e) z=260 mm; (d) z=300 cm.

Respect the Z cuts (Fig. 5.68), the E-Field planes closer to the reflector suffer a strong distortion derived mainly from the interaction between the incident and reflected field on the reflector. From 220 cm this effect takes less force although the dispersion seen in Fig. 5.67 generates quiet zones with an irregular size and shape.

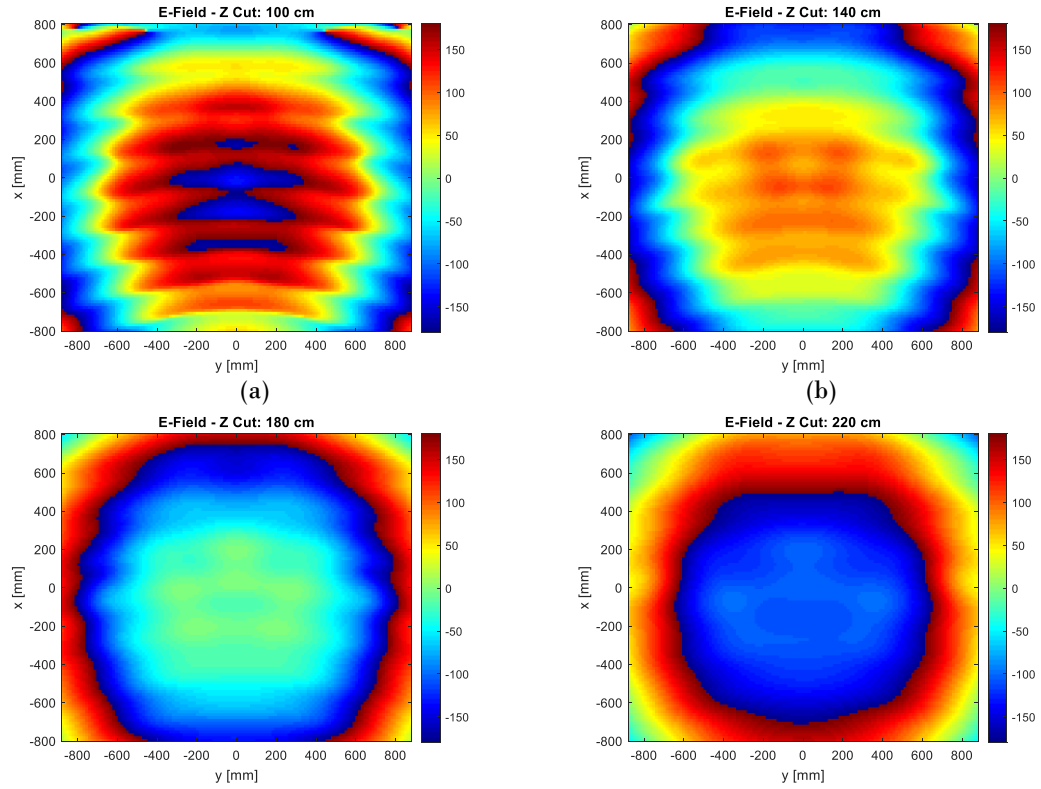

(a) (b) (c) (d)

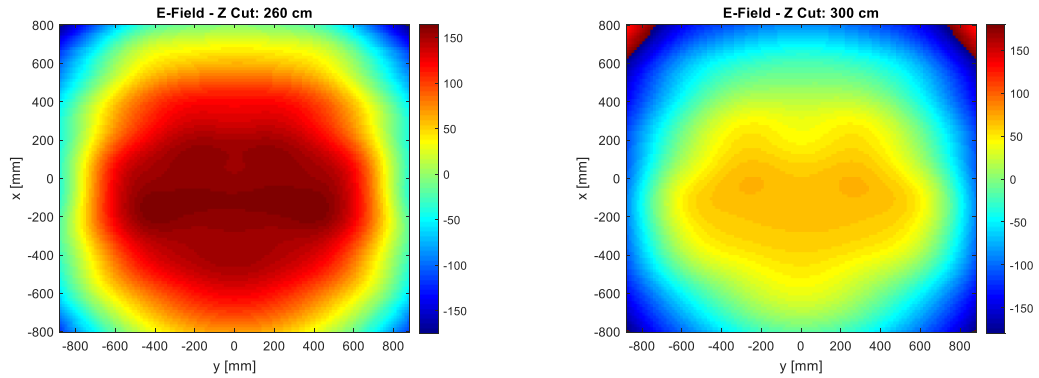

Fig. 5.69. - Design 1.7 GHz One-Layer – Starting point. E-Field Phase – Z Cuts. Y-Polarization: (a) z=100 cm (b) z=140 cm (c) z=180 cm; (d) z=220 cm; (e) z=260 mm; (d) z=300 cm.

Despite this, according to Fig. 5.69 , the phase presents a better behavior than in the previous designs. A distribution in concentric circles can be discerned with greater clarity. The quiet zone in phase, however, also acquires an irregular shape.

The quiet zone measured for this configuration (Fig. 5.70) reaches a size greater than 50 cm in all its cuts at a distance of approximately 230 cm. In terms of surface, the quiet zone adjusted to the requirements could start from 220 cm, where the quiet zone in magnitude is the limiting factor.

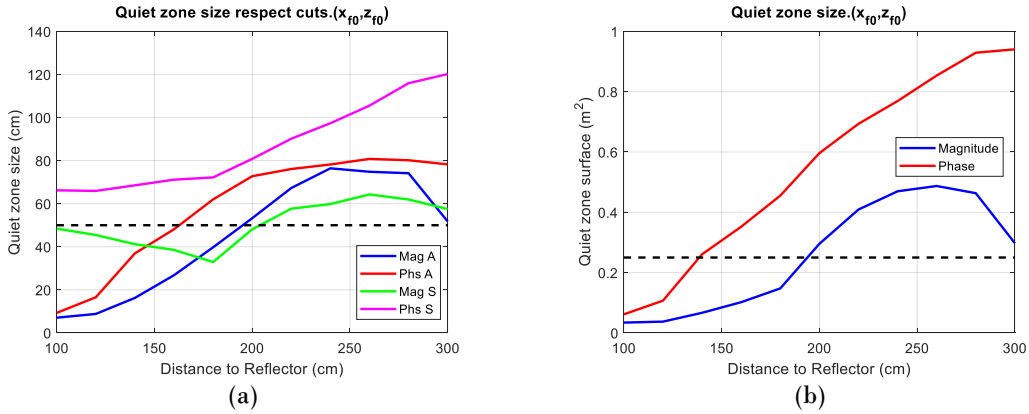

Fig. 5.70. - Design 1.7 GHz One-Layer – Starting point. Quiet zone size (a) and approximate surface (b).

5.5.3.1.- Feed Position.

It has been seen that the initial configuration has good performance in phase but its shape in magnitude is not the desired. For that reason and in an analogous way to the previous designs, it is arranged to modify the distance between the feed and the reflector in a proportional way, maintain the angle of pointing $\theta_{incx} = \theta_0$.

Taking as reference a plane 260 cm from the reflector, the E-Field is represented in Fig. 5.71. In magnitude, note that the size of the quiet zone increases by reducing the distance feed reflector, acquiring a more symmetrical quiet zone shape.

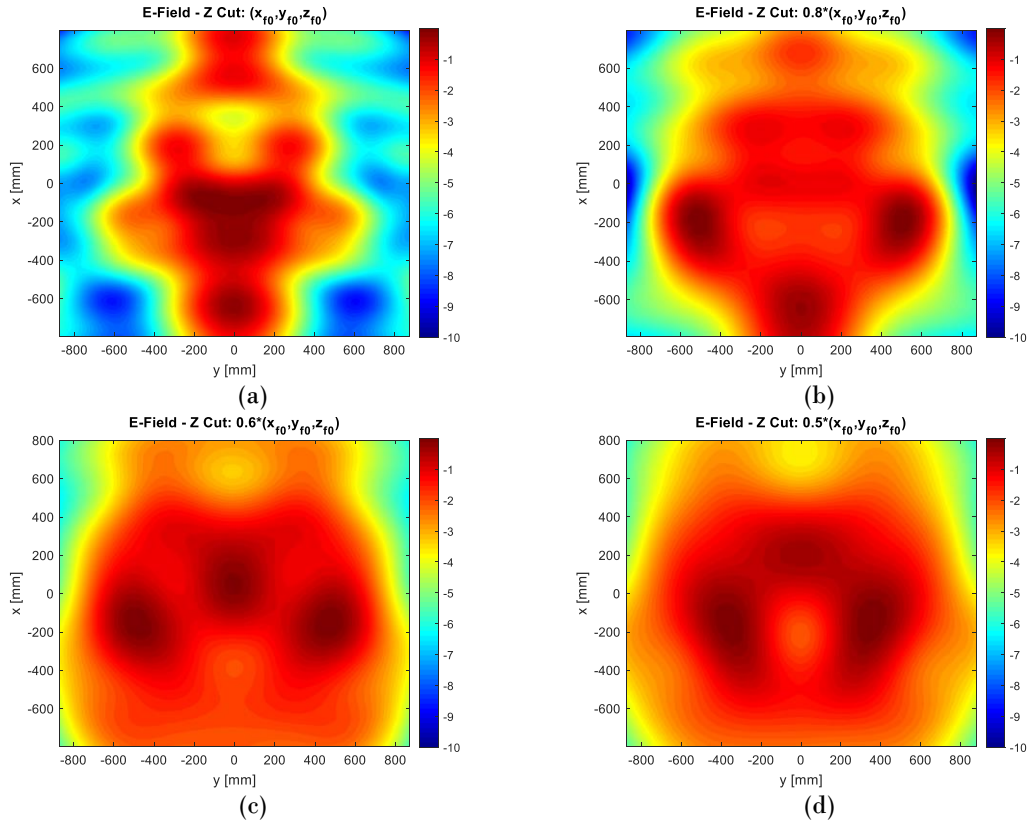

Fig. 5.71. - Design 1.7 GHz One-Layer. E-Field Magnitude at z=260 cm. Y-Polarization: (a) Initial position (b) 80 % of initial position (c) 60 % of initial position; (d) 50 % of initial position.

This behavior is also reflected in the measured quiet zone size comparison (Fig. 5.71) where it is observed that the position with the quiet zone are those where the distance between feed and reflector is reduced by 40 and 50%. Both configurations exceed the threshold of 50 cm marked although the configuration with $(x_f, z_f) = (-512.0, 800.0)\ mm$ will be chosen because in magnitude it exceeds this threshold in a looser way. In phase this configuration has a worse behavior although it is like the one achieved at 60% of the initial position, getting the half meter quiet zone since 2.4 m.

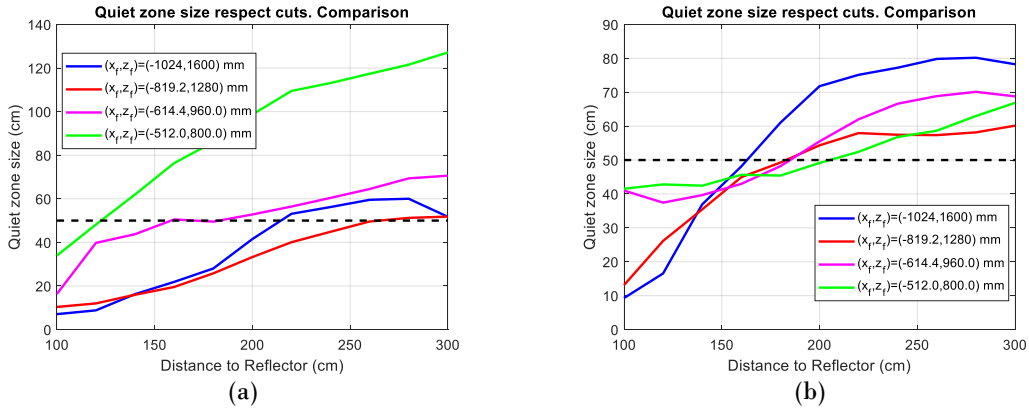

Fig. 5.72. - Design 1.7 GHz One layer – Feed position comparison. Minimum Quiet zone size in magnitude (a) and in phase (b). Approximate surface in magnitude (c) and phase (d).

5.5.3.2.- Incidence Feed Angle (θ_{incx}).

In an analog way to the 28 GHz designs, as the last step to obtain the definitive design, it will be studied which is the most optimal θ_{incx} angle to obtain the best Quiet zone. In Fig. 5.73 it can be discerned that the quiet zone has a behavior like the designs previously seen in the matter of this angle of inclination.

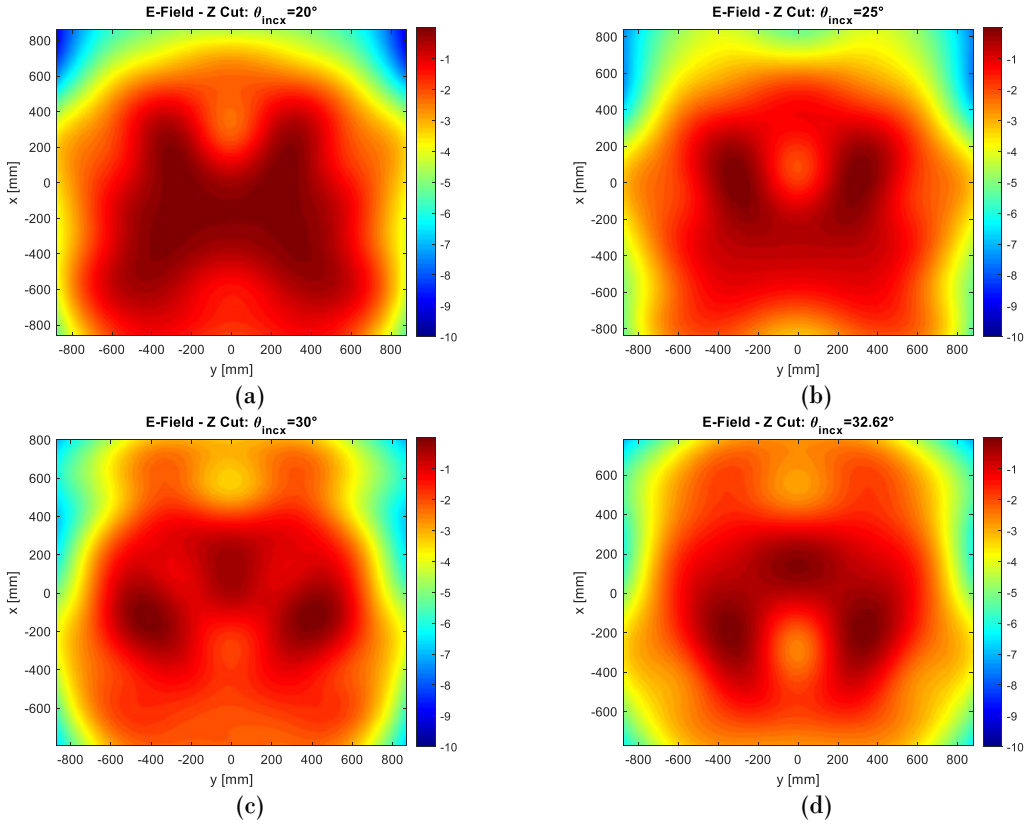

Fig. 5.73. - Design 1.7 GHz One layer. E-Field Magnitude at z=240 cm. Y-Polarization: (a) $\theta_{incx} = \theta_0 - 10 = 20°$; (b) $\theta_{incx} = \theta_0 - 5 = 25°$; (c) $\theta_{incx} = \theta_0 = 30°$; (d) $\theta_{incx} = \theta_{in0x} = 32.62°$;

For θ_{incx} high, it can be seen in the 3D plots as small "holes" appear where the ripple reaches 4 dB, something that will reduce the size of the quiet zone. In the designs for angle of 20 and 25° these small holes are reduced by slightly increasing the quiet zone at their edges.

For the smaller angles, the differences in size can be seen more clearly in Fig. 5.74 Both configurations have a quiet zone size much larger than 50 cm. Once this limit has been exceeded, the configuration for $\theta_{incx} = 25°$ has a Quiet zone that increases more quickly.

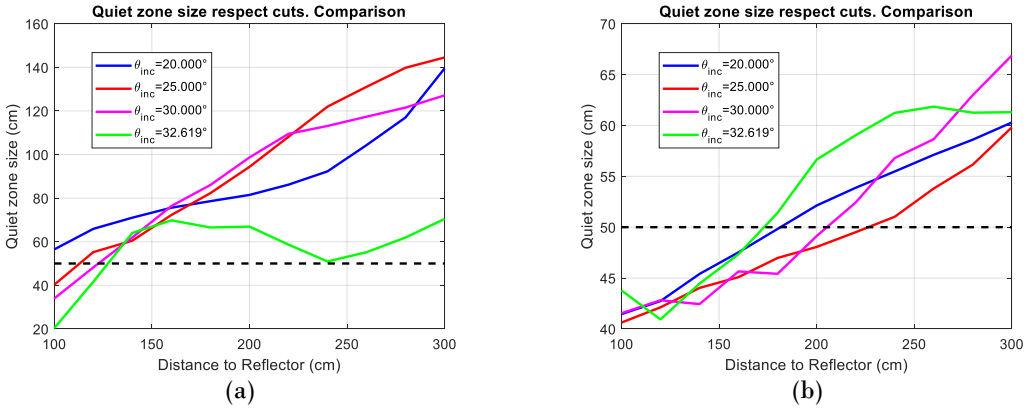

Fig. 5.74. - Design 1.7 GHz One layer – Feed position comparison. Minimum Quiet zone size in magnitude (a) and in phase (b).

Despite this, in phase it is observed that for $\theta_{incx} = 20°$ the quiet zone adjusted to the requirements begins at a distance closer to the reflector than in comparison with $\theta_{incx} = 25°$. That is why it is decided to choose the lowest angle as optimal for the final design.

5.5.3.3.- Definitive Design.

In Table 5.16 summarizes the main physical parameters of the 1.7 GHz design. For the calculation of the drift angle, the planes $E_{zmax} = 180\ cm$, $E_{zmin} = 100\ cm$ haven taken as reference. Note that in this case the drift angle is small (approximately 0.66°) with respect to the 28 GHz designs.

Regarding to its parameters in the equivalent parabolic system, it is observed that in this case there is a greater difference between diameter and focal distance, something that is coherent since the relative distance between feed and reflector is smaller than in 28 GHz designs to have a less restrictive far field condition.

1.7 GHz Design One-Layer. Physical characteristics.		
Symbol	Name/Units	Value
f_0	*Desing frequency [GHz]*	1.700
λ_0	*Wavelength at design frequency [mm]*	176.471
P_x/P_y	*Periodicity of the cells in both axes [mm]*	88.235
h	*Height of the substrate [mm]*	3.810
N_x	*Number of cells in asymmetric cut*	20
N_y	*Number of cells in symmetric cut*	19
D_{tx}	*Total diameter of the reflector in Asymmetric cut [mm]*	1852.94
D_{ty}	*Total diameter of the reflector in Asymmetric cut [mm]*	1764.71
θ_r	*Real angle of radiation. Tilt to rotate the structure [º]*	20.66
Δ_x	*Deviation of the direction of maximum radiation on the Asymmetric Cut [mm]*	-200.00
(x_f, y_f, z_f)	*Coordinates of the feed respect the reflector [mm]*	(512.0,0.0,800.0)
D_x	*Equivalent diameter of the reflector in Asymmetric cut [cm]*	1825.55
D_y	*Equivalent diameter of the reflector in Asymmetric cut [cm]*	1764.71
F	*Focal distance [mm]*	961.546
C	*Clearance [mm]*	105.432
F/D_{tx}	*Relation between focal distance and size of the reflector*	0.519
$(\theta_{incx}, \theta_{incy})$	*Angles of inclination feed [º]*	(20.0,0.0)
(x_c, y_c)	*Coord. of the point in reflector where the feed is pointing [mm]*	(−220.8,0.0)

Table 5.16. - Design 1.7 GHz One-Layer. Physical characteristics overview.

In Fig. 5.75 shows the symmetric and asymmetric cuts of this model. On the one hand, there is a significant improvement in the field respect the initial configuration. The E-Field is concentrated in the desired direction. In addition, it reduces the pattern of polluting interference that was observed in the initial design (Fig. 5.67).

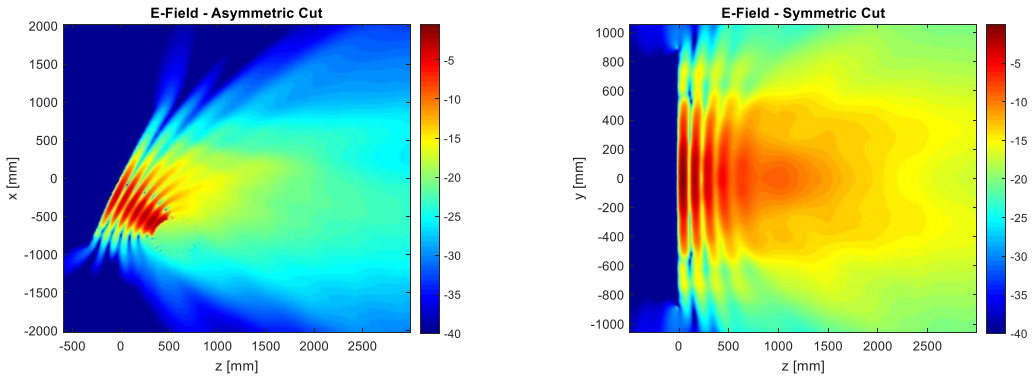

(a) (b)

Fig. 5.75. - Design 1.7 GHz One-layer – Definitive Design. E-Field Magnitude. Y-Polarization: (a) Asymmetric Cut; (b) Symmetric Cut.

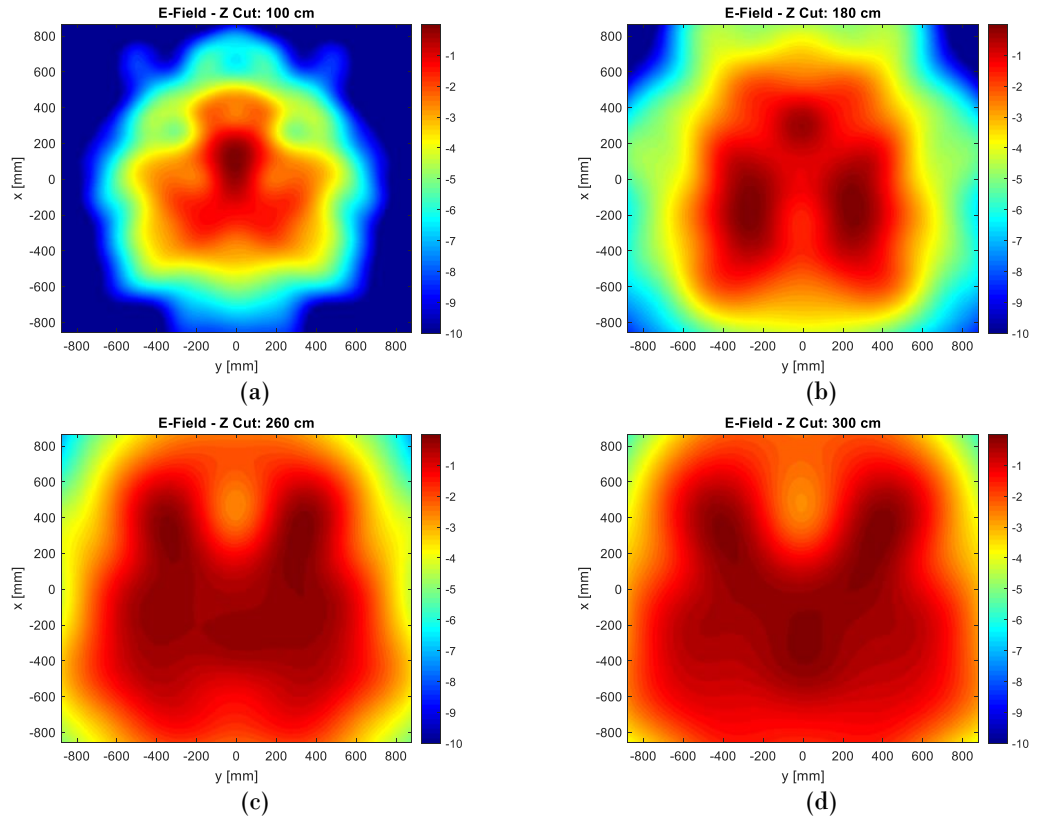

Fig. 5.76. - Design 1.7 GHz One-layer – Definitive Design. E-Field Magnitude – Z Cuts. Y-Polarization: (a) z=100 cm; (b) z=180 cm; (c) z=260 mm; (d) z=300 cm.

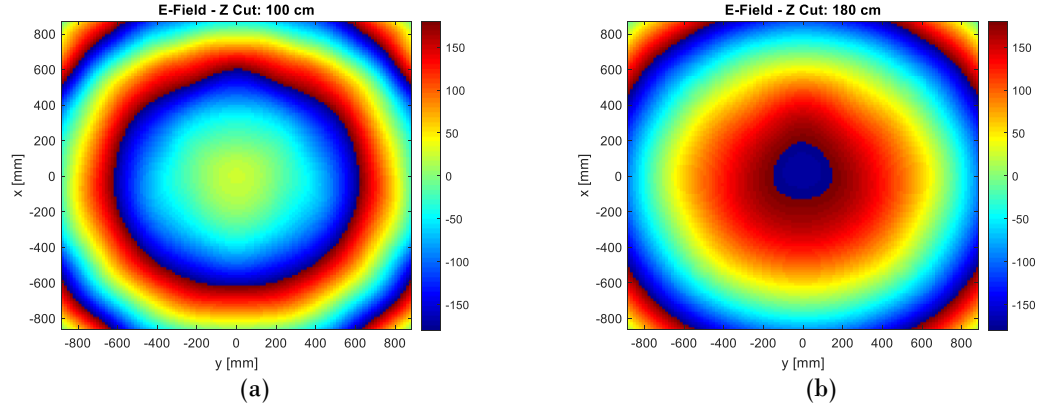

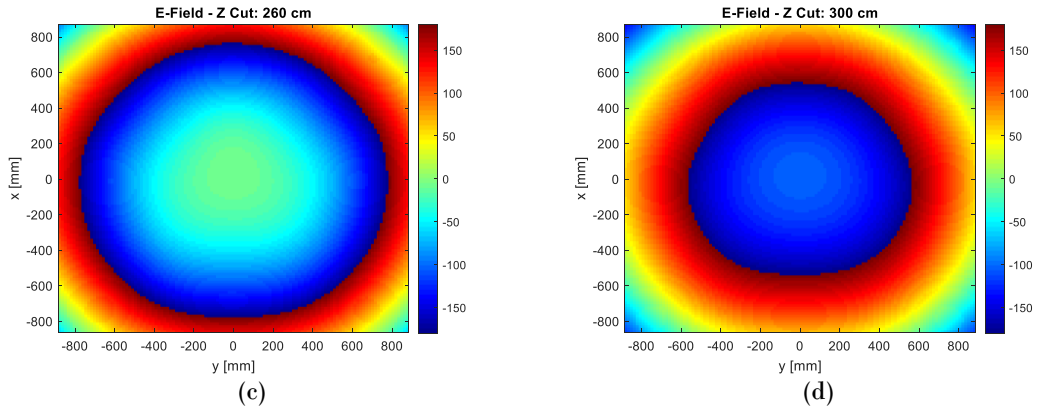

Fig. 5.77. - Design 1.7 GHz One-layer – Definitive Design. E-Field Magnitude – Z Cuts. Y-Polarization: (a) z=100 cm; (b) z=180 cm; (c) z=260 mm; (d) z=300 cm.

On the other hand, there are small irregularities of the electric field in its propagation on the Z axis, especially in the asymmetric cut. The effect of these distortions can be seen in Fig. 5.76 In amplitude the quiet zone acquires a more irregular shape with the small holes mentioned in previous point. In phase the existing ripple is reduced as shown in Fig. 5.77 obtaining a sharp concentric circles phase.

Based on Fig. 5.78, with this design it is possible to obtain a quiet zone adjusted to requirements from 180 cm of the reflector. In amplitude this size of quiet zone reaches a size greater than 1 meter. The phase will then be the most restrictive part, which will move in sizes around 60 cm.

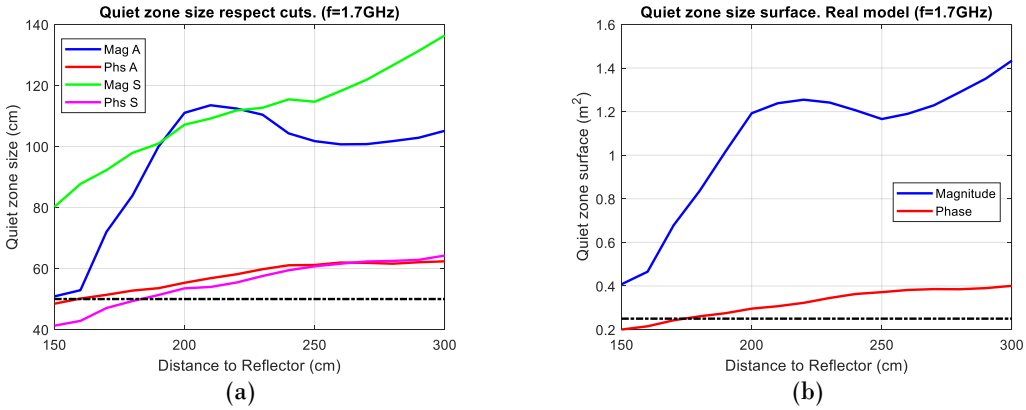

Fig. 5.78. - Design 28 GHz One-Layer – Starting point. Quiet zone size (a) and approximate surface (b).

In Table 5.17 is detailed the location of the quiet zone following the requirements. While the size on Z-axis, as occurs in the previous designs extends to more than 3 meters.

Notice how the quiet zone begins at much smaller relative distance than reflector 28 GHz designs ($0.97D_{tx}$ versus $2.79D_{tx}$). Based on the dimensions of the reflector, this indicates that the CATR system can be placed in narrower anechoic chambers.

1.7 GHz Design One layer. Quiet zone Location.		
	Amplitude	*Phase*
QZ Measured [cm]	*[150,200]*	*[180,230]*
Ap. Surface [cm]	*[150,200]*	*[160,210]*

Table 5.17. - Design 1.7 GHz One layer. Location of the quiet zone respect the center of the reflector.

Regarding the ratio between quiet zone and reflector, along the quiet zone there is an average ration of 47 %, a considerably higher value than the initially assumed 30%.

5.6.- Real Models. Bandwidth Study.

As the last point of the methodology, a simulation of a more real model of the structure will be carried out where there will be omitted aspects in the previous design will be had that will provide more realistic results on the behavior of the antenna.

In all the designs presented in this memory, copper will always be used as a conductor, with a conductivity $\sigma = 5.8 \cdot 10^7 \left[\frac{S}{m}\right]$ and a height of 35 µm is considered for both the patches and the ground plane that conform the reflector.

As previously mentioned, the far field between this described model and the simplified one is prepared, to check the effect of introducing these new variables in the model. The second study lies in the evaluation of X-component comparing it with the optimized component (Y-component). Finally, the real model also allows an in-band study of the proposed structure. With this study it is also possible to calculate an approximate bandwidth of the antenna.

In all the mentioned studies, the size of the quiet zone in the main E-Field cuts will be calculated, in a similar way to the previous point. Regarding frequency, the calculation of the quiet zone will be based on taking the minimum size between the asymmetric and symmetric cut. The approximate bandwidth of this antenna will be calculated by taking that minimum and maximum frequency at which the size of the quiet zone, in the range of distances defined in its final model, meets the requirements. Analogous to the previous point, amplitude and phase of the E-Field will be considered separately.

5.6.1.- Design 28 GHz One-Layer.

5.6.1.1.- Simplify vs. Real model comparison.

On the same area of study seen in the final design, Fig. 5.79 shows the comparison of quiet zone size between simplify and real model for 28 GHz one layer. In amplitude, a great similarity between the different cuts is observed while in phase the differences are more significant. It is calculated that the maximum deviation in distance between curves for the same cut is 15 cm.

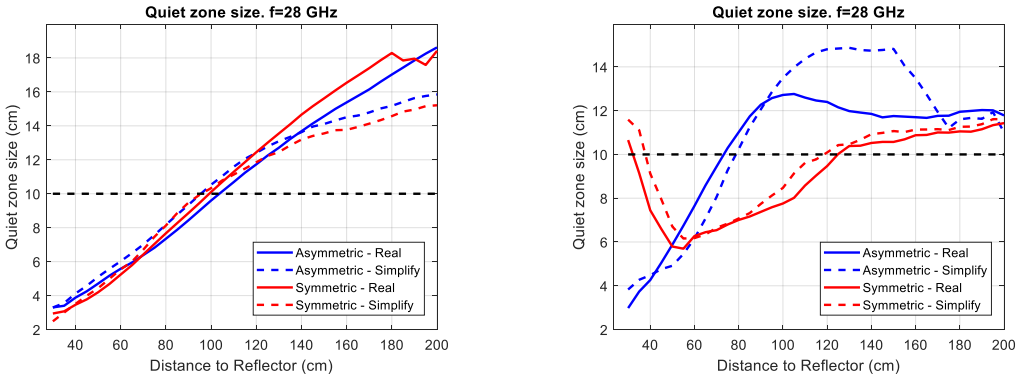

Fig. 5.79. - Design 28 GHz one-layer – Simply versus Real Model comparison: (a) Quiet zone in Amplitude; (b) Quiet zone in Phase. In solid color, the principal cuts of Real Model. In discontinuous color the cuts for the simplified model.

It will then be concluded that the variables introduced in this model do not generate a significant distortion in amplitude and phase, only appears significant differences after cross the 10 cm limit. Implicitly, this study also indicates that placing the feed at a distance from the reflector less than its far field limit, although close to it, does not introduce a strong distortion.

5.6.1.2.- Polarization comparison.

Following the same method as the previous point in Fig. 5.79 the sizes of quiet zone for both polarizations are shown in Fig. 5.80.

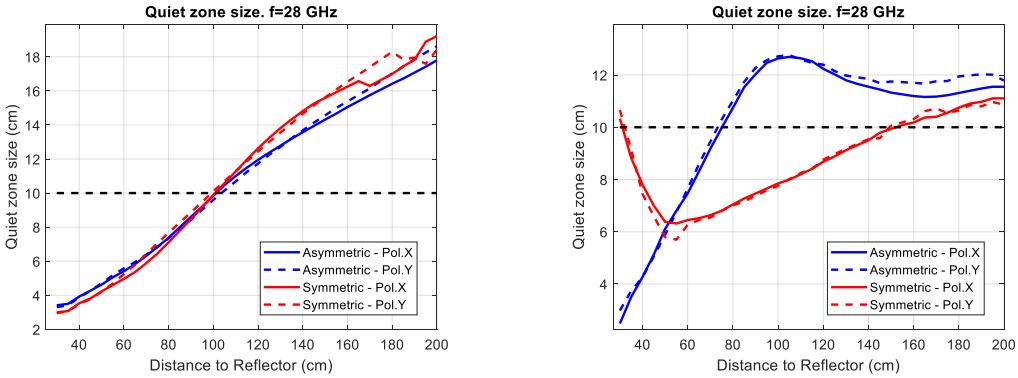

Fig. 5.80. - Design 28 GHz one-layer – Polarization comparison: (a) Quiet zone in Amplitude; (b) Quiet zone in Phase. In solid color, the principal cuts for X-Polarization. In discontinuous color the cuts for Y-Polarization.

The quiet zone size differences are very small between both polarizations. This is mainly explained by the strong symmetry of both polarizations in the feed, which makes the reflector identically influenced by the E-Field and therefore reflected in the same way.

5.6.1.3.- Bandwidth.

Fig. 5.81 shows the quiet zone calculated for a frequency range around 4 GHz respect to the design frequency.

Both graphs show how the frequency fundamentally affects the minimum distance where the quiet zone meets the imposed requirements. In amplitude, it is observed that as the frequency increases, the curve shifts and therefore the minimum distance increases. Regarding phase, also appears a similar behavior: at lower frequencies the size meets the requirements while at frequencies of 28 and 30 GHz this minimum distance is above 150 cm.

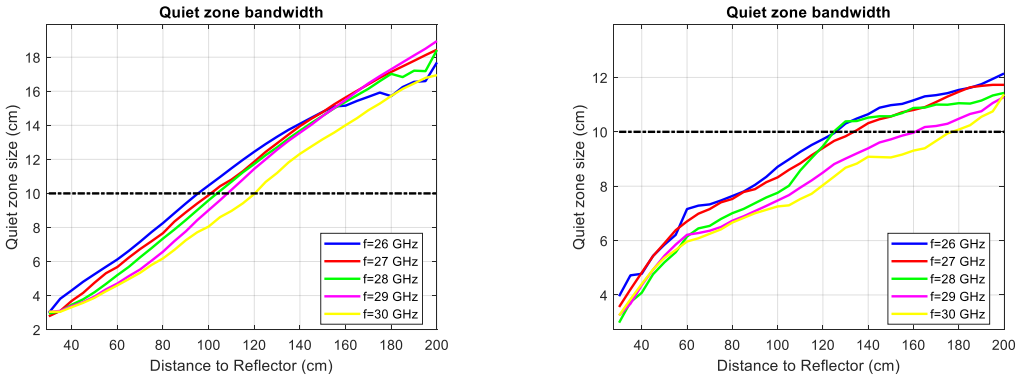

Fig. 5.81. - Design 28 GHz one-layer – Frequency study: Quiet zone in Amplitude (a) and in Phase (b)

Thus, the approximate bandwidth of the antenna under the premises explained before, will be 2 GHz in both components, being between 26 and 28 GHz. This bandwidth is 7.14% respect the central frequency, a percentage of the order of typical values obtained in reflectarray antennas.

5.6.2.- Design 28 GHz Two-layer.

5.6.2.1.- Simplify vs. Real model comparison.

In Fig. 5.82 it is shown the comparison of quiet zone size between the two models for the design of two layers. As in the previous design, there is a great similarity between them, both in phase and amplitude. It is only possible to discern a greater difference in the asymmetric cut of the real model once the threshold of 10 cm has been surpassed.

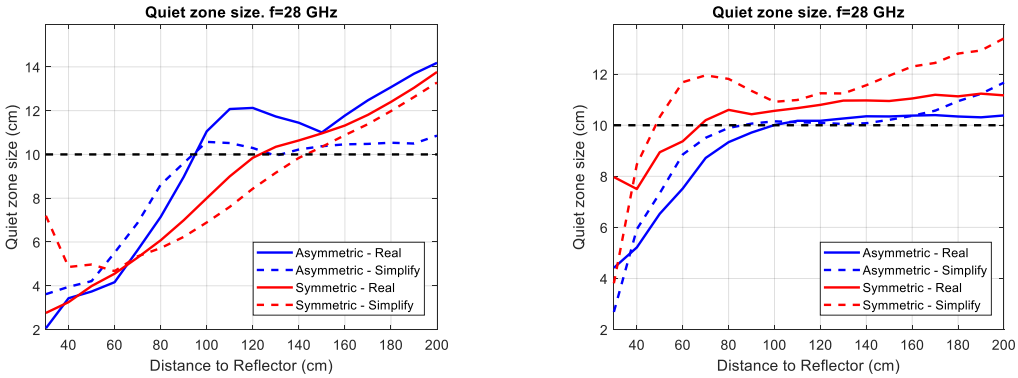

Fig. 5.82. - Design 28 GHz two-layers – Simply versus Real Model comparison: (a) Quiet zone size in Amplitude; (b) Quiet zone size in Phase.

Given the similarity between the models, there is no shift of the quiet zone in amplitude, although if it exists in phase, where it can be considered a quiet zone adjusted to the requirements from 100 cm.

This study corroborates that the effect caused by the *prepeg* joining the two layers or the height of the patches will not be significantly important.

5.6.2.2.- Polarization comparison.

As in the previous design, the polarization in X will follow a quiet zone behavior very similar to the Y polarization (Fig. 5.83). While there is a slight displacement of the minimum distance at which the requirements of 10 cm in amplitude are met. In phase this distance will remain approximately the same.

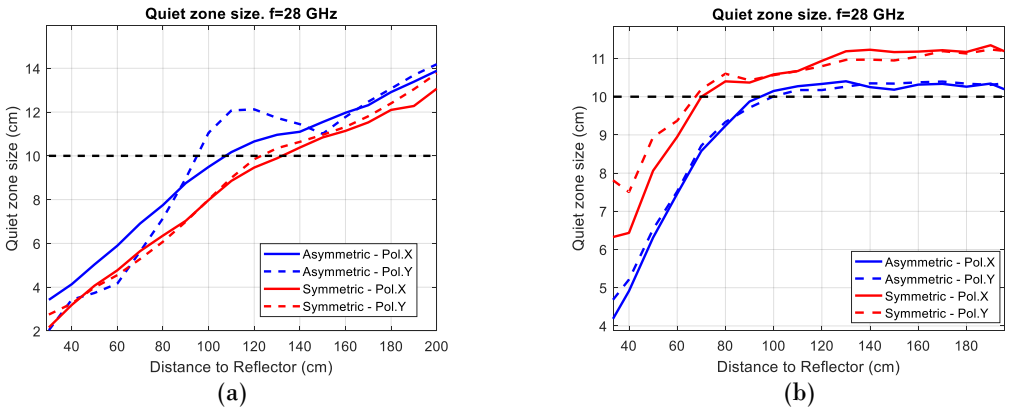

Fig. 5.83. - Design 28 GHz two-layers – Polarization comparison: (a) Quiet zone in Amplitude; (b) Quiet zone in Phase. In solid color, the principal cuts for X-Polarization. In discontinuous color the cuts for Y-Polarization.

Again, it is observed that thanks to the symmetry of the feed, both polarizations will have a very similar behaviour in quiet zone.

5.6.2.3.- Bandwidth.

After the in-band study of this design, it is observed that it does not follow a behavior like the case of the design of a layer. As it has been seen in the simplified model, the electric field is dispersed in two main beams, which makes its quiet zone is reduced. Fig. 5.84 shows how this behavior is accentuated at lower frequencies (Fig. 5.84(b)) and reduced for highs (Fig. 5.84(c)).

The reason for this, is the effect caused by patches for high incidence angles. At higher frequencies, the directivity of the feed and therefore the taper on the reflector increases. This reduces the E-Field level at the top of the patches and their contribution to the reflected field.

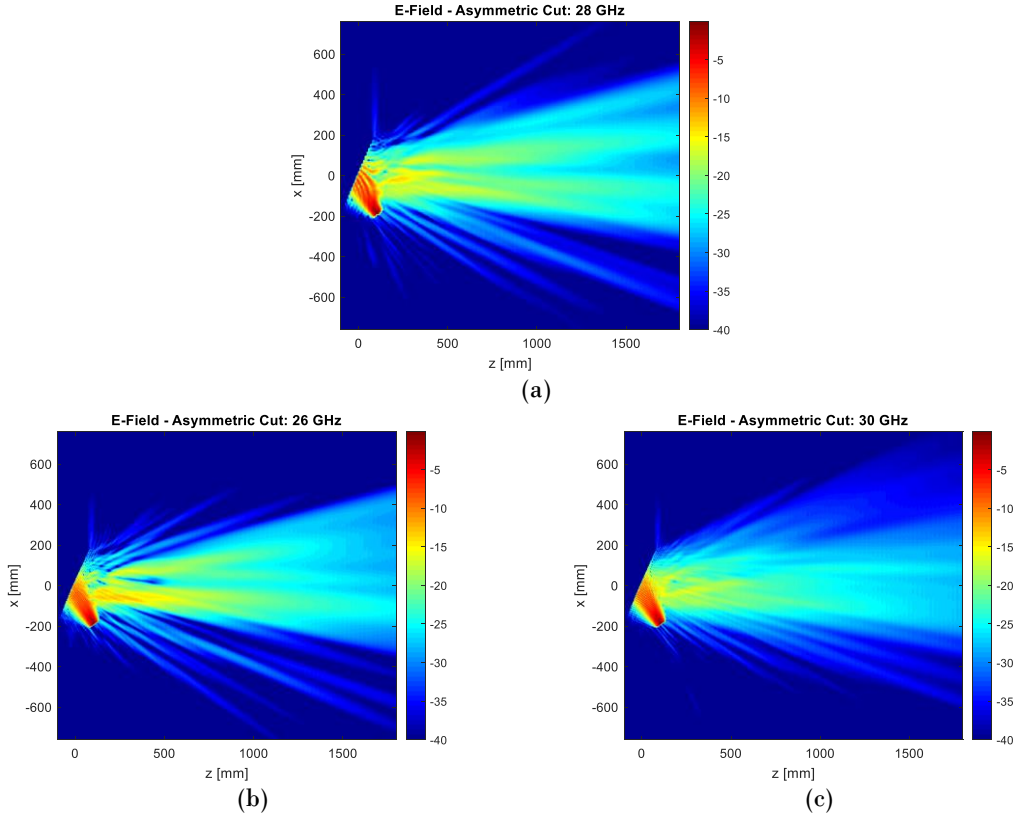

Fig. 5.84. - Design 28 GHz two-layer – Frequency study: Symmetric Cuts: (a) f=28 GHz; (b) f=26 GHz; (c) f=30 GHz.

Due to this effect, it was observed in Fig. 5.85(a) as the size of the quiet zone in amplitude is reduced for frequencies of 26 and 27 GHz and the minimum distance to meet the requirements is increased. However, it is observed that the degradation at low frequencies is small.

A similar behavior can be seen in phase, where the higher frequencies achieve the threshold of 10 cm fixed closer to the reflector. However, it is observed that at 30 GHz a greater distance is required to meet the requirements.

Thus, the operability range of this antenna will be between 26 and 30 GHz in amplitude and between 28 and 30 GHz in phase. In relative terms, the bandwidth is 14.29% and 7.14% in each case. In this sense, the bandwidth is improved in amplitude in values above the normal bandwidth for these antennas.

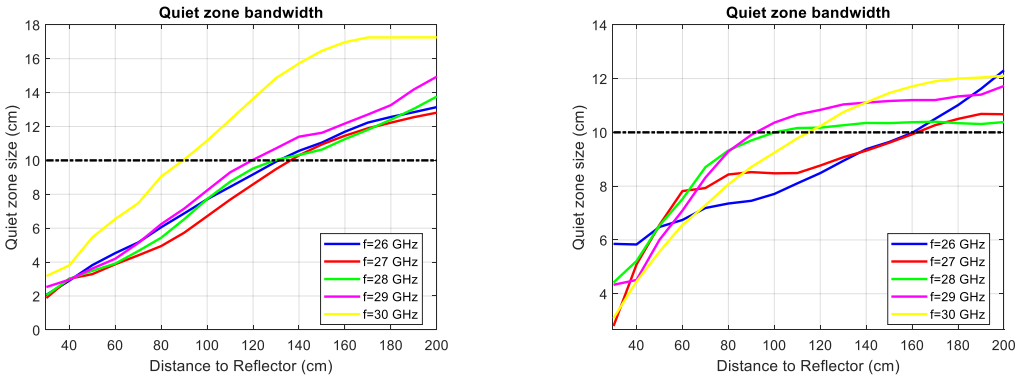

Fig. 5.85. - Design 28 GHz two-layers – Frequency study: Quiet zone size in Amplitude (a) and in Phase (b).

5.6.3.- Design 1.7 GHz.

5.6.3.1.- Simplify vs. Real model comparison.

In relation to 1.7 GHz design, Fig. 5.86 shows the comparative calculation of the quiet zone of both models, where there are more differences between them. This derives from an aspect that appears in the previous point: the ripple. The new variables introduced in the real model increase the ripple and make the quiet zone size reduced compared to the simplify model.

In spite of this, the size of the quiet zone continues above 50 cm in the whole range study in amplitude, and in the same range calculated previously in phase. It is the concluded that the real model will not affect the quiet zone characteristics defined above.

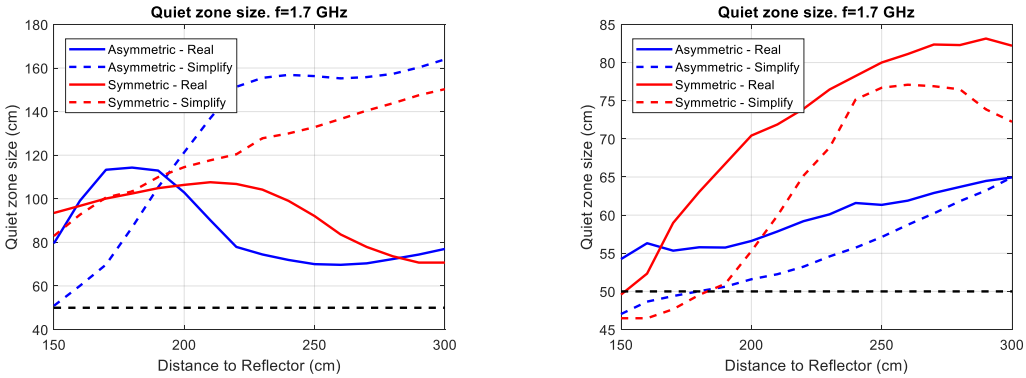

Fig. 5.86. - Design 1.7 GHz one-layer – Simplify versus Real model comparison: (a) Quiet zone size in Amplitude; (b) Quiet zone size in Phase.

5.6.3.2.- Polarization comparison.

Regarding the comparison between polarizations, the differences in their main cuts will also be greater. Despite the radiation pattern symmetry of the feed mentioned, the small variations in the E-Field ripple, cause important differences in the quiet zone calculation.

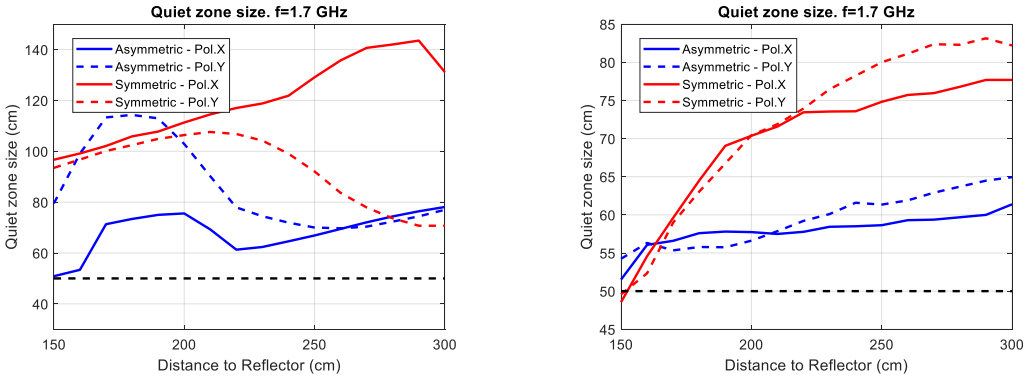

Fig. 5.87. - Design 1.7 GHz one-layer – Polarization comparison: (a) Quiet zone in Amplitude; (b) Quiet zone in Phase. In solid color, the principal cuts for X-Polarization. In discontinuous color the cuts for Y-Polarization.

Another important aspect in view of these results is that the minimum distance where the quiet zone required is placed remains unalterable in both polarizations.

5.6.3.3.- Bandwidth.

Fig. 5.88 shows the in-band behavior of 1.7 GHz design. In amplitude and according to the results obtained in the simulations, the quiet zone acquires an elliptical shape, which makes the size of the quiet zone in its symmetric cut reduced and, in this case, less than the imposed limit.

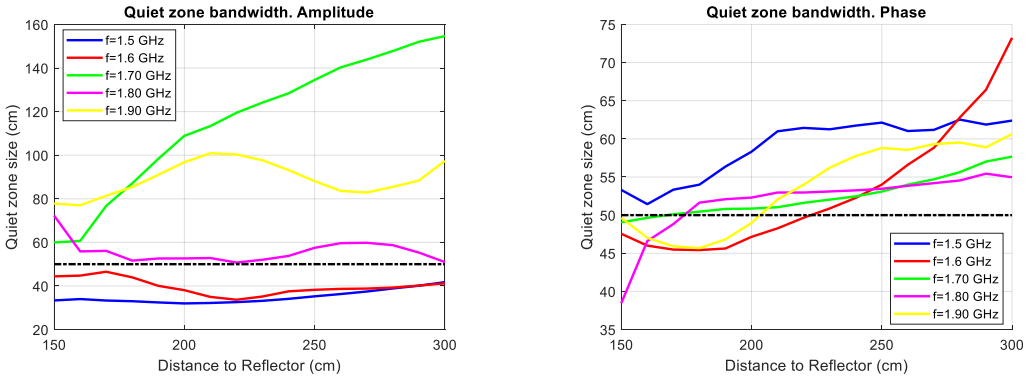

Fig. 5.88. - Design 1.7 GHz one-layer – Frequency study: Quiet zone in Amplitude (a) and in Phase (b)

However, from the design frequency, the eccentricity of this zone is reduced and the curves in both cuts are approaching, which makes the minimum size increase. In relation to frequencies above 1.7 GHz notice how at 1.9 GHz a better performance is achieved than a 1.8 GHz. This derives mainly from the difference in electrical paths for different frequencies.

Regarding phase, it is observed how in all the cuts the limit of 50 cm marked is exceed, although at 1.6 and 1.9 GHz a greater distance between feed and reflector is required.

Thus, the bandwidth for both components will be 200 MHz which corresponds to 11.76% of their central frequency. Respect the average capacity of these antennas, this design achieves a high relative bandwidth. The frequency range in which the operation of the antennas is not degraded will be between 1.7 and 1.9 GHz.

5.7.- Conclusions.

According to the methodology described in the previous chapter, 3 different designs of reflectarray antennas have been designed with a behavior that approaches or reaches the requirements defined in this project.

First, the cell study of the designs has been carried out. For the three cases, it is demonstrated that the substrate Taconic TSM-DS3 [60] has an acceptable behavior, although some degradation, especially in the phase range, can be appreciated for the designs at 28 GHz. Another transverse aspect at both frequencies will be the phase limitation in single-layer designs. A restriction that is eliminated when considering multi-layer designs, although it increases complexity and offers greater sensitivity to high angles of incidence. Regarding the substrate height, from the available combinations it is

possible to select the smallest at 28 GHz, although at 1.7 GHz a larger h is required, which arises as a combination of several substrate layers.

As feed, a type of antenna called axial chokes conical horn antenna will be used. These horns allow to generate directive and symmetrical radiation patterns, with a reduced SLL level. Characteristics that are especially suitable in CATR systems. That said, two antenna designs are proposed for each frequency under study.

With the elements of the antenna studied, it is already to discern the configuration of the reflectarray before the optimization stage. The reflectors of all designs will be elliptical due to the lesser effect of the dispersion on the study area and the system offset configuration (considering a radiation angle not zero, the phase distribution acquired an elliptic shape).

In 28 GHz designs, a very similar initial structure will be used, so the characteristics that distinguishes them will be the phase restriction on their distribution. In the 1.7 GHz design, a good starting point is reached by scaling the distances of the designs to 28 GHz.

The next step will be the process of optimization of the designs. Thanks to the optimization of the position of the feed and the inclination of this respect the reflector, it is possible to improve in form and size the quiet zone generated in all the designs. It is also demonstrated that the use of blocking elements or abrupt changes in the feed position do not get a considerable improvement.

Besides this, it has been observed that the main beam generated by the reflectarray suffers an angular deviation respect the theoretical radiation angle, as well as a shift of the point of the reflector where it is generated. This effect will be corrected by rotating the structure a certain drift angle and considering a certain offset in the area where the quiet zone is located.

In all the proposed designs, it is created circular quiet zones with a size of the quiet zone adjusted to the requirements on the XY plane. For 28 GHz designs, the minimum distance to meet such targets on the Z-axis is greater than the marked limit of 500 cm. However, in the 1.7 GHz, it is achieved to have a quiet zone of 50x50x50 cm^3 within the distance to the maximum reflector, where it is even possible to reach in amplitude sizes of 1 meter over the XY plane, whit ratios near to 50 %. A higher ration than that achieved with a conventional parabolic reflector.

Finally, these antennas are evaluated in a more realistic environment. For all designs, it is possible to conclude that the difference of calculated quiet zones between the real and simplified models is not significantly large, although the greatest discrepancies will occur in the two-layer design, where a greater number of variables will be considered.

It is also corroborated that the symmetry of the field radiated by the feed and patches, make the still zone obtained in both polarizations similar. Due to vulnerability to ripple of the 1.7 GHz design, the quiet zone has a greater difference although their size continues to meet the fixed premises.

Regarding the study in band, the design of a 28 GHz layer has a better performance at frequencies lower than the design frequency reaching a bandwidth of 2 GHz. In two-layer design, it is possible to increase this bandwidth up to 4 GHz in amplitude, being the high frequencies the ones that reach better quiet zones. In 1.7 GHz design, resonance effects appear at certain frequencies that distort the shape of the quiet zone, although it allows to cover a bandwidth of 200 MHz, being the high frequencies the ones with the best behavior.

For the designs of one-layer, it is concluded that in the range of frequencies within this bandwidth, the f_0 will be border frequency, either maximum or minimum for a correct operation of the antenna.

6.- DEVELOP AND BUDGETING.

In the following point it details the organization and economic evaluation of the project reflected in this report.

First, the set of milestones will be expressed in which the project can be divided as well as the duration of each one, detailing the temporal range in which each one has been reached.

Next, it is proposed to make an economic balance about the project and the manufacture of the antenna designs.

6.1.- Project development.

The realization of this project covers two discontinuous time ranges, so the tasks that form it, are grouped according to the time where they have been performed: Period I (11/06/2018 – 01/09/2018) and Period II (01/02/2019 – 26/07/2019).

In the first period (Table 6.1), is based primarily on the bibliographic search and the clear definition of the requirements to be met by the antenna. Once progress had been made in these two tasks, the design methodology was defined and the implementation of those programs that support it.

Before ending this period, it was possible to make a battery of designs whose purpose was to check the methodology and study the most basic variables of antenna, such as the shape of the reflector, the maximum number of layers to consider …

Description	Duration (days)	Start	End
Start	0	11/06/2018	11/06/2018
Bibliographic Search	60	11/06/2018	01/09/2018
Antenna requirements	3	18/06/2018	20/06/2018
Methodology development	15	20/06/2018	04/07/2018
Methodology implementation	19	04/07/2018	31/07/2018
Test Designs	21	01/08/2018	01/09/2018

Table 6.1. Project development – Period I.

At the beginning of the second period (Table 6.2) some points in the methodology were identified that could be improved, so the first task in this second block consisted in modifying the previously programs to introduce these improvements. At this point, for example, it is introduced the study of the cell considering oblique incidence, and therefore the definition of design matrix.

Description	Duration (days)	Start	End
Corrections and methodical improvements	28	01/02/2019	11/03/2019
Bibliographic Search	21	01/02/2018	10/04/2019
Designs	84	12/02/2019	07/06/2019
Documentation	94	13/02/2019	24/06/2019
Deadline	0	16/07/2019	16/07/2019
Presentation	0	26/07/2019	26/07/2019
End	0	26/07/2019	26/07/2019

Table 6.2. Project development – Period II.

A large part of the work carried out in the second block consisted fundamentally in the realization of the designs described in this memory as well as in the writing of this memory. The bibliographic search was continued, more focused on the themes and context in which the project is framed. The detailed Gantt diagram of this project is shown in Fig. 6.1 and Fig. 6.2.

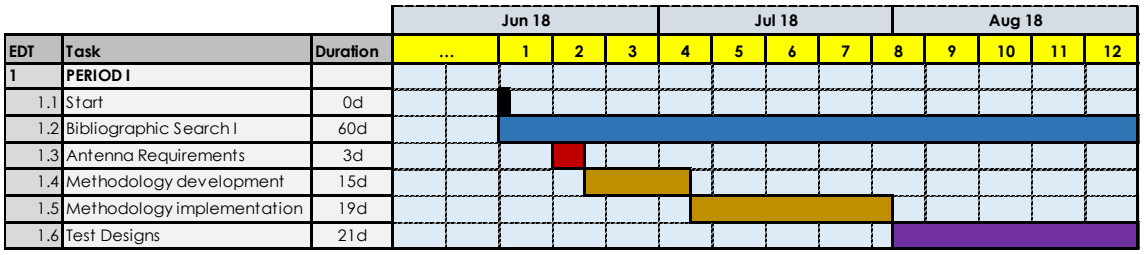

Fig. 6.1.– Project development – Gantt diagram: Period I (11/06/2018 – 01/09/2018).

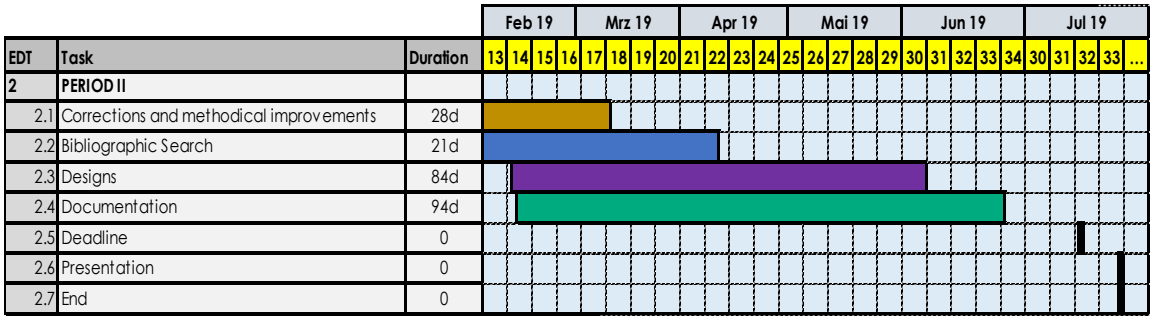

Fig. 6.2.– Project development – Gantt diagram: Period I (11/06/2018 – 01/09/2018).

6.2.- Project costs.

As the second and last point of this chapter, an estimate is made of the cost of this project. The costs considered can be divided into two types: design cost, manufacturing costs. It is worth mentioning that the cost derived from the methodology implementation are considered in the design phase even if they do not strictly belong to this group.

6.2.1.- Design costs.

In reference to the first ones, three sources of cost are differentiated: the cost by licenses (Table 6.3), the cost of personnel (Table 6.4) and the depreciation of equipment (Table 6.5). In the licenses, an overestimated approximation of the cost of these licenses has been made, if their use only stems from said project.

Description	***Cost (€)***
CST Studio Microware 2018 ® - Licenses	4,000.00
Antenna Magus ® - License	
Matlab R2019® - License	3,000.00
Complementary Software (e.g. Office)	500.00
Subtotal	7,500.00

Table 6.3. Design costs – Software costs.

Description	***Working hours (h)***	***€/hour***	***Subtotal (€)***
Msc Engineer Student	755.93	23.56	17,809.71

Table 6.4. Design costs – Personnel costs.

Special mention will have the cost of equipment, for which the monthly depreciation suffered by the equipment used has been calculated, in this case a computer, following the linear method[1].

Description	*Cost (€)*	*Useful life (years)*	*Asset depreciation (€/month)*	*Dedication (months)*	*Subtotal (€)*
Computer	1,200.00	5	18.33	9	165.00

Table 6.5. Design costs – Depreciation costs of assets used.

Description	*Cost (€)*
Software costs	7,500
Personnel costs	17,809.71
Depreciation costs of asset used	165.00
Total	25,474.71

Table 6.6. Design costs – Summary

According to Table 6.6, the cost derived from the design and methodology implementation amounts to 25,474.71 €.

6.2.2.- Manufacture costs.

In relation to the manufacturing costs, it has been calculated the cost of each design described in the project, shown in the following tables. In each one of them the elements are counted separately as well as the structure that supports the antenna.

Description	*Cost (€)*
Substrate Taconic TSM-DS3	79.00
Axial Chokes Conical Antenna	3,000.00
Structure	500.00
Labor force	117.80
Subtotal	3,746.00

Table 6.7. Manufacture costs – 28 GHz Design one-layer.

To calculate the price of the substrate a cost of 2 €/cm is considered for one-layer designs and 6.5 €/cm for two-layer design. Labor is calculated considering a salary of

[1] Depreciation according to linear method consist is the difference between the asset value minus the salvageable value divided by its useful life.

15.71 €/hour and estimating the time in hours in the manufacture of the complete structure.

Note how the designs at high frequency (Table 6.7 and Table 6.8), much of the budget consists of the manufacture of the field source, the horn, as it is the most complex with respect to the rest of elements. By studying the cost independently, we have considered the cost of the horn in both designs at 28 GHz although it could be reused for prototype purposes.

Description	***Cost (€)***
Substrate Taconic TSM-DS3 (two-layers)	234.266
Axial Chokes Conical Antenna	3,000.00
Structure	500.00
Labor force	176,7
Subtotal	3,910.97

Table 6.8. Manufacture costs – 28 GHz Design two-layer.

Of the three designs, the one with the highest cost will be the design at 1.7 GHz (Table 6.9) since in addition to the horn, in this case considerably larger in dimensions than the previous one, a high cost of the substrate is added, by using a reflector with dimensions close to 2 meters. According to Table 6.10, the manufacturing cost of the three designs, amounts to 16,798.45 €.

Description	***Cost (€)***
Substrate Taconic TSM-DS3 (two-layers)	3,705.88
Axial Chokes Conical Antenna	4,000.00
Structure	1200.00
Labor force	235.60
Subtotal	9,141.48

Table 6.9. Manufacture costs – 1.7 GHz Design one-layer.

Description	***Cost (€)***
28 GHz one-layer design	3,746.00
28 GHz two-layers design	3,910.97
1.7 GHz one-layer design	9,141.48
Total	16,798.45

Table 6.10. Manufacture costs – Summary.

Apart from this, the proposed designs suppose an economic saving with respect to their homologue using a parabolic reflector. Especially important is the difference in cost and complexity in the designs at 1.7 GHz, where a parabolic reflector of such dimensions would cost more than 100,000 €.

7.- CONCLUSIONS AND FUTURE LINES.

7.1.- Conclusions.

According to the information detailed in this Master Thesis, the main goal of this project has been the design of prototype reflectarrays for a CATR systems, allowing to compare the advantages or limitations that these antennas introduce to the traditional system design.

In the first place, the context in which the problems are contextualized has been placed, defining the concept of reflectarray antennas, CATR systems and the inherent topic in which these are contextualized, the 5G generation.

With an initial and general idea of the problem, the requirements that the reflectarray antenna had to satisfy were described in detail as well as the programs and tools that are available to make the design.

Knowing these requirements, a methodology has been proposed and defined for the design of reflectarray antennas in CATR systems. A methodology that could be implemented in the software tools available. This design process described will be implemented in the software tools available. This design process described, will be based on the use of the geometry of reflectarray antennas, using its array nature to collimate the electric field according to the requirements set. Thanks to CST software, it will be possible to obtain results of the electric field generated by the antenna faithful to the experimental measurements.

This method is used for the design of 3 different types of antenna, on two different frequency bands. After finishing the design process, the reflectarray models are subjected to a battery of tests, among which stands out a study in band.

In view of the acquired results, it is concluded that the reflectarray antennas have capacity to generate, in a determined zone of space (quiet zone), a wave that can be assumed as plane in the same way that if it was in far field of the antenna. The reflectarrays allow to generate quiet zones like those that would be obtained with its main competitor: parabolic reflector.

On the one hand, all designs corroborate a lower bandwidth than parabolic reflectors but suitable for the application described. On the other hand, it is obtained the good performance offered by these antennas at low frequencies to generate quiet zones of large sizes at a much lower cost and complexity than parabolic reflectors.

It has also been concluded that the proposed methodology allows to design models of antennas adjusted to the requirements marked for low frequencies. In microware bands, the design created from this methodology do not achieve the desired performance.

Based on this and in the absence of an experimental study, it is possible to conclude that reflectarray antennas are a possible substitute for parabolic reflectors thanks to their ease of manufacture, scalability and bandwidth adjusted to the conditions sought in a CATR system.

Numerous concepts acquired during the Master´s Degree have been used in this project, especially regarding to the design of RF components. It has also allowed to delve into the compact range CATR systems, a topic also introduced during the degree. Also, thanks to this project has had the opportunity to obtain an advanced knowledge of the electromagnetic simulator CST ®, a program widely used globally.

7.2.- Future lines.

Finally, it is possible to enumerate some lines of future research that open the completion of this project.

- **Bandwidth.** Although the bandwidth fits the requirements of a sub-band, the increase of this bandwidth would allow to use the reflector in several sub-bands. Multi-layer designs or band optimizations of the design would allow for improved in-band performance.

- **Wider range of substrates.** In cell analysis it was found how the Taconic substrate provided cell behaviors that could be improved using another type of substrate or the use of air layers.

- **New designs in FR1.** In view of the good behavior of the design at 1.7 GHz it is possible to implement, following the same methodology, a battery of designs for the different sub-bands that conform FR1 band. In this sense and unrelated to the project, designs have been made for the sub-bands 1.8-2 GHz; 2.3-2.5 GHz; 2.6-2.8 GHz; 3.4-3.6 GHz.

- **Cost reduction.** Although the lower economic cost of this antenna has been verified, it is possible to reduce the budget substituting for example the feeding horns by antenna arrays. In this sense, it should be verified that the effect would have the use of an array and the distortions that it introduces on the quiet zone.

- **Optimization algorithm.** Due to the limitations of the project, the proposed methodology fixed the size of patches according to a condition in far field, which is a limitation for the design of antennas with near field requirements. A solution to this would be the integration of an optimization algorithm that, based on certain masks required in a certain area of space, modifies the phase distribution in the reflector to collimate an electric field that fits these premises. This block would replace the process of study and optimization seen in this project.

- **Manufacture and measure.** The next step of this project would be the manufacture and measurement of certain prototypes adjusted to the above-mentioned designs. Especially relevant would be the design at 1.7 GHz as it is the best performance presents.

8.- REFERENCES.

[1] D. R. Prado, *"Analisis del campo cercano en reflectarrays para su uso como sondas en sistemas de medida de rango compacto",* Master Thesis, July 2012.

[2] WordPress – Principia Tecnologica: '*Generaciones de Redes Moviles'*: https://principiatechnologica.wordpress.com/generaciones-de-redes-moviles/. Last visit: 05/03/2019

[3] D. Andreev, "*Overview of ITU-T activities on 5G/IMT-2020*" in ITU Workshop 19.06.2018.

[4] Dr.B.T.Geetha, Vidhya.B, "*A Comparative Study of 5G Technology with other Generations of Mobile Teechnologies*" in *IEEE International Conference on Power Control*, Signals and Instrumentation Engineering, 2017.

[5] T. Fisher, *"5G Spectrum and Frequencies: Everything You Need to Know"* in Lifewire: https://www.lifewire.com/5g-spectrum-frequencies-4579825. Last visit: 06/03/2019

[6] 3GPP: Release 15, Specification TS 38.101-1 v15.4.0, December 2018.

[7] National Instruments, "mmWave: The Battle of the Bands", June 2016.

[8] J. Barrett, "5G Spectrum Bands" in Global mobile Supplier Association, February 2017: https://gsacom.com/5g-spectrum-bands/ . Last visit: 06/03/2019.

[9] S. Kavanagh, "What is 5G New Radio (5G NR)" in 5G.co.uk: https://5g.co.uk/guides/what-is-5g-new-radio/ Last visit: 06/03/2019.

[10] MVG: "*5G Antenna Test and measurement systems – Overview*".

[11] Michael D. Foegelle, "RF Measurement in a 5G World" in IEE Instrumentation and Measurement Society, 2018.

[12] Jari Vikstedt, "Introduction of 5G Over-the-Air Measurements" in IEEE, 2018.

[13] Lee Teschler, "Why 5G is going to over-the-air testing" in TEST & MEASUREMENT TIPS:https://www.testandmeasurementtips.com/why-5g-is-going-to-over-the-air-testing-faq/ . Last visit: 13/03/2019.

[14] 3GPP Specification TR 38.810 v16.1.0, December 2018.

[15] R. C. Johnson, *"Compact Range Techniques and Measurements*" in *IEEE Transcations on Antennas and Propagation*, vol. AP-17, n° 5, September 1969.

[16] Deutsches Zentrum für Luft- und Raumfahrt (DLR), "*Compact Test Range of DLR for Antenna and RCS Measurements*".

[17] Microware Vision Group, *"Compact Antenna Test Range"*: https://www.mvg-world.com/en/products/field_product_family/antenna-measurement-2/compact-range-chambers-0 . Last visit: 25/03/2019.

[18] C. Rowell, *"Introduction to CATR Systems"* in OTA Workshop *Rhode&Schwarz*, March 2019.

[19] A. Muñoz-Acevedo, S. Burgos, M.Sierra-Castañer, "*Performance Comparison Between Serrated Edge and Rolled Edge Reflectors Inside CATR Facilities*" in EuCAP 2011.

[20] I. Linares Troncal, "*Diseño de antenas reflectarray de polarizacion circular en banda Ka para comunicaciones en banda ancha vía satélite*", Final Thesis Bachelor's Degree, 2018.

[21] MVG: *Mini-Compact Range* – Datasheet.

[22] R&S® ATS1000 Antenna Test System – 5G antenna characterization with small footprint, Datasheet 2019.

[23] B. I. Lueje, "*Diseño de una antena reflectarray para una megaconstelacion de satélites*", Bachelor's Thesis, July 2017.

[24] D. G. Berry, R. G. Malech, *"The Reflectarray Antenna"* in *IEEE Transactions on Antennas and Propagation*, pp.645-651, November 1963.

[25] P. Robustillo, J. Zapata, J. A. Encinar, "Design of a Contoured-Beam Reflectarray for EuTELSAT European Coverage Using a Stacked-Patch Element Characterized by an Artificial Neural Network" in *IEEE Transactions on Antennas and Propagation,*vol.11 pp.977-980, 2012.

[26] A. C. Gafo, *"Diseño de una antena reflectarray con diagrama de radiación tipo isoflux para aplicación en satélite de cobertura global"*, Bachelor's Thesis, July 2013.

[27] H. Chou, P. Hsueh, *"A dual-band near-field focused reflectarray antenna for RFID applications at 0.9 and 2.4 GHz"* in *Radio Science*, vol.46,Issue 06, December 2011.

[28] S. V. Polenga, A. V. Stankovsky, "MIlimeter-Wave Waveguide Reflectarray" in *2015 International Siberian Conference on Control Communications (SIBCON)*, 2015.

[29] M. Abdollahvand, J. A. Encinar, K. Forooraghi, "Single-Layer Dual-Frequency Reflectarray for Ka-Band Antennas" in *10th European Conference on Antennas and Propagation (EuCAP)*, 2016.

[30] A. P. Infiesta, *"Diseño de Antenna Reflectarray para sistemas celulares 5G",* Bachelor's Thesis, June 2017.

[31] Y. Fujii, S. Yoshimoto, S. Makino, *"The Design Method of Low-cross-polarization Reflectarray Antenna"* in *International Symposium on Antennas and Propagation (ISAP)*, November 2015.

[32] D. R. Prado, M. Arrebola, M. R. Pino, R. Florencio, R. R. Boix, J. A. Encinar, F. Las-Heras, " Efficient Crosspolar Optimization of Shaped-Beam Dual-Polarized Reflectarrays Using Full-Wave Analysis for the Antenna Element Characterization" in *IEEE Transactions on Antennas and Propagation* , vol. 65, no. 2, pp. 623-635, February 2017.

[33] D. R. Prado, J. A. Lopez-Fernandez, M. Arrebola, M. R. Pino, G. Goussetis, *"General Framework for the Efficient Optimization of Reflectarray Antennas for Contoured Beam Space Applications"* in *IEEE Access*, vol. 6, pp.72295 – 72310, 2018.

[34] M. R. Chaharmir, J. Shaker, *"Design of a Multi-Layer Ka-Band Frequency Selective Surface-Backed Reflectarray for Satellite Applications"* in *The 8th European Conference on Antennas and Propagation (EuCAP)*, 2014.

[35] S. Ballandovich, L. Liubina, M. Sugak, *"Design and Analysis of Dual-Band Circular Polarization 3D Printed Reflectarray"* in *Advances in Wireless and Optical Communications*, 2018.

[36] S. Sasaki, T. Muruyama, D. Higashi, *"Reflectarray Antenna Constructed by Arranging Double Omega-Shaped Resonant Elements with Mirror Image for Circular-Polarization Conversion"* in *International Symposium on Antennas and Propagation (ISAP)*, November 2017.

[37] J. Huang, J. A. Encinar, "Reflectarray Antennas", Wiley-IEE Press, 2008.

[38] I. Barriuso, A. L. Gutierrez, M. Lanza, *"Comparison of heuristic methods when applied to the design of reflectarrays"* in Proceedings of the *5th European Conference on Antennas and Propagation (EuCAP)*, April 2011.

[39] D. R. Prado, J. Alvarez, M. Arrebola, *"Efficient, Accurate and Scalable Reflectarray Phase-Only Synthesis Based on the Levenberg-Marquardt Algorithm"* in *ACES Journal*, vol.30, No.12, pp 1246-1255, December 2015.

[40] D. Martinez-de-Rioja, E. Martinez-de-Rioja, Jose A. Encinar, *"Multibeam Reflectarray for Transmit Satellite Antennas in Ka Band Using Beam-Squint"* in *IEEE International Symposium on Antennas and Propagation (APSURSI)*, 2016.

[41] Ahmed H. Abdelrahman, P. Nayeri, *"Single-Feed Quad-Beam Transmitarray Antenna Design"* in *IEEE Transactions on Antennas and Propagation*, vol.64,No.3,March 2016.

[42] M. Arrebola, L. de Haro, Jose A. Encinar, *"Analysis of Dual-Reflector Antennas with a Reflectarray as Subreflector"* in *IEEE Antennas and Propagation Magazine*, vol.50, pp 39-51, December 2008.

[43] Ö. A. Civi, *"Reconfigurable Reflectarrays: Design, Analysis and Fabrication"* in *9th European Conference on Antennas and Propagation (EuCAP)*, April 2015.

[44] H. Theissen, C. Dahl, I. Rolfes, *"An Electronically Reconfigurable Reflectarray Element Based on Binary Phase Shifters for K-Band Applications"* in *German Microware Conference (GeMiC)*, March 2016.

[45] S. Montori, E. Chiuppesi, L. Marcaccioli, *"1-bit RF-MEMS-Reconfigurable Elementary Cell for Very Large Reflectarray"* in *10th Mediterranean Microware Symposium*, August 2010.

[46] H. Yang, F. Yang, S. Xu, *"A 1-Bit Multipolarization Reflectarray Element for Reconfigurable Large-Aperture Antennas"* in *IEEE Antennas and Wireless Propagation Letters*, vol.16, 2017.

[47] F. Venneri, S. Costanzo, G. Di Massa, *"Design of a Reconfigurable Reflectarray Based on Varacaptor Tuned Element"* in *6th European Conference on Antennas and Propagation (EuCAP)*, 2011.

[48] Y. Ismail, A. Faizal, M. Zain, *"Phase Range Analysis of Reflectarrays Patch Cells Printed on Liquid Crystal Substrate"* in *2nd Malaysia Conference on Photonics*, August 2008.

[49] M. Sazegar, A. Giere, Y. Zheng, *"Reconfigurable Unit Cell for Reflectarray Antenna Based on Barium-Strontium-Titanate Thick-Film Ceramic"* in *Proceedings of the 39th European Microware Conference* pp. 598 – 601,October 2009.

[50] S. A. Long, G. H. Huff, *"A Fluidic Loading Mechanism for Phase Reconfigurable Reflectarray Elements"* in *IEEE Antennas and Wireless Propagation Letters*, vol. 10 pp 876 – 879, 2011.

[51] T. H. Hand, S. A. Cummer, *"Reconfigurable Reflectarray Using Addressable Metamaterials"* in *IEEE Antennas and Wireless Propagation Letters*, vol.9, pp 70-74, 2010.

[52] Z. Chang B. You, L. Wu, *" A Reconfigurable Graphene Reflectarray for Generation of Vortex THz Waves"* in *IEEE Antennas and Wireless Propagation Letters*, vol.15, pp. 15137-1540, January 2016.

[53] M. K. Arshad, F. A. Tahir, *"Optimum Microstrip Reflectarray Unit Cell Design for Wide-Band Operation"* in *11th International Conference on Frontiers of Information Technology*, 2013.

[54] J. Huang, *"Bandwidth Study of Microstrip Reflectarray and a Novel Phased Reflectarray Concept"* in *IEEE Antennas and Propagation Society International Symposium*, June 1995.

[55] E. Carrasco, J. A. Encinar, *"Bandwidth Improvement in Large Reflectarrays by Using True-Time Delay"* in *IEEE Transactions on Antennas and Propagation*, vol.56,no 8, August 2008.

[56] M. R. Chaharmir, J. Shaker, H. Legay, *"Broadband Design of a Single Layer Large Reflectarray Using Multi Cross Loop Elements"* in *IEEE Transactions on Antennas and Propagation*, vol. 57, no. 10, October 2009.

[57] D. M. Pozar, *"Bandwidth of Reflectarrays"* in *Electronics Letters*, vol.39, Issue 21, October 2003.

[58] Alvaro F. Vaquero, Daniel R. Prado, Manuel Arrebola, Marcos R. Pino, Fernando Las-Heras, *"Reflectarray Probe Optimization at Millimiter Frequencies"* in *10th European Conference on Antennas and Propagation (EuCAP)*, June 2016.

[59] His-Tseng Chou, *"Floquet Mode Phenomena of Infinite Phased Array Antennas in Near-Field Focus Applications"* in *IEEE Transcations on Antennas and Propagation*, vol.61,no.6, June 2013.

[60] Taconic: TSM-DS3 Dimensionally Stable Low Loss Laminate Datasheet.

[61] FR4 Datasheet. *Farnell reference*: 1644697.
[62] Antenna Magus Report: *Axial-choke conical horn*.
[63] S. D. Targonski, D. M. Pozar, *"Minimization of Beam Squint in Microstrip Reflectarrays Using an Offset Feed"* in *IEEE Anntenas and Propagation Society International Symposium*, July, 1996.